2015-04-06

The Molecular Basis for Impaired Cerebral Myogenic Response in Type 2 Diabetes

Abdelrahman, Khaled

UNIVERSITY OF CALGARY

The Molecular Basis for Impaired Cerebral Myogenic Response in Type 2 Diabetes

by

Khaled Soliman Hamed Abdelrahman

A THESIS

SUBMITTED TO THE FACULTY OF GRADUATE STUDIES

IN PARTIAL FULFILMENT OF THE REQUIREMENTS FOR THE

DEGREE OF DOCTOR OF PHILOSOPHY

GRADUATE PROGRAM IN CARDIOVASCULAR AND RESPIRATORY SCIENCES

CALGARY, ALBERTA

APRIL, 2015

Abstract

Cognition and brain function are dependent on appropriate control of blood flow within the cerebral circulation. Cerebral blood flow is controlled through the interplay of several physiological mechanisms that regulate the contractility of vascular smooth muscle cells (VSMCs) within the wall of cerebral arteries. The myogenic response of cerebral arteries is a crucial mechanism that is responsible for maintaining adequate brain blood flow. This fundamental mechanism is due to cellular processes intrinsic to VSMCs including: 1) Ca^{2+}-calmodulin-dependent activation of myosin light chain kinase and phosphorylation of LC_{20}, 2) Rho-associated kinase (ROK)-dependent phosphorylation of myosin phosphatase targeting subunit 1 (MYPT1) and suppression of myosin light chain phosphatase activity, and 3) dynamic reorganization of the actin cytoskeleton. Inappropriate regulation of one or more of these mechanisms may contribute to the dysfunctional control of cerebral diameter and flow, predisposing type 2 diabetic patients to ischemic and hemorrhagic stroke. Here, we employed Goto-Kakizaki (GK) rats, a type 2 diabetic rat model, to identify the molecular basis for the dysfunctional myogenic constriction in early and established type 2 diabetes. We detected an enhanced basal myogenic tone in prediabetic GK cerebral arteries at low intraluminal pressure that progressed with the severity of diabetes such that the myogenic response was lost in arteries of GK rats with established diabetes. Our biochemical evidence shows that there are parallel, progressive alterations in MYPT1 and LC_{20} phosphorylation, as well as actin polymerization downstream of ROK that are consistent with the evolution of dysfunctional myogenic response. These findings provide a better understanding of the underlying defects responsible for dysfunctional control of cerebral arterial diameter and blood flow in type 2 diabetes.

Acknowledgments

I would like to thank my supervisor Dr. William Cole for his continuous support, encouragement and guidance. I would also like to thank my supervisory committee members, Dr. Michael Walsh, Dr. Andrew Braun and Dr. Robert French for their advice and valuable suggestions. I would like to acknowledge the contribution of Emma Walsh who helped with pressure myography experiments and preparation of protein samples for western blot experiments, Dr. Ahmed El-Yazbi who helped troubleshooting some of the western blot experiments for quantifying LC_{20} and MYPT1 phosphorylation, Dr. Moreno-Domínguez and Dr. Colinas-Miranda who helped troubleshooting some of the western blot experiments for quantifying G-actin and FAK phosphorylation, and Christine Campbell who helped with some real time-PCR experiments. I am very grateful to Alberta Innovates-Health Solutions and the Killam Foundation for supporting my stipend during the doctoral program. Finally, I would like to thank all the members of the Cole laboratory for their valuable input and suggestions. Thanks to my wife, daughter and parents for their understanding and assistance.

To my family

Table of Contents

List of Figures

List of Symbols, Abbreviations and Nomenclature

Abbreviation	Full name
$[Ca^{2+}]_i$	Cytosolic free Ca^{2+} concentration
Akt	Protein kinase B
ARP2/3	Actin-related proteins 2 and 3
BK_{Ca}	Large-conductance Ca^{2+}-activated potassium channels
CaM	Calmodulin
cAMP	Cyclic adenosine 3':5'-monophosphate
CAS	Crk-associated kinase
COF	Cofilin
cGMP	Cyclic guanosine 3':5'-monophosphate
CPI-17	C-kinase potentiated Protein phosphatase-1 inhibitor
DMPK	Myotonic dystrophy protein kinase
eNOS	Endothelial nitric oxide synthase
F-actin	Filamentous actin
FAK	Focal adhesion kinase
G-actin	Globular actin
GAPDH	Glyceraldehyde-3-phosphate dehydrogenase
GDP	Guanosine 5'-diphosphate
GK	Goto-Kakizaki
GTP	Guanosine 5'-triphosphate
H1152	ROK inhibitor
HRP	Horseradish peroxidase
HSP	Heat shock protein
ILK	Integrin linked kinase
iNOS	Inducible nitric oxide synthase
IP3	Inositol 1,4,5-trisphosphate
IRS	Insulin receptor substrate
K_v	Voltage-gated potassium channels
LC_{20}	20 kDa myosin regulatory light chain
LIMK	Lim kinase
LZ	Leucine zipper

MAPK	Mitogen activated protein kinase
MLCK	Myosin light chain kinase
MLCP	Myosin light chain phosphatase
MYPT1	Myosin phosphatase targeting subunit 1
NO	Nitric oxide
N-WASP	Neuronal Wiskott–Aldrich syndrome protein
PBS	Phosphate-buffered saline
PCR	Polymerase chain reaction
PI3K	Phosphatidylinositide 3-kinase
PKA	Protein kinase A
PKC	Protein kinase C
PKG	Protein kinase G
PPARγ	Peroxisome proliferator-activated receptor gamma
qPCR	Quantitative polymerase chain reaction
RBD	Rho-binding domain
RhoGEF	Rho guanine nucleotide exchange factor
ROK	RhoA-associated kinase
SD	Sprague Dawley
SDS	Sodium dodecyl sulfate
SDS-PAGE	Sodium dodecyl sulfate - polyacrylamide gel electrophoresis
SFK	Src family kinase
SR	Sarcoplasmic reticulum
TBS	Tris-buffered saline
TBST	Tris-buffered saline with Tween
TRPC	Transient receptor potential, canonical family
VASP	Vasodilator-stimulated phosphoprotein
VGCCs	Voltage-gated calcium channels
VSMCs	Vascular smooth muscle cells
WR	Wistar rat
ZIPK	Zipper interacting protein kinase

Chapter One: General introduction to the cerebral myogenic response and type 2 diabetes

1.1 Cerebral circulation

Cognition and brain integrity are dependent on appropriate control of blood flow within the cerebral circulation to provide an adequate supply of oxygen and nutrients, as well as the removal of carbon dioxide and metabolic by-products. Carotid and vertebral arteries are considered the major arteries that conduct blood from the heart to the brain. Blood is distributed through a circle of arteries at the base of the brain, known as the Circle of Willis (Alpers et al., 1959). This circular arrangement is crucial to support brain activity by providing alternate routes for blood flow in any circumstance of blockade in one of the main arteries in the circle. The major cerebral arteries arising from the Circle of Willis are anterior, middle, and posterior cerebral arteries (Figure 1.1). These three arteries are pial vessels, running along the surface of the brain and give rise to arterioles that supply blood to deeper structures within the brain (Putnam, 1937).

1.2 Structure of cerebral arteries

The cerebral arterial wall is composed of three major layers: tunica adventitia, tunica media and tunica intima (Figure 1.2). The tunica adventitia contains connective tissues including elastin, collagen, fibroblast cells, mast cells and macrophages that provide attachment to the surrounding structures, support and protection of the vessel (Mulvany & Aalkjaer, 1990).

The tunica media represents the major layer of the cerebral arterial wall. It is composed of multiple layers of spindle-shaped smooth muscle cells arranged circumferentially along the length of the vessel. The thickness of the smooth muscle layer is dependent on the size of the

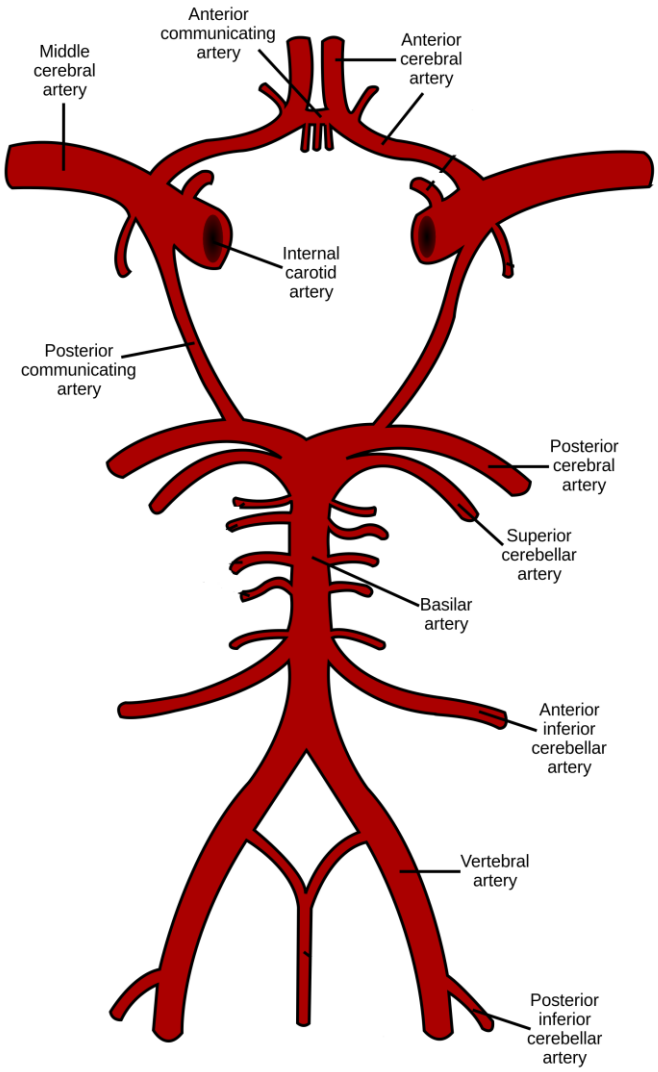

Figure 1.1: The Circle of Willis and cerebral arteries

The Circle of Willis is the specialized, anatomical structure of cerebral arteries at the base of the brain. The anterior section of the Circle of Willis arises from the branching of the internal carotid artery into the left and right middle and anterior cerebral arteries. The posterior section of the Circle of Willis is formed due to the branching of the basilar artery into the left and right posterior cerebral arteries. The left & right anterior and posterior communicating arteries close the Circle of Willis (modified from www.wikipedia.org).

vessel and may range from two to three layers in arterioles sized 30-100 μm in diameter to four to 10 layers in arteries of > 100 μm in diameter (Shiraishi et al., 1986).

The tunica intima is a single sheet of endothelial cells lining the tunica media. Cerebral endothelial cells form tight junctions that constitute the blood-brain barrier which permits only selective movement of circulating molecules to the brain (Ge et al., 2005). Endothelial cells have the ability to sense shear stress generated from blood flow across the luminal surface of the vessel and actively respond to regulate cerebral blood flow under dynamic physiological conditions through the release of relaxing factors and gap junction-mediated coupling (Socha et al., 2012).

1.3 Cerebral blood flow

Blood flow to the brain can be described by Poiseuille's law, which states that flow is dependent on pressure change (ΔP), blood viscosity (η), the length of the vessel (L), and the fourth power of the vessel radius (r) according to the equation $F = (\pi \times \Delta P \times r^4)/8\eta L$ (Cipolla, 2009). The systemic vascular resistance is the resistance to flow due to peripheral circulation that must be overcome by the heart to deliver adequate blood to body organs. As predicted from the above-mentioned equation, vascular resistance is largely dependent on vessel diameter. Therefore, arterioles (<100 μm in diameter) and small arteries (~100-300 μm in diameter) are the major determinants of the peripheral vascular resistance and, hence, are referred to as resistance vessels (Harper et al., 1984). According to Poiseuille's law, small changes in resistance vessel diameter will have a major impact on the blood flow to the brain and are a determinant of local hemodynamics. Insufficient flow to the brain can lead to ischemia while excessive flow can provoke capillary rupture and blood–brain barrier disruption (Faraci & Heistad, 1990).

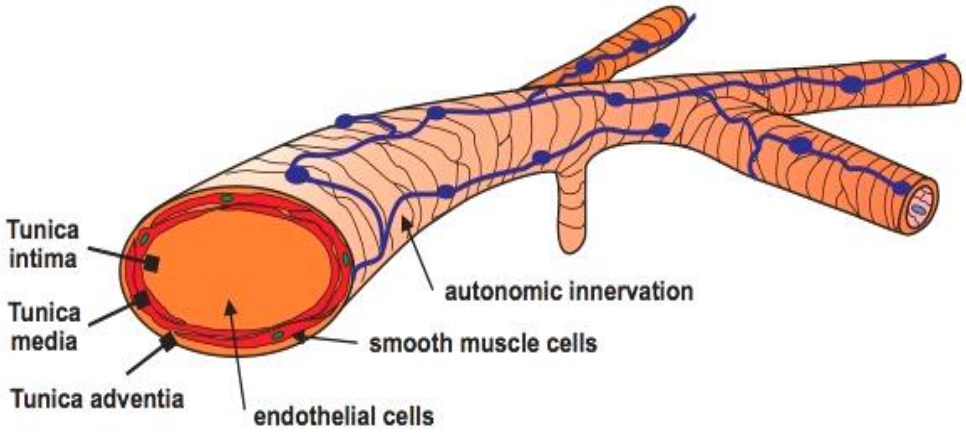

Figure 1.2: Structure of the cerebral artery

The wall of cerebral arteries is composed of three major layers: the tunica adventitia, tunica media and tunica intima. The tunica intima constitutes a single layer of endothelial cells. The tunica media is made of multiple layers of VSMCs depending on the vessel diameter. The tunica adventitia represents the connective tissue around the vascular wall including collagen, elastin, fibroblasts and perivascular nerves.

Cerebral blood flow is a function of several physiologic factors that regulate the contractile state of vascular smooth muscle cells (VSMCs) within the walls of cerebral vessels. These factors can be intrinsic to VSMC or extrinsic in nature, e.g. circulating or locally released vasoactive molecules. Adequate regulation of cerebral blood flow is achieved through the interplay of multiple intrinsic and extrinsic factors that frequently exert opposing vasoconstrictor and vasodilatory influences on VSMCs (Davis & Hill, 1999; Cole & Welsh, 2011). The myogenic response will be discussed in the next section as one of the factors intrinsic to VSMCs that regulate vascular diameter.

1.4 The myogenic response

More than 100 years ago, Bayliss (1902) made the seminal observation that resistance arteries exist in a state of partial constriction owing to the mechanical stress of intraluminal pressure. This ability of resistance arteries to react to intraluminal pressure is known as the *myogenic response.* The development of myogenic tone by VSMCs in response to pressure change permits flow autoregulation by reducing flow with pressure elevation and permitting dilation and increased flow with pressure reduction. Each resistance artery/arteriole has a different operating range of intraluminal pressure; e.g. the rat middle and posterior cerebral arteries exhibit myogenic constriction between ~60 to 130 mmHg (Davis & Hill, 1999; Schubert & Mulvany, 1999; Johnson et al., 2009), but penetrating arterioles are active between ~20 and 140 mmHg (Cipolla & Bullinger, 2008). Outside this autoregulatory pressure range, changes in diameter and flow with pressure elevation are proportional, with inadequate flow observed at low pressure (< 60 mmHg) and excessive flow at high pressure (>120 mmHg) (Osol et al., 2002).

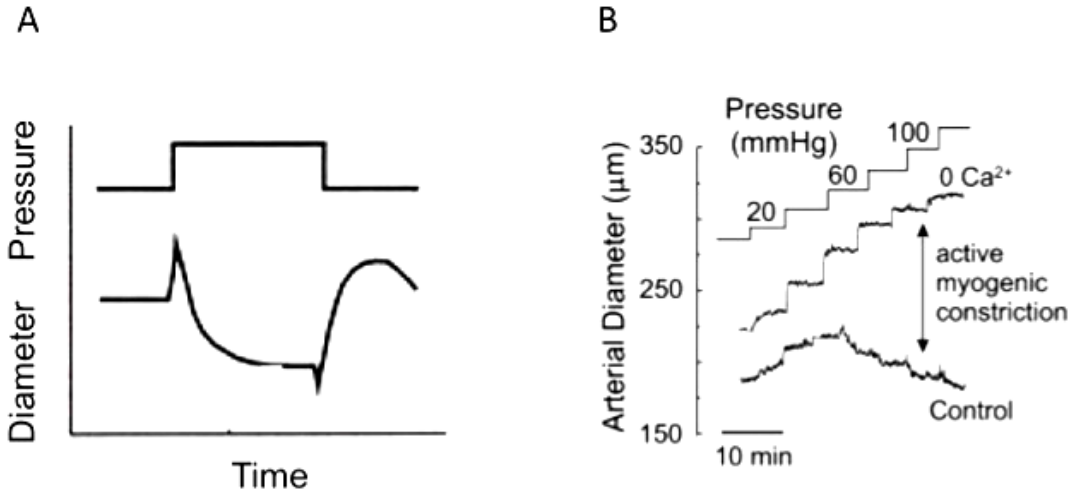

Figure 1.3: The myogenic response of small resistance arteries.

Panel A: Diagrammatic representation of a typical myogenic constriction of a cerebral resistance artery in response to a step increase in intraluminal pressure. Intraluminal pressure elevation and reduction elicits a spontaneous vasoconstriction and vasodilation, respectively.

Panel B: Representative traces of the pressure-diameter relationship in rat middle cerebral artery for intraluminal pressures between 10 to 120 mmHg in 20 mmHg incremental steps, in 2.5 mM external Ca^{2+} (Control) followed by zero external Ca^{2+} (0 Ca^{2+})-containing Krebs' solution. The difference in diameter in the presence and absence of external Ca^{2+} represents the active myogenic constriction. (Figure is modified from Cole & Welsh 2011)

The myogenic response has been widely studied *in vitro* by pressure myography using isolated, pressurized vessels. This technique offers the ability to track changes in vessel diameter in response to intraluminal pressure changes in the absence of extrinsic metabolic, neuronal, and endothelial influences. Figure 1.3 shows pressure myography trace for rat cerebral artery in response to a series of intraluminal pressure steps from 10 to 120 mmHg in increments of 20 mmHg. In the absence of extracellular Ca^{2+}, the vessel dilates passively in response to pressure elevation. The difference in diameter in the presence and absence of extracellular Ca^{2+} corresponds to the extent of active myogenic constriction due to pressure-dependent activation of myogenic mechanisms of contraction intrinsic to VSMCs.

1.4.1 Modulation of the myogenic response by extrinsic factors

Although the myogenic response is due to cellular mechanisms that are inherent to VSMC, the modulatory effect of external vasoactive molecules is also crucial to match blood flow to metabolic demands under dynamic physiological situations. Extrinsic modulation evokes either vasoconstriction or vasodilation that is superimposed on the basal level of intrinsic myogenic tone. These extrinsic vasoactive molecules include factors from the endothelium (including nitric oxide, prostacyclin, endothelin-1, and thromboxane A_2), perivascular nerves (e.g. nitric oxide, calcitonin gene-related peptide, and serotonin), the blood (e.g. angiotensin II), or locally released from astrocytes (e.g. prostaglandins and K^+ ions) (Davis & Hill, 1999; Walsh & Cole, 2013).

1.4.2 Physiological importance of the myogenic response

The ability of resistance arteries to react to changes in intraluminal pressure is crucial for proper cardiovascular function. The myogenic response contributes to peripheral vascular resistance and, accordingly, blood pressure regulation. It also allows the resistance arteries to

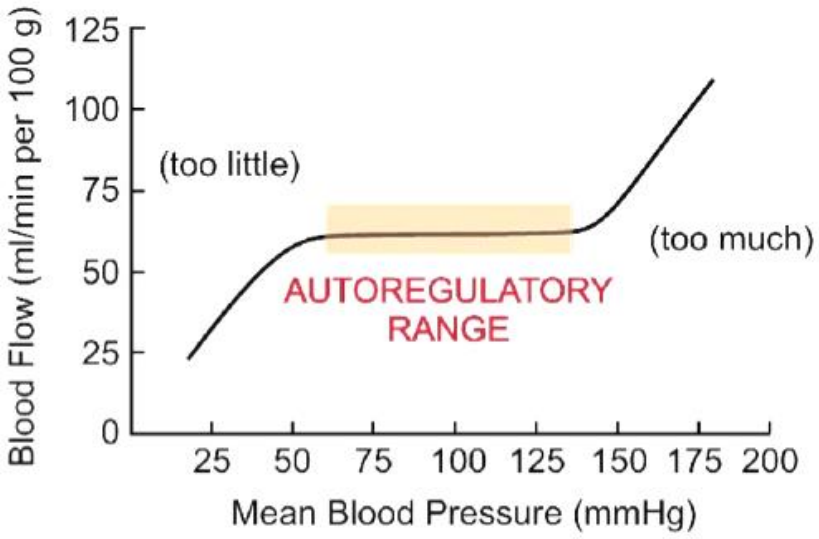

Figure 1.4: Blood flow-perfusion pressure relationship.

The myogenic response maintains a relatively constant blood flow across a wide range of perfusion pressure (between ~50 and ~140 mmHg) in rat cerebral arteries. Outside the autoregulatory range, there is either too little or too much blood flow owing to the lack of myogenic regulation of cerebral arterial diameter.

dilate and constrict to maintain adequate blood flow to different body organs, e.g. brain and kidney. In the brain, it was found that blood flow is maintained at an almost constant level when cerebral perfusion pressure is between 50-140 mmHg, which is consistent with the operating range for the myogenic response of pressurized cerebral arteries (Figure 1.4) (Cipolla, 2009).

Pressure autoregulation of upstream vessel diameter by the myogenic response is also required to maintain capillary hydrostatic pressure constant during variations in systemic arterial pressure. Thus, the myogenic response serves as a protective mechanism that shields downstream structures, such as thin-walled arterioles, capillaries and the blood-brain-barrier, from the damaging effects of high intravascular pressure (Blum et al., 2005; Loutzenhiser et al., 2006). Therefore, an abnormal cerebral myogenic response observed in animal models of hypertension, stroke and diabetes could have major consequences for brain function (Cole & Welsh, 2011).

1.5 Contemporary view of the molecular mechanisms of the myogenic response

A fundamental concept of our understanding of the regulation of VSMC contraction holds that phosphorylation of myosin 20 kDa regulatory light chains (LC_{20}) and force development are a function of the balance between the activities of myosin light chain kinase (MLCK) and myosin light chain phosphatase (MLCP) (Somlyo & Somlyo, 2003). Previous research has focused on the regulation of MLCK, but control of MLCK activity alone was postulated to be insufficient to fully explain the myogenic response (Osol et al., 2002; Schubert et al., 2008). Recent methodological advances have improved the sensitivity of detection and quantification of protein phosphorylation levels in the small amounts of proteins obtained from short segments of pressurized resistance arteries (2-3 mm in length and <200 μm in diameter). This has facilitated the direct analysis of other signaling pathways that could contribute to the control of VSMC contractility of resistance arteries. MLCP inhibition due to phosphorylation of

myosin phosphatase targeting subunit 1 (MYPT1) by Rho-associated kinase (ROK) was found to play a crucial role in the myogenic response. MYPT1 phosphorylation increases the sensitivity of the contractile apparatus to activator Ca^{2+} (i.e. a leftward shift in the LC_{20} phosphorylation or force versus $[Ca^{2+}]_i$ relationships), a mechanism of Ca^{2+} sensitization (Johnson et al., 2009; El-Yazbi et al., 2010). Recent findings also indicate a role for dynamic reorganization of the actin cytoskeleton in the myogenic response. Specifically, increased actin polymerization with pressure elevation is postulated to strengthen connections and facilitate increased force transmission between the contractile apparatus and plasma membrane/extracellular matrix (Cipolla et al., 2002; Gerthoffer, 2005; Gunst & Zhang, 2008; Moreno-Domínguez et al., 2014) (Figure 1.5). This contemporary understanding of the molecular basis of the three mechanisms is largely based on findings obtained using cerebral resistance arteries and to lesser extent skeletal muscle resistance arterioles (e.g. gracilis or cremaster arterioles) of rats and rabbits (Davis & Hill, 1999; Johnson et al., 2009; El-Yazbi et al., 2010). Details of each mechanism will be explained in the following sections.

1.5.1 The mechanosensor

A mechanosensor is the molecular structure that senses the change in intraluminal pressure and transmits the signal to the contractile apparatus to elicit vasoconstriction. Candidates for this mechanosensor include stretch-activated cation channels (Carlson & Beard, 2011), pressure-evoked sphingosine-1-phosphate signaling (Lidington et al., 2013), membrane-associated enzymes (e.g. metalloproteinases) (Lucchesi et al., 2004), cadherins (Jackson et al. 2010), mechanical-activation of G protein-coupled receptors (Mederos et al., 2008), and integrin adhesion signaling (Hill & Meininger, 2012; Walsh & Cole, 2013).

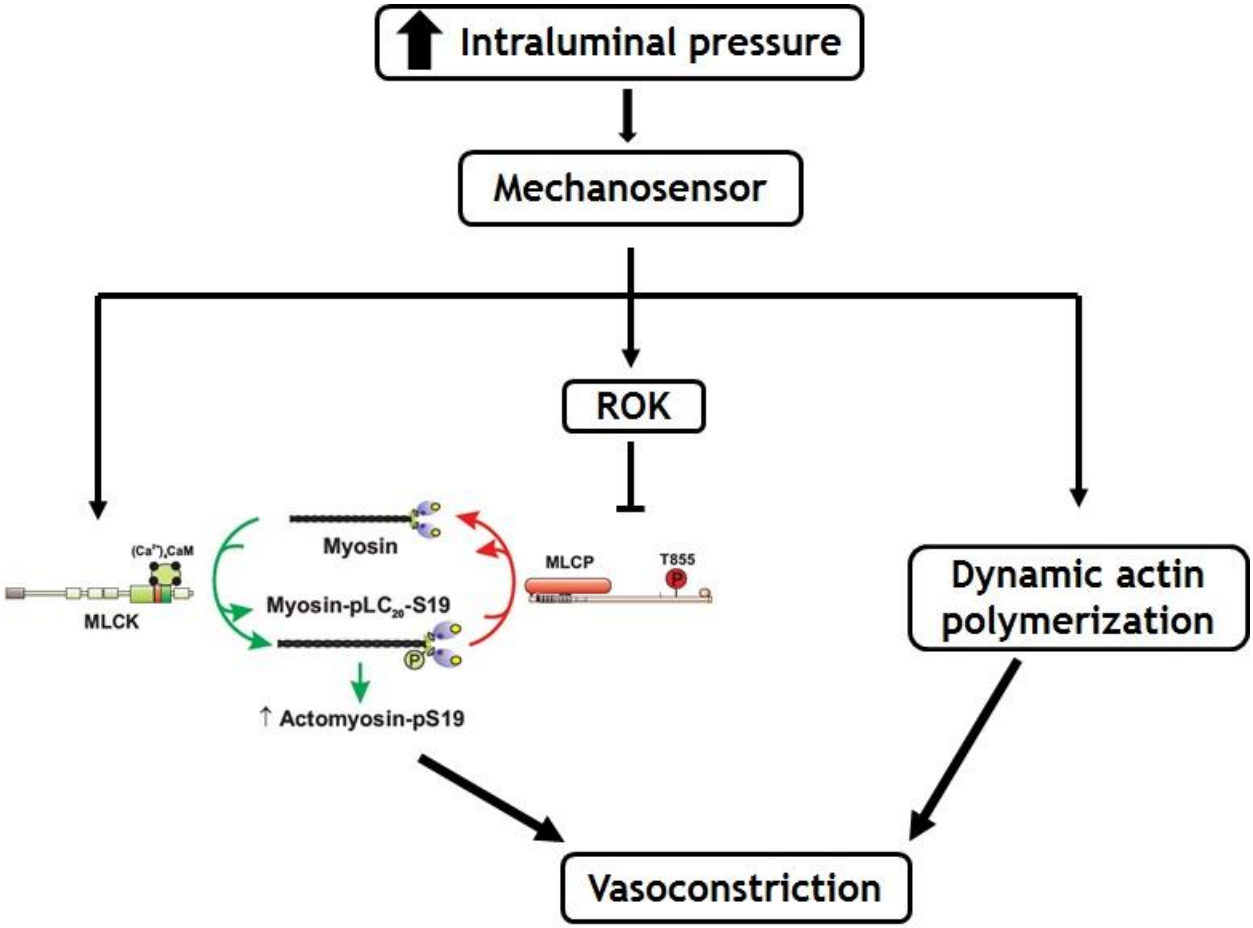

Figure 1.5: Simplified outline for the mechanisms responsible for the myogenic response

Mechanical activation of mechanosensor(s) in response to intraluminal pressure elevation activates MLCK (via increased Ca^{2+} entry and release), and actin polymerization, and inhibits MLCP activity via ROK-mediated phosphorylation of MYPT1. LC_{20} phosphorylation is controlled by the balance between MLCK and MLCP activities. Vasoconstriction is achieved by pLC_{20}-dependent changes in cross-bridge cycling to generate force, as well as dynamic actin cytoskeletal reorganization to transmit force.

Integrins are transmembrane glycoproteins that are connected to the extracellular matrix via interaction with matrix proteins, such as collagen, laminin and fibronectin. Integrins are also connected to the cytoskeleton via interaction with integrin adhesion proteins that transduce the mechanical force across the plasma membrane (Martinez-Lemus et al., 2005; Davis et al., 2001; Martinez-Lemus, 2014). Davis et al (2001) and Martinez-Lemus et al (2005) have provided direct evidence to support the role of integrins in the myogenic response that is suppressed by integrin-specific peptides and blocking antibodies in skeletal muscle resistance arterioles. This role for integrins in the rat cerebral artery has been supported by recent data obtained in the Cole laboratory using integrin-blocking antibodies (Colinas et al., 2015).

Smooth muscle integrins are associated with membrane dense plaques that are structural analogues of focal adhesions of cultured cells (Gunst & Zhang, 2008). Integrin activation induces phosphorylation of tyrosine residues and activation of focal adhesion kinase (FAK) and Src family kinases (SFK) (Gunst & Zhang, 2008). Specifically integrin activation was found to trigger autophosphorylation of Tyr-397 (Y397) on FAK and Tyr-416 (Y416) on SFK that were directly linked to development of myogenic constriction in cerebral arteries (Colinas et al., 2015). Substrates for activated FAK and SFK have not been fully identified, but candidates, based on agonist- and depolarization-induced tyrosine phosphorylation in airway and vascular smooth muscles, include the cytoskeletal proteins paxillin and talin (Pavalko et al., 1995; Tejani et al., 2011), the adaptor protein p130 Crk-associated kinase (CAS) (Tang & Tan, 2003), p42/44 mitogen-activated protein kinase (MAPK) (Spurrell et al., 2003) and RhoA guanine nucleotide exchange factors (RhoGEF) that are essential for RhoA/ROK activation (Lessey et al., 2012). Moreover, activation of integrins has been linked to activation of the L-type Ca^{2+} channel in

vascular smooth muscles via a tyrosine phosphorylation cascade involving FAK and SFK and other adhesion proteins, such as paxillin and vinculin (Wu et al., 2001).

Another mechanosensor in the myogenic response has been proposed to be Gq/11-coupled receptors (specifically Angiotensin II receptors type 1, AT1 receptors). AT1 receptors in response to mechanical stretch adopt an active conformation that enables G protein coupling, activation of phospholipase C, opening of non-selective cation channels, and membrane depolarization (Mederos et al., 2011).

1.5.2 LC_{20} and the myogenic response

Force generation in smooth muscle during the myogenic response is initiated by cross-bridge cycling that is regulated at the level of thick (myosin) filaments. Each smooth muscle myosin molecule consists of: (i) two myosin heavy chains (MHC) that have intertwined coiled-coil tail sequences and N-terminal globular ATPase heads, and (ii) two pairs of 20 kDa regulatory light chains (LC_{20}) and 17 kDa essential light chains localized at the neck region of each MHC (Figure 1.6). LC_{20} monophosphorylation at residue Ser-19 (S19) or diphosphorylation at S19 and Thr-18 (T18) leads to an increase in ATPase activity of the myosin heads and consequently the activation of cross-bridge cycling. The balance between MLCK and MLCP activities determines the level of LC_{20} phosphorylation and, thereby, determines the extent of force generation via the interaction between actin and myosin filaments (Somlyo & Somlyo, 2000; Somlyo & Somlyo, 2003; Cole & Welsh, 2011).

A

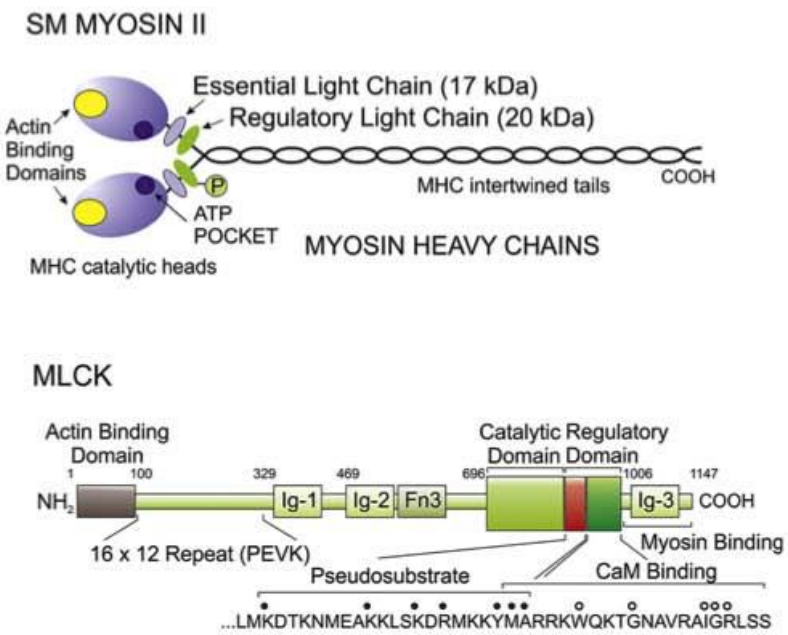
SM MYOSIN II
Essential Light Chain (17 kDa)
Regulatory Light Chain (20 kDa)
Actin Binding Domains
MHC intertwined tails
COOH
P
ATP POCKET
MYOSIN HEAVY CHAINS
MHC catalytic heads
MLCK
Actin Binding Domain
Catalytic Domain
Regulatory Domain
1
100
329
469
696
1006
1147
NH2
Ig-1
Ig-2
Fn3
Ig-3
COOH
16 x 12 Repeat (PEVK)
Pseudosubstrate
Myosin Binding
CaM Binding
...LMKDTKNMEAKKLSKDRMKKYMARRKWQKTGNAVRAIGRLSS
MLCP
PP1c-δ
ROK
T697 T855
M20
1030
1
39
170
198
296
NH2
35RVxF38
Ankyrin Repeats
D/E
MYPT1
Myosin Binding
LZ

B

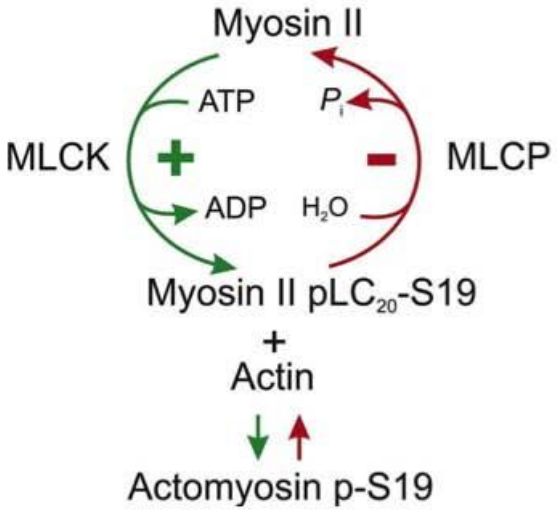
Myosin II
ATP
Pi
MLCK
+
−
MLCP
ADP
H2O
Myosin II pLC20-S19
+
Actin
Actomyosin p-S19

Figure 1.6: The domain structure of smooth muscle myosin II, myosin light chain kinase and myosin light chain phosphatase.

Panel A: Diagrammatic representations of smooth muscle myosin II, myosin light chain kinase (MLCK) and myosin light chain phosphatase (MLCP). Smooth muscle myosin II is composed of two heavy chains (MHC) with actin binding domains and ATP pockets, two 17 kDa essential light chains and two 20 kDa regulatory light chains (LC_{20}). MLCK is composed of an N-terminal actin binding domain, a C-terminal catalytic domain, a pseudosubstrate autoinhibitory domain and a $(Ca^{2+})_4$-CaM binding regulatory domain. MLCP is composed of a catalytic subunit (PP1cδ), a myosin phosphatase targeting subunit (MYPT1) and a small subunit, M20 of unknown function. Thr-697 (T697) and Thr-855 (T855) (rat numbering) are two major sites on MYPT1 for ROK-mediated phosphorylation.

Panel B: Diagrammatic representation showing that the level of LC_{20} phosphorylation is dictated by the balance in the activities of MLCK and MLCP. Phosphorylation of LC_{20} at Ser-19 (S19) permits myosin ATPase activation, leading to cross-bridge cycling and force generation. (Figure is modified from Cole & Welsh 2011)

1.5.3 Ca^{2+}-dependent activation of MLCK and the myogenic response:

The primary mechanism for initiation of contraction in VSMC involves an increase in the cytosolic free calcium concentration $[Ca^{2+}]_i$ in response to smooth muscle cell membrane depolarization, neurotransmitters released from nerve terminals, G protein-coupled receptor activation by circulating ligands, or an increase in intraluminal pressure. The increase in $[Ca^{2+}]_i$ is due to Ca^{2+} influx from the extracellular space, and release from intracellular compartments such as the sarcoplasmic reticulum (SR). The historical view of the myogenic response holds that constriction is initiated by a mechanosensor that senses the change in circumferential wall tension and stimulates non-selective cation channel activity. This leads to membrane potential (E_m) depolarization, activation of voltage-gated calcium channels (VGCCs), Ca^{2+} influx and increased $[Ca^{2+}]_i$ (Knot & Nelson, 1998; Davis & Hill, 1999). Later it was shown that pressure elevation also evokes phospholipase C-γ1 (PLCγ1)-mediated production of 1,2-diacylglycerol (DAG) and inositol 1,4,5-trisphosphate (IP3) (Jarajapu and Knot, 2002; Gonzales et al., 2014). IP3 evokes the release of Ca^{2+} from internal Ca^{2+} stores within the SR in the form of Ca^{2+} waves that propagate through the cytosol (Mufti et al., 2010). DAG might also contribute to membrane depolarization by activating non-selective cation channels (Large et al., 2009). Ca^{2+}, from extracellular and intracellular sources, binds to CaM to form the $(Ca^{2+})_4$-CaM complex. Force is initiated when MLCK is activated by the Ca^{2+}-CaM complex leading to phosphorylation of LC_{20} at the S19 site. This phosphorylation is necessary and sufficient for actomyosin ATPase activation, cross-bridge cycling and smooth muscle contraction (Walsh et al., 1982). Although VGCCs are considered the influx pathway for Ca^{2+} required for contraction, additional influx pathways may also contribute to the increase in $[Ca^{2+}]_i$, such as Canonical Transient Receptor

Potential (TRPC) cation channels and reverse mode sodium-calcium exchanger (Potocnik & Hill, 2001; Brayden et al., 2008).

Physiological control of cerebral blood flow is dependent on sustained changes in arterial diameter; i.e. on tonic rather than phasic contraction of VSMCs. Therefore, the extent of the VSMC depolarization must be tightly controlled such that appropriate changes in $[Ca^{2+}]_i$ are achieved in the absence of action potentials (regenerative activation of VGCCs and action potential will result in phasic rather than tonic contractions). This control is provided by a compensatory activation of voltage-gated K^+ (K_V) channels and large conductance Ca^{2+}-activated K^+ channels (BK_{Ca}) (Knot & Nelson, 1995; Ledoux et al., 2006). The activation of at least three different types of voltage-dependent channels in rat cerebral arteries, including Kv1.2/1.5/1.6, Kv2.1/9.3 and Kv7 subunit-containing channels, have been postulated to regulate depolarization associated with intraluminal pressure elevation (Plane et al., 2005; Zhong, Abd-Elrahman, et al., 2010; Zhong, Harhun, et al., 2010). The activation of BK_{Ca} channels has been attributed to the release of Ca^{2+} from the SR in the form of transient, spatially-restricted elevations in $[Ca^{2+}]_i$ at the inner surface of the sarcolemma referred to as Ca^{2+} sparks (Brayden & Nelson, 1992; Yang et al., 2009) (Figure 1.7).

1.5.4 Ca^{2+} sensitization and the myogenic response

Ca^{2+}-dependent activation of MLCK is necessary, but not sufficient for the myogenic response. This view is suggested by the minimal elevation in arterial wall $[Ca^{2+}]_i$ over the level attained at 60-80 mmHg, yet force generation increases substantially with further pressure elevation to maintain diameter constant or provide for additional constriction at >80 mmHg (Osol et al., 2002). Moreover, rat cerebral and skeletal muscle arterioles exhibit a significant depolarization (~25 mV) upon an increase in intraluminal pressure from 10 to 60 mmHg, yet

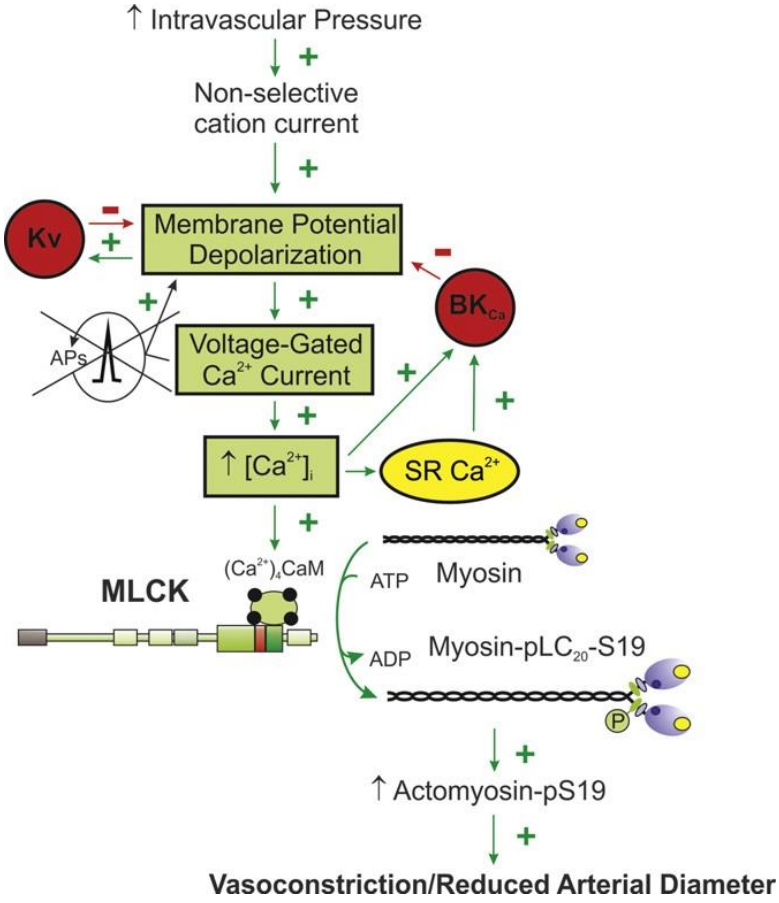

Figure 1.7: Pressure-dependent activation of MLCK in the myogenic response

Diagrammatic representation of the historical model of the mechanisms contributing to the myogenic response. Increased intraluminal pressure evokes depolarization by activating non-selective cation current. Membrane depolarization results in voltage-dependent Ca^{2+} current, a rise in cytosolic free Ca^{2+} concentration ($[Ca^{2+}]_i$) and vasoconstriction due to Ca^{2+}-calmodulin ($(Ca^{2+})_4$-CaM)-mediated activation of MLCK and phosphorylation of LC_{20} at S19. Two negative-feedback mechanisms involving voltage-gated K^+ channels (K_V), activated by membrane depolarization, and Ca^{2+}-activated K^+ channels (BK_{Ca}), activated by a rise in $[Ca^{2+}]_i$, prevent generation of action potentials (AP) and, therefore, permit precise control of arterial diameter (Figure is modified from Cole & Welsh 2011).

very little depolarization (~5-10 mV) was detected between 60 and 120 mmHg (Knot & Nelson, 1998; Davis & Hill, 1999). Inhibition of MLCP activity and Ca^{2+} sensitization was suggested to be a possible additional mechanism contributing to the development of myogenic constriction in resistance arteries (Johnson et al., 2009). This mechanism was originally implicated as a cause of increased force generation in response to agonists, such as angiotensin II, thromboxane A_2 and serotonin, acting on G protein-coupled receptors (i.e. $G_{12/13}$) (Cavarape et al., 2003; Somlyo & Somlyo, 2003; Wilson et al., 2005). An obligatory contribution of Ca^{2+} sensitization to the myogenic response was suggested using a highly sensitive three-step western blotting procedure to quantify phosphoprotein content in segments of pressurized rat middle cerebral arteries in the Cole laboratory (Johnson et al., 2009; Moreno-Domínguez et al., 2013).

1.5.4.1 MLCP inhibition and agonist-induced contraction

Smooth muscle MLCP is a trimeric serine/threonine phosphatase composed of ~38 kDa catalytic subunit PP1c-δ, 110-130 kDa regulatory myosin-targeting subunit (MYPT1), and ~20 kDa M20 subunit of unknown function (Figure 1.6) (Somlyo & Somlyo, 2003; Cole & Welsh, 2011). As a regulatory subunit, MYPT1 enhances the specific activity of PP1c-δ in dephosphorylating phospho-LC_{20}. The regulation of MLCP activity occurs through phosphorylation of multiple sites on MYPT1 that are known to exert a strong inhibitory effect on MLCP activity. In the setting of agonist-induced contraction, activation of $G_{12/13}$-coupled receptors induces Ca^{2+} sensitization by activating the small GTPase, RhoA, which is an upstream activator of ROK that mediates MYPT1 phosphorylation and inhibition of MLCP activity (Somlyo & Somlyo, 2003; Swärd et al., 2003; Cole & Welsh, 2011).

Two major ROK phosphorylation sites on MYPT1, Thr-697 (T697) and Thr-855 (T855) (amino acid numbering based on rat MYPT1 sequence), have been suggested to play a role in

MLCP inhibition (Feng et al., 1999; Murányi et al., 2002). Interestingly, Chen et al. (2015) have shown that MYPT1-T697, but not T855 phosphorylation contributes to force maintenance in bladder smooth muscles. Protein kinase C (PKC) also contributes to agonist-induced Ca^{2+} sensitization via an indirect inhibition of MLCP. PKC is activated downstream of G_q-coupled receptor occupancy and phosphorylates 17 kDa PKC-potentiated protein phosphatase 1 inhibitor protein (CPI-17) at Thr-38. Phosphorylated CPI-17 is a potent inhibitor of MLCP and directly suppresses PP1c-δ activity (Eto, 2009). The ROK-dependent phosphorylation of MYPT1 and PKC-induced CPI-17 phosphorylation shifts the MLCK:MLCP activity ratio in favor of the kinase, leading to an elevation in LC_{20} phosphorylation and contraction without a further change in $[Ca^{2+}]_i$, hence the name, Ca^{2+} sensitization.

1.5.4.2 ROK-dependent inhibition of MLCP and the myogenic response

The ability of ROK inhibitor and over-expressed, dominant-negative RhoA or ROK to block myogenic constriction in the absence of a significant change in $[Ca^{2+}]_i$ was interpreted to indicate a role in the myogenic response for inhibition of MLCP by ROK-mediated phosphorylation (Gokina et al., 2005; Jarajapu & Knot, 2005; Schubert et al., 2008). Furthermore, activation of ROK-mediated Ca^{2+} sensitization was directly confirmed by the recent development of a highly-sensitive biochemical approach that permits quantification of phosphoproteins (e.g. phospho-LC_{20} and phospho-MYPT1) in single segments of pressurized arteries (Johnson et al., 2009; El-Yazbi et al., 2010). The updated view of the myogenic response, based on data obtained for cerebral and skeletal muscle resistance arteries, postulates that within the pressure range over which the myogenic response functions (~ 60 to 120 mmHg), changes in wall tension are detected by a mechanosensor(s), possibly integrins, resulting in the translocation and activation of RhoA at the plasma membrane. RhoA subsequently activates

ROK that in turn phosphorylates MYPT1 at T855 (rat isoform). Phosphorylation of MYPT1 at T855 is associated with inhibition of MLCP activity and an alteration of the MLCK-MLCP balance favoring LC_{20} phosphorylation (reviewed in Somlyo & Somlyo, 2003; Cole & Welsh, 2011). This view is supported by the finding that ROK inhibitor, H1152, abolished myogenic constriction and suppressed the increased phosphorylation of MYPT1-T855 and LC_{20} associated with pressure elevation (Johnson et al., 2009; Moreno-Domínguez et al., 2013). In rat middle cerebral arteries, increased phosphorylation at T697 was not detected following pressure elevation within the physiological pressure range and was only detected at supra-physiologic pressure (to 140 mmHg) or following treatment with serotonin at 80 mmHg (El-Yazbi et al., 2010). No change in CPI-17 phosphorylation was detected in rat cerebral or skeletal muscle arterioles with pressure elevation (Johnson et al., 2009; Moreno-Domínguez et al., 2013). These observations suggest that phospho-CPI-17-mediated inhibition of MLCP does not play a role in the myogenic response. MYPT1 exhibited basal phosphorylation (at 10 mmHg intraluminal pressure) at both T697 and T855, suggesting that MLCP is partially inhibited under these conditions, possibly contributing to the basal level of constriction in resistance arteries for appropriate blood flow and blood pressure control at low pressure (Figure 1.8).

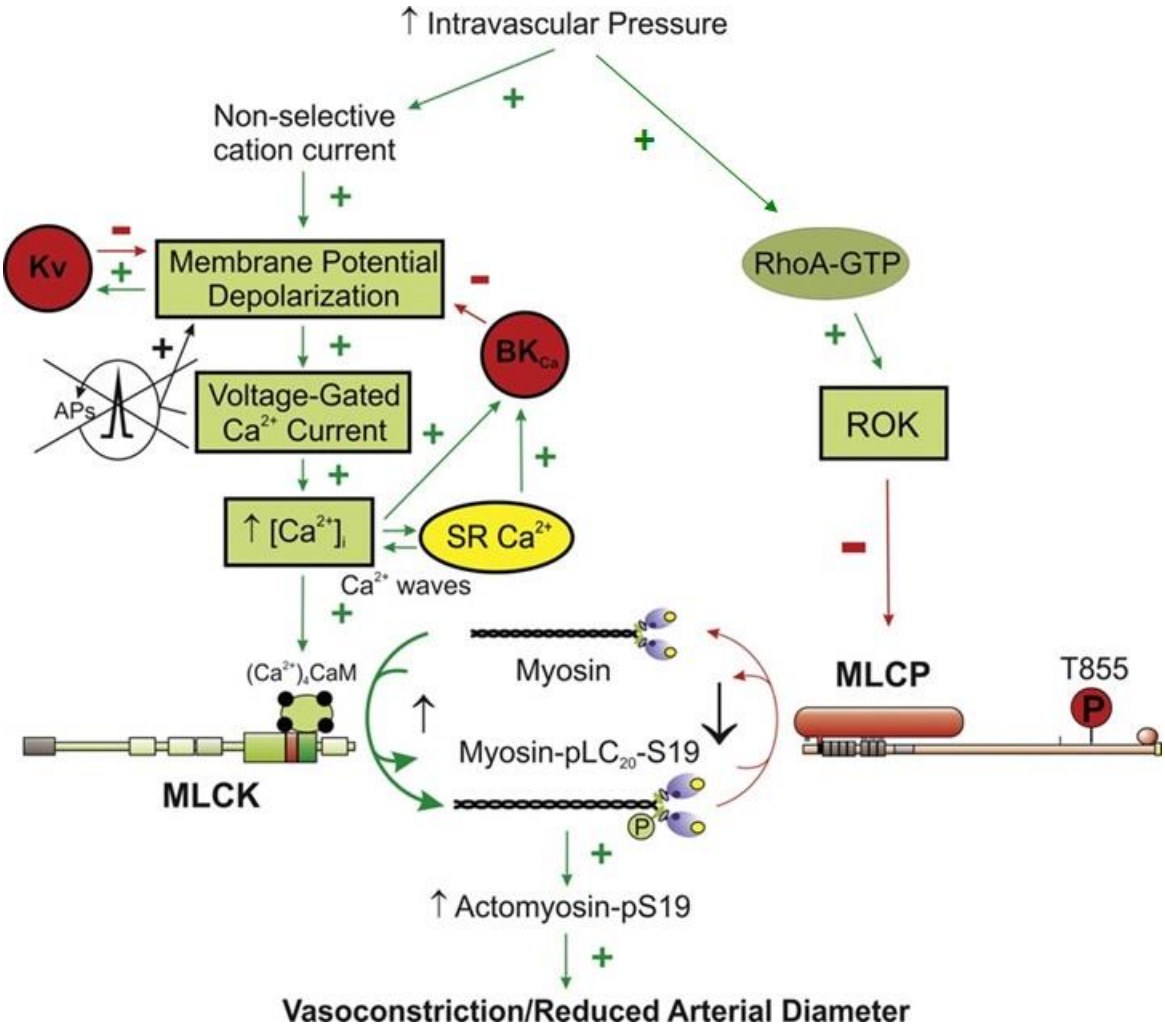

Figure 1.8: Pressure-dependent inhibition of MLCP and the myogenic response

Diagrammatic representation of the updated model for the myogenic response involving: (i) the historical Ca^{2+}-activated/MLCK mechanism (presented in Fig. 1.7) and (ii) a parallel MLCP inhibition/Ca^{2+} sensitization mechanism. Pressure elevation evokes Ca^{2+} sensitization via RhoA activation (RhoA-GTP), ROK activation, and phosphorylation of myosin targeting subunit (MYPT1) of MLCP at T855 by ROK. Phosphorylation of MTPT1 leads to suppression of MLCP activity, enhanced LC_{20} phosphorylation and force generation in the myogenic response within the physiological pressure range (Figure is modified from Cole & Welsh 2011).

1.5.5 Actin cytoskeleton reorganization and the myogenic response

1.5.5.1 Actin cytoskeleton reorganization as a mechanism essential for VSMC contraction

Accumulating evidence suggests that dynamic reorganization of the actin cytoskeleton can influence force development during smooth muscle contraction. Smooth muscle actin includes "contractile actin" that interacts with myosin and contributes to cross-bridge cycling, and "cytoskeletal actin" that forms a subsarcolemmal network between contractile filaments, the cell membrane and extracellular matrix to enhance force transmission. Cytoskeletal actin exists as either filamentous (F-actin) or globular actin (G-actin). The model of dynamic cytoskeleton reorganization postulates that the cytoskeletal actin pool polymerizes and depolymerizes during smooth muscle contraction and relaxation, respectively. Contractile stimuli trigger *de novo* actin polymerization from the available G-actin pool under the cell membrane and around adhesion plaques. Actin filaments of the contractile apparatus are anchored to the cytoplasmic tails of integrins by a complex of adhesion proteins, and to each other at cytosolic dense bodies (Cipolla et al., 2002; Gerthoffer, 2005; Gunst & Zhang, 2008). Thus, the cortical actin cytoskeleton is an essential element that connects and reinforces integrin adhesion complexes (Figure 1.9).

Moreover, classic cadherins, that are postulated to be another mechanosensor candidate in the myogenic response, localize in specialized sites of cell-to-cell adhesion that are termed adherens junctions. At the adherens junctions, cadherins can establish linkages with the actin cytoskeleton and therefore may also contribute to the mechanosensory pathway(s) that "sense" force and coordinate signaling between VSMC for effective vessel constriction (Juliano, 2002; Jackson et al., 2010).

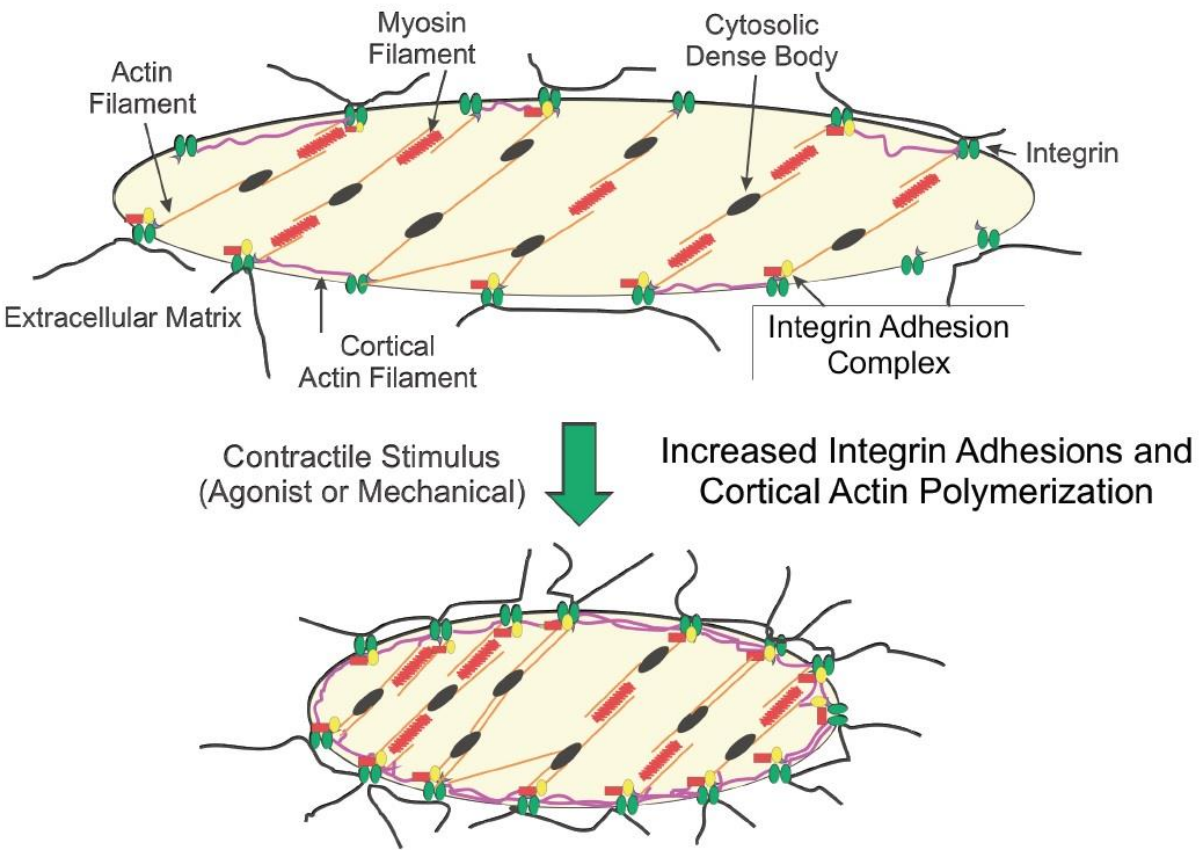

Figure 1.9: The role of cortical actin cytoskeleton dynamics in VSMC contraction

Diagrammatic representation of the changes in the cortical actin cytoskeleton and integrin attachments to the extracellular matrix as a function of contractile stimulation (agonist or mechanical) involving increased attachment of integrins to the extracellular matrix, integrin adhesion expansion and increased polymerization of cortical actin (modified from Gunst & Zhang, 2008).

This subsarcolemmal meshwork is important for transmission of force generated by the contractile apparatus to the cell membrane, extracellular matrix and neighboring VSMCs. Therefore, dynamic processes of actin cytoskeletal reorganization enhance force transmission by stiffening and strengthening these interactions. The importance of actin polymerization for smooth muscle contraction is supported by the effects of actin polymerization inhibitors on the contractile responses of a variety of smooth muscle tissues. Contractility was markedly attenuated in airway, vascular, and uterine smooth muscles upon treatment with latrunculin B (which sequesters G-actin monomers) or cytochalasin D (which caps the fast-growing ends of actin filaments) (Youn et al., 1998; Cipolla et al., 2002; Shaw et al., 2003; Moreno-Domínguez et al., 2014).

The role of actin polymerization in the VSMC contraction was first suggested upon treatment of rat aorta with cytochalasin D that substantially inhibited the contraction induced by norepinephrine or a high concentration of external K^+, in the absence of any change in $[Ca^{2+}]_i$, phospho-LC_{20} or myosin ATPase activity, which suggested that cytoskeleton reorganization does not affect the MLCK:MLCP balance (Saito et al., 1996). Later on, the evidence for actin polymerization in smooth muscle contraction was further supported by the direct measurement of changes in G-actin and/or F-actin levels after application of contractile stimuli. Several methods have been used including DNase I inhibition assay, fluorescence imaging, electron microscopy and differential centrifugation (Mehta & Gunst, 1999; Bárány et al., 2001; Cipolla et al., 2002; Flavahan et al., 2005; Zhang et al., 2007). Quantification of F-actin and G-actin levels at rest and after stimulation with acetylcholine (canine trachea) or norepinephrine (carotid artery) indicated that a small pool of G-actin (~10 to 12%) undergoes polymerization, with F-actin increasing from ~70 to 80% at rest up to ~80 to 92% after stimulation (Tang & Tan, 2003; Zhang et al.,

2007; Kim et al., 2008). All these observations are consistent with the presence of two actin pools in the smooth muscle, one being used in the contractile apparatus to generate force, and the other that is dynamic and undergoes reversible polymerization and depolymerization. It is worth noting that the contractile actin is associated with tropomyosin and stabilized in the filamentous form. This interaction with tropomyosin blocks the access of the actin severing proteins such as cofilin, thus it abolishes the dynamics of contractile actin in the process of contraction and relaxation. Cortical actin is not associated with tropomyosin that permits the dynamics of the cortical actin pool as it is accessible to actin polymerization modulators such as cofilin (Walsh & Cole, 2013).

1.5.5.2 Pressure-evoked actin cytoskeleton remodeling

Several lines of evidence have suggested that the myogenic response of rat cerebral arteries cannot be solely attributed to increased MLCK and decreased MLCP activities. These observations include: (i) treatment of vessels with cytochalasin D or latrunculin B, that inhibit actin polymerization, completely suppressed the myogenic constriction of resistance arteries (Gokina & Osol, 2002; Flavahan et al., 2005; Moreno-Domínguez et al., 2013); (ii) maximal stoichiometric phosphorylation of LC_{20} of 0.5 mol P $mole^{-1}$ is detected at pressures above 80 mmHg, yet diameter is maintained or reduced between 80 and 120 mmHg despite the increased distending force of intraluminal pressure (Moreno-Domínguez et al., 2014); (iii) depletion of RhoA in rat cerebral arteries in organ culture abolished the pressure-dependent constriction between 15 and 80 mmHg without affecting LC_{20} phosphorylation (Corteling et al., 2007); (iv) in Rho-depleted cerebral arteries, inhibition of MLCP by microcystin caused an increase in LC_{20} phosphorylation without appreciable change in contractility (Corteling et al., 2007); (v) inhibition of PKC abolished the myogenic response of rat cerebral artery without a change in the

phosphorylation of LC_{20}, CPI-17 or MYPT1 (Johnson et al., 2009); (vi) under three experimental conditions, including an increase in intraluminal pressure from 80 to 120 mmHg, the addition of serotonin at 80 mmHg, and pressurization to 80 mmHg in the presence of serotonin, pressure- or agonist-induced constriction was not associated with any further detectable change in LC_{20} phosphorylation (Moreno-Domínguez et al., 2014). These observations suggested that the myogenic response in rat cerebral arteries might involve a third mechanism that is independent of changes in the level of LC_{20} phosphorylation. Thus, dynamic actin cytoskeleton reorganization was investigated as the most plausible third mechanism contributing to the myogenic response in cerebral arteries. A pressure-dependent decrease in G-actin content was detected upon pressure elevation from 10 to 80 or 120 mmHg in cerebral arteries (Moreno-Domínguez et al., 2013). Experiments using latrunculin B did not show any effect on the basal diameter (at 10 mmHg) or the extent of serotonin-induced constriction at 10 mmHg. However, latrunculin B induced vasodilation up to the passive diameter observed at zero extracellular Ca^{2+} in vessels pressurized to 80 mmHg without a detectable change in the phosphorylation of LC_{20}. Latrunculin B also dilated serotonin-preconstricted vessels at 80 mmHg, and vessels constricted upon pressure elevation from 10 to 80 mmHg after serotonin pretreatment (Moreno-Domínguez et al., 2014). The lack of an effect of latrunculins at low intraluminal pressure suggests that their effect on the diameter is not likely due to disruption of the contractile actin filaments (Luykenaar et al., 2009; Moreno-Domínguez et al., 2014). These findings suggest an obligatory role for dynamic actin polymerization in the pressure-dependent constriction of cerebral resistance arteries.

1.5.5.3 Cellular signaling mechanisms involved in actin cytoskeleton dynamics

The current understanding of signal transduction pathways of actin polymerization is largely directed by studies from the Gunst laboratory using airway smooth muscle activated by agonists (Gunst & Zhang, 2008). This view holds that the newly formed cortical actin is connected to membrane-associated dense plaques at the cytoplasmic domain of β-integrins through linker proteins such as talin and vinculin. Thus, β-integrins connect the extracellular matrix to the contractile machinery and support efficient force transmission. Several proteins are recruited to the adhesion plaques on stimulation, e.g. FAK, talin, paxillin, vinculin (Opazo Saez et al., 2004). These proteins among others are thought to serve as scaffolding domains that initiate actin polymerization via the actin nucleation initiating factor N-WASP (neuronal Wiskott-Aldrich syndrome protein) pathway (Zhang et al., 2007) (Figure 1.10).

1.5.5.3.1 The Neuronal Wiskott-Aldrich syndrome protein (N-WASP) pathway

Two mechanisms have been proposed as the upstream activation signals for N-WASP. The first mechanism involves FAK activation by autophosphorylation at Y397 in response to integrin activation (Tang & Gunst, 2001). FAK catalyzes the tyrosine phosphorylation of paxillin that consequently activates N-WASP via the adaptor protein CrkII and the small GTPase Cdc42 (Tang & Gunst, 2004; Tang et al., 2005). An alternate pathway for N-WASP activation involves phosphorylation of the integrin adhesion protein p130 Crk-associated substrate (CAS) by SFK. Phosphorylation of CAS increases its binding to CrkII and N-WASP. Activation of N-WASP through either pathway exposes a binding site for the actin related protein (ARP) 2/3 complex to initiate actin polymerization and branching (Tang & Gunst, 2004; Tang et al., 2005). p130 CAS also lies upstream of profilin, which binds to actin monomers and can promote actin polymerization. Binding of the profilin-actin complex to N-WASP can bring actin monomers

closer to the ARP2/3 complex nucleation site of a growing actin filament (Gutsche-Perelroizen et al., 1999).

1.5.5.3.2 The Cofilin pathway

The cofilin pathway is considered a second level of regulating actin polymerization by ROK along with its well-established role in Ca^{2+} sensitization. Cofilin is an actin depolymerizing factor that binds to and severs actin filaments providing G-actin monomers, and actin filaments with barded ends that act as nucleation sites for *de novo* formation and branching of actin filaments by the ARP2/3 complex. Cofilin is phosphorylated at S3 by LIM kinase that is activated by ROK-mediated phosphorylation. Phosphorylation of cofilin abolishes its actin binding and severing function (Moriyama et al., 1996; Bernard, 2007). Data from the Cole laboratory have showed that activation of the RhoA/ROK pathway in the myogenic response promotes actin polymerization through phosphorylation of cofilin and subsequent suppression of cofilin-mediated actin severing and depolymerization (Moreno-Domínguez et al. 2014). In another view, it would appear that activation of the ROK-mediated phosphorylation of cofilin would alleviate cofilin's ability to cap and sever actin filaments, thus preventing the formation of new actin filaments essential for force development. However, the role of cofilin phosphorylation in force development was supported by studies employing swine carotid artery that suggested that this pathway is constitutively active with cofilin phosphorylated and inactive (Tejani et al., 2011). The authors proposed that cofilin phosphorylation does not play a role in the development of the myogenic response, yet the N-WASP pathway is the major determinant of actin polymerization at that stage. Subsequently, when cofilin becomes dephosphorylated, it expresses actin-severing properties to support dynamic actin polymerization and filament branching during the force maintenance phase of the myogenic response (Walsh & Cole, 2013).

1.5.5.3.3 The Heat Shock Protein 27 (HSP27) pathway

HSP27, a chaperone protein, has been implicated in the regulation of dynamic actin polymerization. The unphosphorylated protein caps actin filaments, inhibiting actin polymerization. Phosphorylated HSP27 is translocated from the cytoskeleton to the cytosol alleviating HSP27-mediated inhibition of actin polymerization (Gerthoffer & Gunst, 2001). Studies in rat gracilis arteries pretreated with PKC inhibitor, GF109203X, showed an inhibition of myogenic tone with no change in CPI-17 phosphorylation (Moreno-Domínguez et al., 2013). However, increased intraluminal pressure decreased G-actin content in a GF109203X-sensitive manner. The pressure-evoked decline in G-actin was accompanied by a GF109203X-sensitive increase in phosphorylation of HSP27 in rat cerebral middle arteries (Moreno-Domínguez et al., 2014). These studies provided direct evidence for the role of PKC-mediated phosphorylation of HSP27 in the regulation of actin polymerization in cerebral arteries.

1.5.5.3.4 The Vasodilator-stimulated phosphoprotein (VASP) pathway

Another level of regulation for actin polymerization involves VASP. VASP is a member of the Ena/VASP family of proteins that plays a role in regulation of actin dynamics and filament elongation. VASP facilitates integrin adhesion assembly and promotes actin polymerization by serving as an anti-capping protein (Bear & Gertler, 2009). Phosphorylation of VASP inhibits VASP/actin interaction and abolishes VASP-induced actin polymerization. Three major phosphorylation sites have been characterized in VASP, S153, S235, and T274. S153 is predominantly phosphorylated by protein kinase A (cAMP-dependent protein kinase) and has been implicated in VASP targeting. S235 is predominantly phosphorylated by protein kinase G (cGMP-dependent protein kinase). T274 can be phosphorylated by both kinases. Both S235 and T274 are located within the actin-binding domain and are involved in dynamic actin cytoskeleton

reorganization (Harbeck et al., 2000; Walsh & Cole, 2013). In the control of myogenic response of cerebral resistance arteries, VASP dephosphorylation was found to play a crucial role in the dynamic process of actin reorganization (X. Zhong, unpublished observations).

1.6 Consequences of a dysfunctional cerebral myogenic response

Given the crucial role that the myogenic response plays in normal physiological function, it is predictable that dysfunctional myogenic regulation of arterial diameter is associated with several vascular pathologies. A lack of blood flow autoregulation, enhanced myogenic constriction at low pressure and/or reduced force generation with increasing pressure is observed in several conditions that have an impact on neurologic function in humans, including hypertension, cerebral vasospasm, type 2 diabetes, hemorrhagic and ischemic stroke (reviewed in Cole & Welsh, 2011). Impaired dilation at low perfusion pressure compromises blood flow and increases the risk of ischemia. Conversely, reduced myogenic constriction leading to uncontrolled, elevated levels of blood flow (i.e. 'breakthrough') in malignant hypertension, hemorrhagic stroke and type 2 diabetes is associated with blood-brain barrier disruption, small vessel rupture, and edema (reviewed in Cole & Welsh, 2011). Advances in the treatment of inappropriate cerebral autoregulation require a detailed understanding of the molecular basis of the myogenic response and the defects responsible for abnormal myogenic control of blood flow in the disease state.

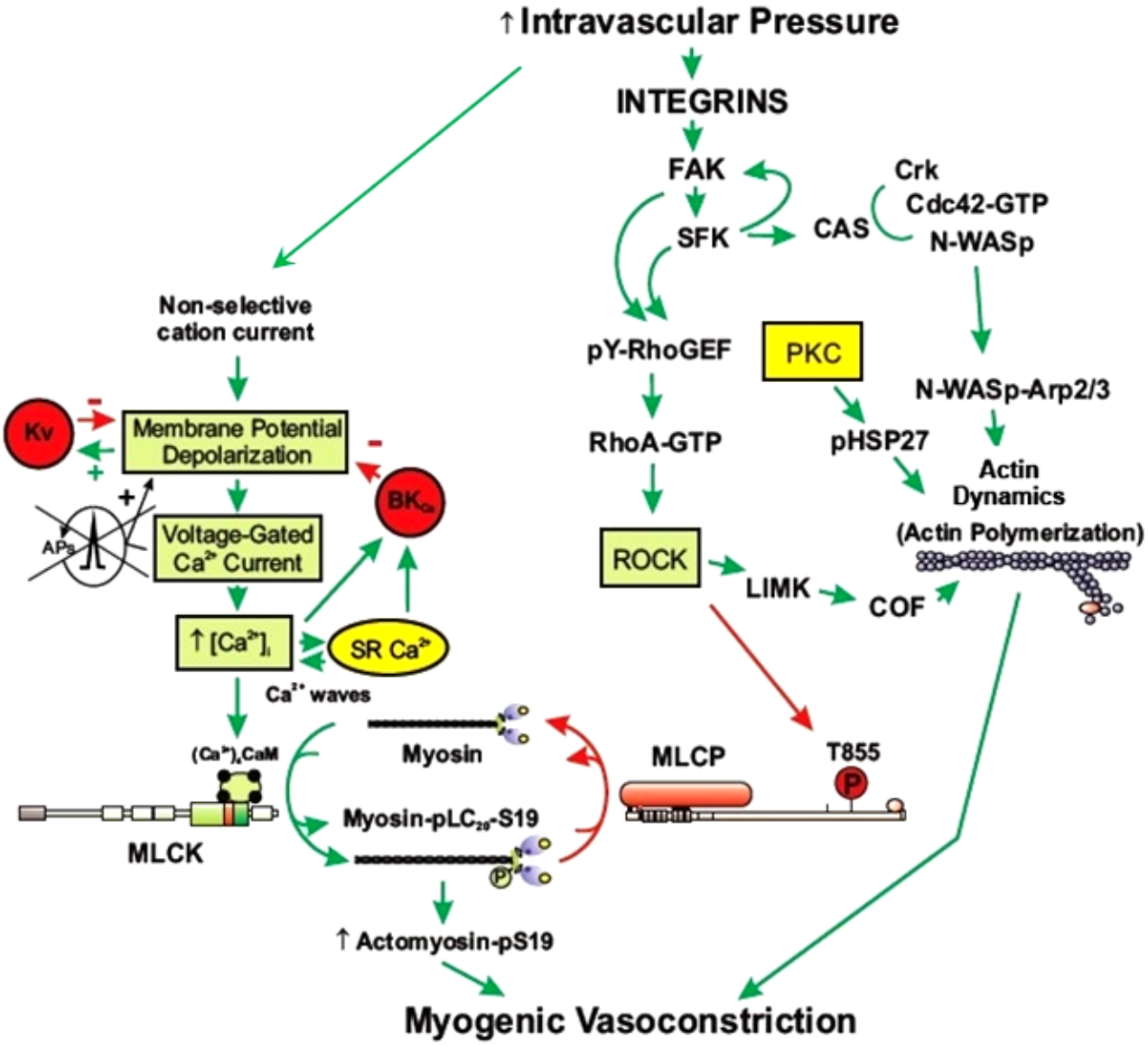
↑Intravascular Pressure
INTEGRINS
FAK
SFK
CAS
Crk
Cdc42-GTP
N-WASp
Non-selective cation current
pY-RhoGEF
PKC
N-WASp-Arp2/3
Kv
Membrane Potential Depolarization
RhoA-GTP
pHSP27
Actin Dynamics
BKCa
APs
Voltage-Gated Ca2+ Current
ROCK
LIMK
COF
(Actin Polymerization)
↑ [Ca2+]i
SR Ca2+
Ca2+ waves
(Ca2+)4CaM
Myosin
MLCP
T855
P
Myosin-pLC20-S19
MLCK
↑ Actomyosin-pS19
Myogenic Vasoconstriction

Figure 1.10: Detailed contemporary model for the molecular basis of the myogenic response

Intravascular pressure elevation stimulates integrins leading to FAK activation by autophosphorylation at Y397. FAK autophosphorylation permits SFK binding and its subsequent autophosphorylation at Y416 and activation. SFK in turn phosphorylates FAK to further enhance its catalytic activity, leading to the tyrosine phosphorylation and activation of RhoGEFs that regulate RhoA and ROK that phosphorylates MYTP1-T855 to suppress MLCP activity. Intravascular pressure also evokes depolarization, increases VGCC activity, a rise in cytosolic Ca^{2+} concentration ($[Ca^{2+}]i$) and vasoconstriction due to $(Ca^{2+})_4$-CaM-mediated activation of MLCK and phosphorylation of LC_{20}. Negative-feedback mechanisms involving K_v and BK_{Ca} potassium channel activation prevent action potentials (AP) due to regenerative depolarization permitting precise control of membrane potential and $[Ca^{2+}]i$. The resulting activation of MLCK and inhibition of MLCP lead to increased pLC_{20} content. SFKs within adhesions also phosphorylate p130 CAS (CAS) which serves as an adaptor for Crk and Cdc42 that together result in the activation of N-WASP and its association with Arp2/3 to permit actin nucleation. ROK and PKC contribute to the control of actin dynamics via suppression of cofilin (COF)-mediated severing of actin filaments by LIM kinase (LIMK)-mediated phosphorylation of cofilin, and removal of actin filament capping through phosphorylation of HSP27, respectively.

At present, no convincing explanation is available for these alterations in myogenic constriction. However, altered K^+ channel expression and/or RhoA/ROK signaling were associated with an abnormal myogenic response in hypertension as an example (Loirand et al., 2006; Moreno-Domínguez et al., 2009). *The focus of this thesis research was to understand how type 2 diabetes alters the myogenic response that may predispose diabetic patients to ischemic and/or hemorrhagic stroke*.

1.7 Diabetes Mellitus

Diabetes mellitus is a chronic metabolic disturbance characterized by fasting and/or postprandial hyperglycemia. Rather than a single disease entity, diabetes mellitus is a heterogeneous syndrome that is caused by an absolute or relative lack of insulin, resistance to the action of insulin, or both (Tsui et al., 2011).

Type 1 diabetes is due to autoimmune pancreatic beta cell destruction resulting in an absolute deficiency of insulin. In North America, type 1 diabetes accounts for 5–10% of all patients with diabetes. Type 2 diabetes manifests primarily as a condition of insulin resistance along with some degree of insulin deficiency. Type 2 diabetes makes up about 90% of all cases of diabetes and the prevalence is rising rapidly both in Canada and worldwide (Tsui et al., 2011). People with type 2 diabetes have a two-fold to four-fold increase in their risk of developing cardiovascular diseases (hypertension, myocardial ischemia, heart failure and stroke), retinopathy, kidney diseases and renal failure. The high mortality rate among diabetic patients is mostly due to cardiovascular complications (Ganne et al., 2007; Goralski & Sinal, 2007; Sarwar et al., 2010). According to current WHO projections, the number of diabetic patients will double by 2030 due, almost exclusively, to an increase in type 2 diabetes, one of the fastest growing

disorders in Canada, with 60,000 new cases annually.[1,2] Treatment of cardiovascular complications associated with type 2 diabetes is and will continue to be a significant burden on our health care system (Goralski & Sinal, 2007). Thus, understanding the molecular basis for the vascular dysfunction in type 2 diabetes may provide new therapeutic targets and interventions to improve morbidity and mortality in diabetic population.

1.7.1 Insulin and insulin receptor signaling

Insulin is a strategic hormone that is not solely crucial for metabolism, but also for the control of vascular function through an influence on vasomotion and vascular remodeling (Anfossi et al., 2009). Vascular endothelium and VSMCs express insulin receptors with intrinsic tyrosine kinase activity as are present in better recognized metabolic tissues such as liver and skeletal muscles. Insulin receptor activation triggers a highly integrated signaling network through tyrosine phosphorylation of insulin receptor substrates (IRSs). Phosphorylated IRS works as a docking protein for phosphatidylinositol 3-kinase (PI3K) and the adaptor proteins Grb2/Sos, which in turn activates two main signaling pathways: the PI3K/Akt or protein kinase B (PKB) pathway and the Ras/mitogen-activated protein kinase (MAPK) pathway, respectively (Muniyappa et al., 2007; Muniyappa & Quon, 2007). The PI3K/Akt pathway is responsible for the metabolic actions of insulin including glucose transporter (GLUT-4) translocation, glucose uptake, glycogen synthesis and lipid metabolism. Moreover, it is responsible for the anti-apoptotic actions and nitric oxide (NO) generation in the vasculature. MAPK pathway activation elicits transcription of genes involved in cell growth, cell differentiation, synthesis of proinflammatory and prothrombotic molecules, and production of mediators involved in extracellular matrix formation (reviewed in Muniyappa et al., 2007; Anfossi et al., 2009).

[1] http://www.who.int/mediacentre/factsheets/fs236/en/
[2] http://www.diabetes.ca/diabetes-and-you/what/prevalence/

1.7.2 Insulin effects on the vascular endothelium

A key physiological mechanism of insulin action on the vascular wall is the production of NO by the endothelium. Insulin activates the PI3K pathway and triggers Akt-mediated phosphorylation of endothelial nitric oxide synthase (eNOS) at S1177 that is crucial for eNOS activation and NO production. Furthermore, insulin increases eNOS mRNA and protein expression in endothelial cells and the microvasculature (Muniyappa et al., 2007; Muniyappa & Quon, 2007). NO released from the vascular endothelium diffuses to the underlying VSMC layer stimulating the synthesis of cGMP from GTP leading to vasodilation. cGMP-mediated vasodilation is mainly due to activation of PKG that, through a cascade of phosphorylation events, has been shown to inhibit mechanisms responsible for VSMC contraction. Specifically, PKG-mediated phosphorylation leads to (i) inhibition of intracellular release of Ca^{2+} from the SR; (ii) phosphorylation of MYPT1-S696/S854 thus inhibiting the ROK-mediated phosphorylation of T696/T855 resulting in activation of MLCP and dephosphorylation of LC_{20}; (iii) phosphorylation of VASP and suppression of cytoskeleton reorganization; and (iv) phosphorylation of RhoA and inhibition of the ROK pathway (reviewed by Moncada & Higgs 2006). Moreover, PKG through modulation of gene expression and protein synthesis acts as an anti-proliferative signal in VSMC and promotes the phenotypic switch toward the contractile phase (Anfossi et al., 2009). Under physiological conditions, the hemodynamic actions of insulin increase blood flow and promote glucose disposal by first increasing the number of perfused capillaries due to dilation of terminal arterioles and, second, by dilating the upstream resistance vessels that support an overall increase in blood flow within the vascular tree. On the other hand, MAPK activation by insulin increases gene expression and protein release of endothelin-1, which promotes vasoconstriction and VSMC proliferation (Lam et al., 2003). Thus, in the

endothelium, insulin-induced modulation of blood flow is dependent on the balance between PI3K- and MAPK-mediated effects on VSMC and endothelial function.

1.7.3 Insulin effects on VSMCs

Occupancy of insulin receptors with insulin in VSMCs leads to activation of both PI3K and MAPK pathways in a manner similar to that reported for the vascular endothelium (Anfossi et al., 2009). Specifically, the PI3K/Akt pathway mediates inducible NOS (iNOS) protein synthesis and activation leading to NO production/release. VSMC-derived NO influences VSMC in an autocrine fashion (Tsai & Kass, 2009). Activation of the MAPK pathway leads to the proliferation and migration of VSMCs (Doronzo et al., 2006). One additional aspect of insulin action on VSMCs that has a strong potential proatherogenic influence via MAPK is its ability to activate geranylgeranyltransferase. This enzyme promotes an essential post-translational modification of RhoA, geranylgeranylation. This modification is crucial for membrane anchoring of RhoA allowing it to become a target for activation by GTP and is mediated exclusively by the MAPK pathway (Wang et al., 2004). It is worth noting that most of the data explaining insulin signaling in VSMCs were obtained from experiments conducted in cultured cells. The assumption is that identical mechanisms are present in native, fully differentiated, contractile VSMC; however, this has not been demonstrated.

1.7.4 Altered insulin signaling in the vasculature

Insulin resistance is defined as a less than expected response of target organs to insulin. It is a common feature of obesity, abnormal glucose tolerance and type 2 diabetes. Increased release of insulin is a compensatory response of pancreatic beta cells to insulin resistance leading to hyperinsulinemia. Insulin resistance does not only involve resistance to the metabolic effects of insulin, but is also seen as a decrease in the response of the vasculature to the hormone

(Dandona et al., 2005; Muniyappa et al., 2007). Vascular insulin resistance is believed to be a major risk factor for atherosclerosis and cardiovascular disease in type 2 diabetic patients. Several mechanisms have been proposed to explain the vascular dysfunction associated with insulin resistance including: altered insulin signaling, elevation of free fatty acid levels, and the presence of low grade chronic inflammation accompanied by elevated levels of cytokines and inflammatory markers. Among these mechanisms, several studies have shown that altered insulin signaling plays a major role in the development of vascular dysfunction in insulin-resistant states (reviewed by Anfossi et al., 2009).

Altered insulin signaling in vascular tissues results in loss of the beneficial effects of insulin. As previously mentioned, insulin activates two main pathways: (i) the PI3K/Akt pathway that mediates vasodilation and anti-atherogenic actions mainly via NO release, and (ii) the MAPK pathway that mediates hypertensive and pro-atherogenic actions through synthesis and secretion of endothelin-1, RhoA activation, and enhanced VSMC migration and proliferation. The most supportive evidence explaining the molecular basis for insulin resistance postulates a selective impairment of the vasodilating and anti-atherogenic PI3K/Akt pathway of insulin signaling, whereas the MAPK signaling pathway remains unaffected. Moreover, the compensatory hyperinsulinemia associated with the insulin-resistant state may over-activate the MAPK pathway, favoring vasoconstriction and VSMC proliferation (Figure 1.11). This preferential signaling may contribute to abnormal vascular tone during insulin resistance and would represent a significant risk factor for vascular dysfunction and development of cardiovascular disease in type 2 diabetes (Wang et al., 2004; Nigro et al., 2006; Muniyappa et al., 2007; Anfossi et al., 2009).

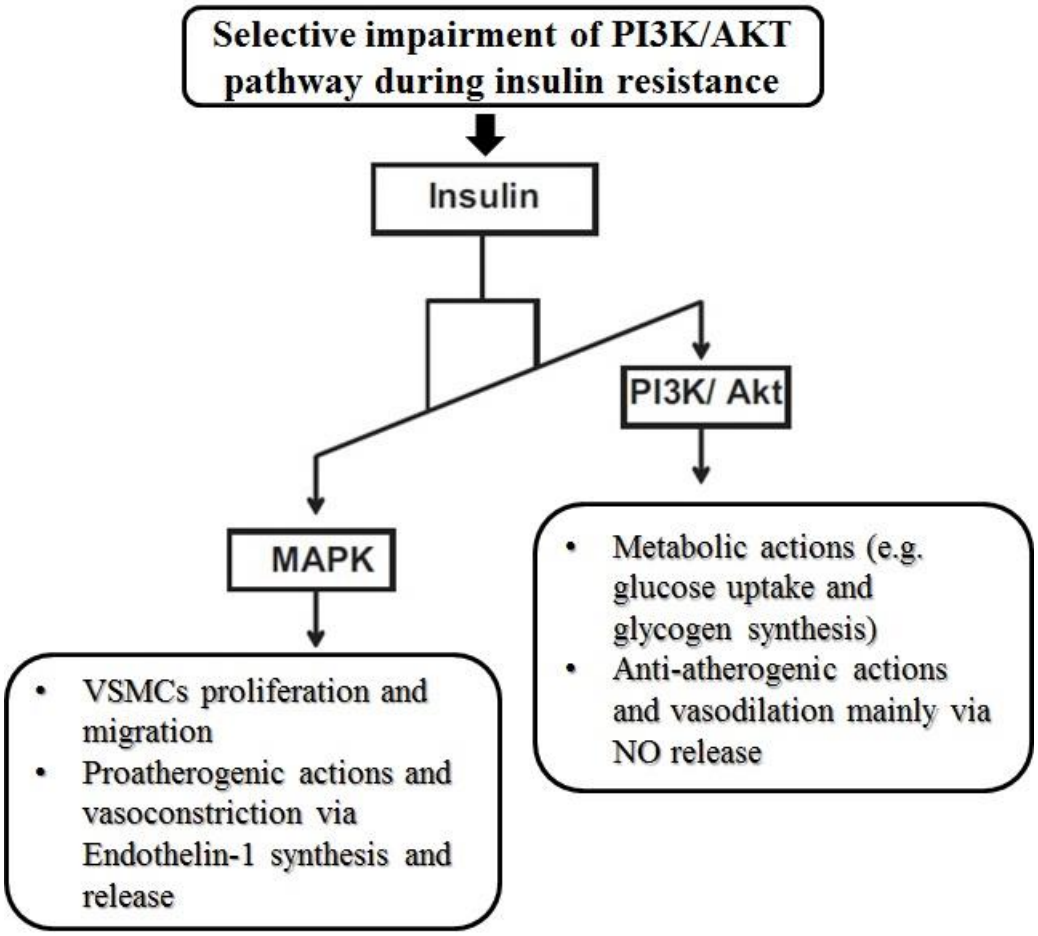

Figure 1.11: Selective impairment in insulin signaling pathways during insulin resistance

Selective impairment in the activation of the PI3K/Akt pathway of insulin signaling in the insulin-resistant state is postulated during states of insulin resistance. This impairment leads to imbalance between the metabolic, anti-atherogenic and vasodilatory actions of insulin, mainly mediated by nitric oxide (NO), and the proatherogenic, VSMC proliferative and vasoconstrictor actions of the hormone, mainly mediated by the MAPK pathway and endothelin-1 synthesis and release (Figure is modified from Anfossi et al., 2009).

1.7.5 Abnormal vascular tone in type 2 diabetes

There is considerable consensus that vasoconstriction evoked by various agonists is augmented and endothelium-dependent relaxation is blunted in resistance vessels from multiple vascular beds obtained from different animal models and patients with type 2 diabetes. For instance, endothelium-dependent relaxation in response to acetylcholine was blunted while phenylephrine-induced contraction was enhanced in femoral arteries from diabetic hypertensive rats (Lu et al., 2011). Contractions induced by serotonin, angiotensin II, phenylephrine and high $[K^+]$ were significantly greater in aortic and mesenteric artery smooth muscle strips isolated from *db/db* mice, model of obesity, diabetes, and dyslipidemia due to impaired leptin receptor activity, compared to control mice (Guo et al., 2005). Vascular dysfunction in aorta and mesenteric arteries was observed as increased smooth muscle contractility to phenylephrine and impaired endothelium-dependent relaxation to acetylcholine in *ob/ob* mice, an obese, insulin-resistant mouse model characterized by lack of leptin (Okon et al., 2003). Isolated coronary microvessels from type 2 diabetic human patients exhibited an increased level of VSMC LC_{20} phosphorylation (Clements et al., 2009). Endothelin-1-induced contraction was enhanced in mesenteric arteries of the Goto-Kakizaki (GK), a non-obese type 2 diabetic rat model (Matsumoto et al., 2010). Serotonin-induced contractions were also augmented in carotid arteries of GK rats (Matsumoto et al., 2014). Ishida et al (2012) have shown an enhanced prostaglandin E2-induced contraction in mesenteric arteries from GK rats. When tested, the exaggerated contractile response of most of the vascular beds identified above was due to an increase in ROK activity rather than its level of expression (Didion et al., 2005; Didion et al., 2007; Matsumoto et al., 2010; Matsumoto et al., 2014; Rao et al., 2013).

The mechanism (s) responsible for enhanced ROK activity in VSMC of type 2 diabetic animal models has not been clearly characterized; however, a few candidate mechanisms have been suggested including: (i) increased oxidative stress that stimulates the kinase activity (Loirand et al., 2006; Didion et al., 2007); (ii) loss of endothelium-derived NO that normally functions to suppress ROK activity (Sauzeau et al., 2000); and/or (iii) selective impairment of insulin- and insulin receptor-mediated signaling via the IRS-1/PI3K/Akt pathway that suppresses RhoA activation and ROK activity in VSMC (Sandu et al., 2000; Begum, 2003; Lee et al., 2009). The latter mechanism can provide a plausible link between insulin resistance and abnormal vascular tone detected in the type 2 diabetic vasculature. Alternatively, impaired endothelium-dependent relaxation has been attributed to overproduction of reactive oxygen species leading to inactivation of NO (Hamilton & Watts, 2013). The loss of the vasodilatory influence of NO in diabetic vasculature may contribute to the augmented constriction to various agonists (Didion et al., 2005; Muniyappa & Quon, 2007).

1.7.6 Dysfunctional myogenic response in type 2 diabetes

At the level of pressure-dependent regulation of blood flow, several studies have provided evidence of a compromised myogenic response in multiple vascular beds from type 2 diabetic animal models and type 2 diabetic patients (Abd-Elrahman et al., 2015). However the reported defects in myogenic behavior are not consistent. For instance, an enhanced myogenic response was reported in mesenteric arteries of obese type 2 diabetic *db/db* mice (Su et al., 2008; Lagaud et al., 2014). Cerebral arterioles of the BBZDR/WOR rat, a type 2 diabetic model that develops hyperinsulinemia, hyperglycemia and hyperlipidemia, show enhanced pressure-dependent autoregulation after 5 to 8 months of diabetes (Jarajapu et al., 2008). In skeletal muscle arterioles of Zucker diabetic fatty rats, an enhanced myogenic response and augmented

vasoconstrictor responses due to diminished NO signaling were detected at the prediabetic and diabetic stages (Lesniewski et al., 2008). In contrast, a loss of myogenic responsiveness was reported in cerebral and coronary arteries of 18-22 week GK rats (Kelly-Cobbs et al., 2011; Kold-Petersen et al., 2012; Abdelsaid et al., 2014) and in resistance arteries isolated from gluteal fat biopsies from diabetic patients (Schofield et al., 2002). Longitudinal studies of GK rats suggest that the dysfunction may progress from a condition of enhanced myogenic constriction in young animals (8 weeks) to a state of impaired (lost) myogenic constriction due to structural remodeling at 18 weeks of age (Kelly-Cobbs et al., 2011). Along the same lines, a compromised myogenic response in mesenteric arteries from 18-week GK rats was attributed to vascular remodeling. The remodeling response was inhibited by an endothelin-1 receptor blocker after the onset of diabetes in GK rats (6-8 weeks) and restored vascular structure (Harris et al., 2008; Sachidanandam et al., 2009).

1.8 Rationale of the study

It is evident from the previously discussed reports that both agonist- and pressure-dependent contraction of VSMCs are affected in type 2 diabetes. Although these studies provided evidence for abnormal pressure-dependent constriction in several animal models of type 2 diabetes, the defects in cellular signaling underlying the abnormal myogenic behavior have not been identified. These findings prompted us to investigate the pressure-dependent constriction of cerebral resistance arteries in a well-established rat model of type 2 diabetes, the GK rat. Specifically, we analyzed the molecular basis for the abnormal myogenic behavior of cerebral arteries from GK rats and determined whether the extent of dysfunction progresses with severity of the diabetic condition. Our focus was directed to the regulation of Ca^{2+} sensitization and the actin polymerization pathways based on our contemporary understanding of their roles in

the development of myogenic tone and evidence from Kold-Petersen et al. (2012) that the change in cytosolic [Ca^{2+}] associated with pressurization was not affected in GK cerebral arteries.

1.9 Major objectives

The major objectives of the work presented in this thesis were:

1) To investigate the abnormal myogenic response in cerebral arteries of GK rats, the progression of the myogenic dysfunction with age and disease condition, and the role of ROK in the abnormal control of cerebral arterial diameter of this type 2 diabetic rat model (Chapter 3).

2) To determine the biochemical basis for the dysfunctional myogenic behavior in GK rats by detecting changes in the phosphorylation status of the contractile proteins and defects in dynamic actin cytoskeletal reorganization with disease progression (Chapter 4).

3) To identify plausible upstream signaling defects that may be responsible for triggering changes in the phosphorylation of contractile proteins and actin polymerization and, thereby, the dysfunctional myogenic regulation of cerebral arterial diameter in GK rats.

1.10 Significance

The application of physiological, pharmacological and biochemical approaches employed in this study offer an exclusive opportunity to define the molecular basis of the dysfunctional control of the myogenic response in an animal model of type 2 diabetes. Defective myogenic regulation may explain the abnormal cerebrovascular autoregulation that is a significant risk factor for stroke, cerebral ischemia and death. Understanding how type 2 diabetes affects the molecular mechanisms of the myogenic response may permit the identification of novel therapeutic targets for reversing/minimizing the alterations present at early stages of type 2 diabetes, thus retarding the progress of diabetic cardiovascular complications and reducing the level of morbidity and mortality associated with this disease.

Chapter Two: Materials & Methods

2.1 The Goto-Kakizaki (GK) rat model of type 2 diabetes

The diabetic animal model employed in this research was the Goto-Kakizaki (GK) rat. It is one of the commonly used animal models of spontaneous type 2 diabetes. The GK model was established in Japan by selective breeding of Wistar rats (WR) that exhibited the highest normal blood glucose levels in an oral glucose tolerance test. After several generations of inbreeding, impaired insulin secretion in response to glucose intake was a constant feature of the inbred GK strain (Goto et al., 1988; Ostenson & Efendic, 2007). During the long-term inbreeding of GK rats (>20 years) the animals have maintained stable levels of glucose intolerance (Portha, 2005).

Until the end of the 1980s, GK rats were bred only in Sendai, Japan (Goto et al., 1988). Colonies were then initiated with breeding pairs from Japan in Paris, France; Stockholm, Sweden; Cardiff, UK; Coimbra, Portugal; London, UK; Aarhus, Denmark; and Seattle, USA (Portha et al., 2009). Despite the fact that GK rats have been bred in various colonies over the past 25 years with a maintained and stable degree of glucose intolerance, other characteristics such as β-cell number, insulin content and islet metabolism and secretion have been found to differ between some of the different colonies. This suggests that different local breeding environments and/or newly introduced genetic changes may contribute to the contrasting phenotypic properties detected in various colonies (Portha et al., 2012). These contrasting properties might in part account for discrepancies between some of the characteristics reported in the literature and described in this thesis.

As mentioned earlier, GK rats originate from WR, thus WRs are used as the control animals. The body weight of adult GK rats is ~10-30% lower than age-matched control WR

(Ostenson & Efendic, 2007; Portha et al., 2009; Portha et al., 2012). Unlike most commercially available genetic models of type 2 diabetes, diabetes in GK rats is polygenic in origin, which makes them a good surrogate for the human disease. Although the majority of type 2 diabetic patients in Western countries are overweight or obese, in Asia 60% are non-obese, "lean" diabetics (Burnetti, 2007). Moreover, this model permits the study of diabetes-related characteristics without the confounding influence of hyperlipidemia or obesity (Nie et al., 2011).

Several reports have described β-cell dysfunction and insulin resistance as the two major factors in the pathogenesis of type 2 diabetes in GK rats. Reduction in β-cell mass occurs during fetal development of GK rats followed by mild hyperglycemia that appears after weaning at the age of 3-4 weeks that impairs the ability of β-cells to secrete insulin in response to increased glucose concentration later in life (Portha, 2005). Substantial β-cell failure was evident at 14-16 weeks of age and was coincident with a sharp rise in the blood glucose level as a result of a failure in insulin secreting capacity of pancreatic beta cells (O'Rourke et al., 1997; Cao et al., 2011; Gao et al., 2011). The loss in β-cell mass and function is attributed to decreased β-cell neogenesis as a result of gestational metabolic impairment and an acquired loss of β-cell differentiation in response to chronic exposure to high blood glucose levels (Portha, 2005; Ostenson & Efendic, 2007).

Insulin resistance in GK rats has been reported in several studies although there is no general consensus on the exact age of onset (Liu et al., 2011; Nie et al., 2011; Noll et al., 2011; Akash et al., 2013). Standaert et al. (2004) detected a systematic insulin resistance in GK rats at 8 weeks, which was evident from defects in several signalling components related to insulin action, such as IRS-1. Ueta et al. (2005) have also detected systemic insulin resistance at 4 to 5 weeks of age in GK rats. The same conclusion was supported by experiments described by Cao

et al. (2011). Hyperinsulinemia was observed between 8-12 weeks of age in GK rats as feedback compensation to insulin resistance which also back up the evidence suggesting the development of insulin resistance as early as 4 to 5 weeks (O'Rourke et al., 1997; Gao et al., 2011).

Accordingly, GK rats employed in the experiments reported in this thesis were divided into two age groups: 8-10 weeks and 18-20 weeks. The 8-10 week age group represents the insulin resistant, prediabetic stage of type 2 diabetes associated with normo- or mild hyperglycemia and normoinsulinemia. On the other hand, the 18-20 weeks age group represents an overt diabetic condition associated with severe hyperglycemia and hyperinsulinemia.

2.2. Ethical approval

All animal experiments were conducted according to a protocol reviewed by the Animal Care Committee of the Cumming School of Medicine, University of Calgary and conforming to the standards of the Canadian Council on Animal Care. A total of ~100 rats were used in the completion of this study. Male WR and GK rats (7 weeks, 170-200 g; Charles River, Montréal, Québec, Canada) were divided in two groups. One group was employed in the study at 8-10 weeks of age and the other group was kept in the animal facility of the University of Calgary on a normal diet and employed in the study at 18-20 weeks of age.

2.3 Intact cerebral arterial pressure myography

Rats were killed by halothane inhalation followed by exsanguination. The brain was removed and transferred to ice-cold Krebs' solution of the following composition (in mmol l^{-1}): NaCl 120, $NaHCO_3$ 25, KCl 4.8, NaH_2PO_4 1.2, $MgSO_4$ 1.2, glucose 11, $CaCl_2$ 2.5 (pH 7.4 when aerated with 95% air–5% CO_2). Rat middle and posterior cerebral arteries from both hemispheres were removed, dissected free of the surrounding connective tissue, cut into segments of 2-3 mm

in length and employed in pressure myography, as previously described (Johnson et al., 2009; El-Yazbi et al., 2010; Moreno-Domínguez et al., 2014).

Arterial segments were cannulated and mounted in a myograph chamber connected to a pressure controller (Living Systems, Burlington, VT, USA) and external arterial diameter measured by edge detection (IonOptix, Milton, MA, USA). Endothelial cells were removed from all arteries by briefly passing a stream of air through the vessel lumen and confirmed by the loss of vasodilatation to 10 μmol l^{-1} bradykinin (Figure 2.1).

Arteries were allowed to warm to 37 $^{\circ}$C for 20 min in Krebs' solution, then pressurized to 60 mmHg and allowed to develop spontaneous tone over 30-45 min. All arteries were then subjected to two five minute pressure steps from 20 to 80 mmHg to ensure the development of a stable level of pressure-dependent myogenic constriction. Preparations that exhibited leaks (indicated by a spontaneous, transient drop in intraluminal pressure) or a lack of stable myogenic constriction during these test steps were discarded. When a stable myogenic response was detected, pressure was reduced to 10 mmHg for ~10 min before application of an appropriate pressure protocol.

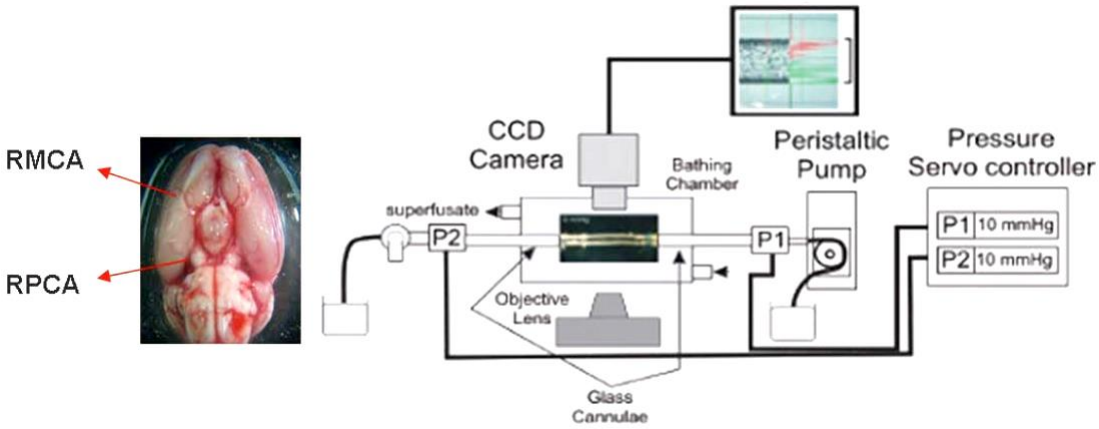

Figure 2.1: Schematic representation of arterial pressure myography.

A segment of rat middle cerebral artery (RMCA) or posterior cerebral artery (RPCA) was mounted between two glass cannulae within a bathing chamber filled with Krebs' solution at 37 °C. Intraluminal pressure was detected by proximal (P1) and distal (P2) pressure transducers and controlled by an adjustable pressure servo controller connected to a peristaltic pump. The pressurized vessel was visualized via an inverted microscope and a CCD camera coupled to a computer. Image capture and outer arterial diameter recordings were achieved by IonOptix software. (Figure is modified from Cole & Welsh, 2011)

2.3.1 Pressure protocol 1

To evaluate the cerebral myogenic response in GK rats compared to WR controls, and determine the effect of ROK on myogenic tone, vessels were subjected to a series of pressure steps from 10 to 140 mmHg in 20 mmHg increments. The first set of pressure steps was applied in normal Krebs' solution (control conditions). Pressure was then reduced to 10 mmHg, raised to 80 mmHg and H1152 (0.5 μmol l^{-1}; Sasaki et al., 2002; Johnson et al., 2009; Moreno-Domínguez et al., 2013) was added to the superfusate until the vessels developed a stable arterial diameter, then dropped back to 10 mmHg before a second series of pressure steps. Pressure was then reduced to 10 mmHg again and the superfusate replaced with zero Ca^{2+}-containing Krebs' saline solution (i.e. no added Ca^{2+} and 2 mmol l^{-1} EGTA) before a third series of pressure steps to determine the passive diameter of the artery at each pressure (Figure 2.2).

2.3.2 Pressure protocol 2

Analysis of the phosphorylation of MYPT1 (T855, T697), FAK-Y397 and LC_{20} was accomplished using vessels flash-frozen after a pressure protocol involving two five min steps to 80 mmHg and 10 min at 10 mmHg before a 10 min step to a test pressure of 10, 60 or 120 mmHg (Figure 2.2). For some measurements of MYPT1 and LC_{20} phosphorylation, vessels were treated with H1152 (0.5 μmol l^{-1}) after a stable arterial diameter was achieved at the test pressure as previously described (Johnson et al., 2009). The same protocol was used for G-actin determination but pressurized vessels were transferred to F-actin stabilization buffer instead of flash-freezing (Moreno-Domínguez et al., 2014).

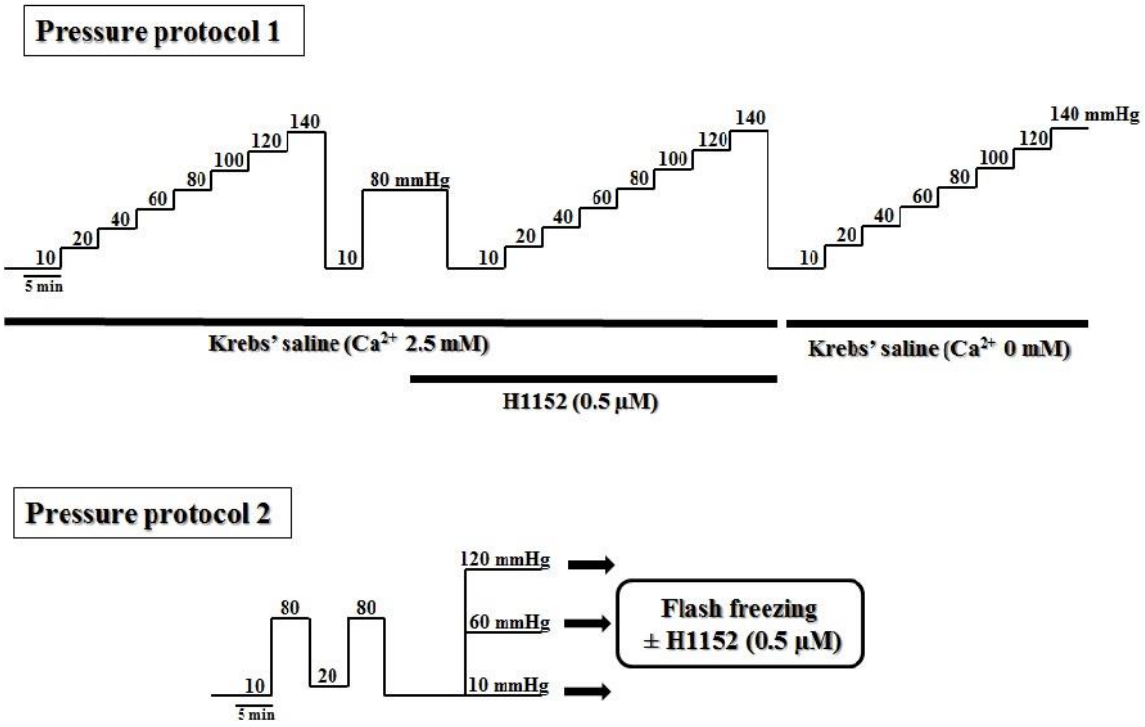

Figure 2.2: Experimental protocols for pressure myography

Pressure protocol (1) was employed to detect changes in the pressure-diameter relationship of rat cerebral arteries in the presence and absence of H1152 (0.5 µM). At the end of each experiment arterial passive diameter was detected in the absence of Ca^{2+} in the bathing solution.

Pressure protocol (2) was employed to flash-freeze rat cerebral arteries at 3 different pressures of 10, 60 and 120 mmHg for the biochemical determination of phosphoproteins and G-actin content in the presence and absence of H1152 (0.5 µM) by western blotting.

2.4 RT-PCR and real-time qPCR

RT-PCR and real-time quantitative PCR (qPCR) were carried out as previously described (Thorneloe et al., 2001; Plane et al., 2005). Total RNA was extracted from rat brain and endothelium-denuded, intact rat middle cerebral arteries using a RNeasy Mini kit with DNase treatment (Qiagen, Mississauga, Canada) and first strand cDNA synthesized using the Sensiscript RT kit (Qiagen) with oligo d(T) primer. Primer pairs to detect RhoA, MYPT1 and ROK2 were designed to permit quantification of transcript abundance in mRNA samples of rat cerebral arteries by real-time qPCR. Rat brain mRNA was used as a positive control to confirm the viability of all primer pairs employed. The sequences of subunit-specific primers (5'–3') that were designed in-house were:

RhoA (108 bp):

Forward CAGCAAGGACCAGTTCCCAGA

Reverse AGCTGTGTCCATAAAGCCAACTC

MYPT1 (103 bp):

Forward AGGAAGCAATGGAAGAGCTA

Reverse CCTCGCGTCTCTAAGCATTA

ROK2 (85 bp):

Forward CTAACAGTCCGTGGGTGGTTCA

Reverse TCCACCTGGCAT GTACTCCATC

β-actin (98 bp):

Forward TATGAGGGTTACGCGCTCCC

Reverse ACGCTCGGTCAGGATCTTCA.

All other primers were purchased from Qiagen (Mississauga). Each primer set used: (i) had an efficiency of >90% that did not differ by >5% at an annealing temperature of ~58 °C, (ii) produced a single peak with no evidence of additional amplicons or dimer formation during melt curve analysis, and (iii) yielded amplicons of an expected size. QPCR was performed with SYBR-Green and a reaction with a hot start at 95 °C for 15 min, followed by 40 cycles of 94 °C for 15 seconds, 58 °C for 30 seconds and 72 °C for 30 seconds. Negative control wells were included by adding water as a blank control. Threshold cycle was determined using a Bio-Rad iCycler and vendor-supplied software, and transcript abundance was calculated by the $2^{-\Delta\Delta Ct}$ method using *β*-actin as the reference for normalization (Livak & Schmittgen, 2001).

2.5 Vessel flash-freezing and protein extraction

At the end of protocol 2 in each pressure myograph experiment, vessels were maintained at a constant intraluminal pressure and immersed in a wet ice-cold mixture of 10% trichloroacetic acid (TCA) and dithiothreitol (DTT; 10 mmol l^{-1}) in acetone. Vessel segments were then carefully removed from the cannula and left in ice cold TCA/DTT/acetone for 15 min. Segments were then washed in wet ice-cold acetone containing DTT for 15 min, lyophilized overnight (freeze dry system, LABCONCO) and stored at −80 °C prior to protein extraction. The cannulated ends were dissected from each lyophilized vessel segment and discarded (to avoid including tissue that was not subjected to the test pressure) before protein extraction.

Proteins were extracted from vessels by adding ~30-70 μl of sample buffer (4% SDS, 100 mmol l^{-1} DTT, 10% glycerol, 0.01% bromophenol blue, 60 mmol l^{-1} Tris-HCl, pH 6.8) according to vessel size and number of vessels pooled. Each sample contained one to two pooled rat cerebral arteries for a single *n* value. Samples were heated at 95 °C for 10 min and rotated overnight at 4 °C before gel electrophoresis.

2.6 Western blotting

2.6.1 Measurement of LC_{20} phosphorylation

Measurement of LC_{20} phosphorylation was performed as previously described (Takeya et al., 2008; Johnson et al., 2009). Unphosphorylated and monophosphorylated LC_{20} were separated by Phos-tag™ SDS-PAGE with Mn^{2+}-Phos-tag™ incorporated in the gel mixture. The Phos-tag™ ligand in the presence of Mn^{2+} interacts with phosphoryl groups of phosphorylated proteins, which retards the movement of phosphoproteins through the gel leading to separation of phosphorylated and unphosphorylated isoforms.

The stacking gel (4.5 %) was made of 4.5% acrylamide, 0.12% *N,N'* methylenebisacrylamide, 0.1% SDS, 125 mM Tris-HCl pH 6.8, 0.1% ammonium persulphate and 0.17% TEMED. The resolving gel (10%) was composed of 10% acrylamide, 0.32% *N,N'* methylenebisacrylamide, 0.1% SDS, 375 mM Tris-HCl pH 8.8, 0.05% ammonium persulphate, 0.07% TEMED, 50 μM Phos-tag™ acrylamide, and 100 μM $MnCl_2$. Minigels of 1.5 mm thickness were employed for electrophoresis at 30 mV for ~ 1.5 h in a Mini Protean cell (Bio-Rad) with the running buffer containing: 0.1% SDS, 25 mM Tris-HCl and 192 mM glycine. After electrophoresis, gels were washed in transfer buffer (25 mM Tris-HCl, 192 mM glycine,

and 20% methanol) containing 2 mM EDTA for 15 min to chelate Mn^{2+}. Gels were then equilibrated in transfer buffer without EDTA for 10 min at 4 ˚C.

Proteins were then transferred to PVDF membrane (0.2 μm pore size, BioRad) at 100 mV for 80 min at 4 ˚C. Membranes were washed with PBS for 5 min after transfer, and proteins were cross-linked and fixed on the membrane by soaking the membrane in PBS containing 0.25% glutaraldehyde at room temperature for 45 min. Membranes were then washed (2×5min) in Tris-buffered saline solution (TBS; 137 mM NaCl; 3 mM KCl; 20 mM; Tris-HCl pH 7.5) prior to blocking. Membranes were then blocked by 1% ECL blocking solution (GE Healthcare) in 0.1% TBST (TBS plus 0.1% (v/v) Tween-20) at room temperature for 2 hours.

The detection sensitivity was enhanced by using a three-step protocol to allow the quantification of phosphoproteins using only small amounts of proteins obtained from each 2-3 mm-long pressurized cerebral artery segment. Membranes were incubated overnight with the rabbit polyclonal LC_{20} antibody (Santa Cruz; 1:1000) in 0.1% TBST at 4 ˚C to detect all forms of LC_{20} (unphosphorylated and phosphorylated forms). Next day, membranes were washed (4×5min) in 0.05% TBST, incubated with biotin-conjugated goat anti-rabbit IgG (Chemicon; 1:40,000) in 0.1% TBST for 1 hour at room temperature, washed (4×5min) in 0.05% TBST, and incubated with horseradish peroxidase (HRP)-conjugated streptavidin (1:200,000; Pierce) in 0.1% TBST for 30 min at room temperature. Membranes were then washed (4×5min) in 0.05% TBST and (1×5min) with TBS, followed by development of the signal using Supersignal West Femto reagent (Pierce) or Amersham ECL advanced reagents (GE Healthcare). The signal was detected with a chemiluminescence imaging analyzer (LAS3000mini, Fujifilm). Images were then analyzed with Multi Gauge v3.0 software (Fujifilm).

2.6.2 Measurement of MYPT1 protein and phosphorylation at T855 & T697

Electrophoresis was carried out as detailed in section 2.6.1 without adding Phos-tag™ and Mn^{2+} to the resolving gel mixture. Three different loading levels of the same samples were employed for the quantification of MYPT1 protein and phosphorylation at T855 and T697 of MYPT1. After electrophoresis, gels were cut at the 70 kDa molecular weight marker. High molecular mass proteins (upper gel) were transferred to nitrocellulose membranes (0.2 μm pore size, BioRad) at 100 mV for 2 hours at 4 °C in transfer buffer containing: 25 mM Tris-HCl, 192 mM glycine, 1% SDS, and 20% methanol. Low molecular mass proteins (lower gel) were transferred to 0.2 μm nitrocellulose membrane at 100 mV for 90 min at 4 °C in transfer buffer containing: 25 mM Tris-HCl, 192 mM glycine, and 20% methanol. Membranes were then rinsed with PBS (1×5min) and fixed in PBS containing 0.25% glutaraldehyde for 15 min. Membranes were washed with 0.05% TBST (2×5min) and then blocked with 5% non-fat dried milk in 0.1% TBST for 2 hours. A three-step protocol was used as described in section 2.6.1 for the measurement of MYPT1 or phospho-MYPT1-T855/T697 in membranes containing high molecular mass proteins by incubating with rabbit polyclonal MYPT1, T855 or T697 phospho-specific MYPT1 antibody (Millipore; 1:1000) overnight at 4 °C and continuing the protocol as detailed in section 2.6.1. A two-step approach was used for actin and GAPDH measurements using membranes containing low molecular mass proteins by incubating membranes with rabbit polyclonal, pan-actin antibody (Cytoskeleton; 1:1000) or anti-GAPDH antibody (Santa Cruz, 1:1000) at 4 °C overnight. Next day, membranes were washed with 0.05% TBST (4×5min) and incubated with HRP-conjugated anti-rabbit IgG (Rockford; 1:10,000) in 0.1% TBST containing 1% milk at room temperature for 30 min. Membranes were then washed with 0.05% TBST (4×5min) then TBS (1×5min) followed by detection as described in section 2.6.1.

2.6.3 Measurement of FAK phosphorylation at Y397

Electrophoresis was carried out as detailed in section 2.6.2. After electrophoresis, gels were transferred to nitrocellulose membrane (0.2 μm pore size, BioRad) at 100 mV for 2 hours at 4 °C in transfer buffer containing: 25 mM Tris-HCl, 192 mM glycine, and 20% methanol. Membranes were then rinsed with PBS (1×5min) and fixed in PBS containing 0.25% glutaraldehyde for 15 min. Membranes were washed (2×5min) with 0.05% TBST and then blocked with 5% bovine serum albumin in 0.1% TBST for 2 hours. After blocking membranes were cut at the 100 kDa marker and a three-step protocol was used as described in section 2.6.2 for the measurement of phospho-FAK-Y397 on membranes containing high molecular mass proteins (upper part of the membrane) by incubating with rabbit polyclonal, Y397 phospho-specific FAK antibody (Millipore; 1:1000) overnight at 4 °C. A two-step approach was used for actin content measurement on membranes containing low molecular mass proteins (lower part of the membrane), as described in section 2.6.2.

2.6.4 Measurement of ROK2 expression

Electrophoresis was carried out as detailed in section 2.6.2. After electrophoresis, gels were transferred to nitrocellulose membrane (0.2 μm pore size, BioRad) at 100 mV for 2 hours at 4 °C in transfer buffer containing: 25 mM Tris-HCl, 192 mM glycine, 1% SDS, and 20% methanol. Membranes were then rinsed with PBS and fixed in PBS containing 0.25% glutaraldehyde for 15 min. Membranes were washed with 0.05% TBST and then blocked with 5% non-fat dried milk in 0.1% TBST for 2 hours. After blocking membranes were cut at the 100 kDa marker and a three-step protocol was used as described in section 2.6.1 for the measurement of ROK2 content on membranes containing high molecular mass proteins (upper part of the

membrane) by incubating with rabbit polyclonal, ROK2 antibody (Millipore; 1:1000) overnight at 4 °C. A two-step approach was used for actin content measurement on membranes containing low molecular mass proteins (lower part of the membrane) as described in section 2.6.2.

2.6.5 G-actin determination

G-actin content was determined as previously described (Walsh et al., 2011; Moreno-Domínguez et al., 2014) for individual rat cerebral artery segments pressurized to 10, 60 or 120 mmHg. Each vessel was transferred to F-actin stabilization buffer (Cytoskeleton, Denver, CO, USA) containing: 50 mmol l^{-1} PIPES (pH 6.9), 50 mmol l^{-1} KCl, 5 mmol l^{-1} $MgCl_2$, 5 mmol l^{-1} EGTA, 5% v/v glycerol, 0.1% Nonidet P40, 0.1% Triton X-100, 0.1% Tween 20, 0.1% 2-mercaptoethanol, 0.001% anti-foam C, and then homogenized in 100 μl of stabilizing buffer at room temperature. The homogenate was centrifuged at 100,000 *g* for 1 hour at 22 °C to separate G- and F-actin; 30 μl of the high-speed supernatant containing G-actin was carefully removed and added to 30 μl of 2× sample buffer. Samples were then heated at 95 °C for 10 min and stored at −20 °C before western blotting. Electrophoresis was performed as described in section 2.6.2. Following electrophoresis, proteins were transferred to a 0.2 μm nitrocellulose membrane at 100 mV for 90 min at 4 °C, in transfer buffer containing 25 mmol l^{-1} Tris-HCl, 192 mmol l^{-1} glycine and 20% methanol. Membranes were then washed in PBS for 5 min, incubated in 0.25% glutaraldehyde in PBS for 15 min to fix proteins on the membrane and washed (2×5min) with TBST (25 mM Tris-HCl pH 7.5, 150 mM NaCl, 0.05% Tween 20). Membranes were blocked with 5% non-fat dried milk in TBS containing 0.1% Tween 20 (0.1% TBST) for 2 hours and then cut at the 35 kDa molecular mass marker. The high molecular mass proteins were incubated with rabbit polyclonal actin antibody (1:1000 dilution; Cytoskeleton) while the low molecular mass proteins were incubated with goat polyclonal SM-22α antibody (Novus Biologicals; 1:2000

dilution). Both antibody incubations were performed overnight at 4 ˚C in 1% non-fat dried milk in 0.1% TBST. A standard two-step western blotting protocol was sufficient to detect G-actin and SM-22 in individual rat cerebral arteries. Membranes were washed (4×5min) in TBST and incubated for 1 hour in 1% non-fat dried milk in 0.1% TBST containing anti-rabbit IgG–horseradish peroxidase-conjugated secondary antibody (1:10,000 dilution) or anti-goat IgG–horseradish peroxidase-conjugated secondary antibody (1:5000 dilution), respectively. After incubation with secondary antibodies, the membranes were washed (4×5min) with TBST and (1×5min) with TBS before chemiluminescence signal detection as described in section 2.6.1.**2.7 Serum glucose and insulin measurements**

Serum glucose and insulin values for the rats used in this study were kindly shared by Dr. Mishra (Braun Laboratory, University of Calgary). Blood glucose was measured by IDEXX Laboratories, an independent analytical service company. Serum insulin levels were quantified using a commercial ELISA kit (Millipore) designed for rat and mouse insulin; the analytical procedure was performed according to the manufacturer's recommendations (Mishra et al., 2014).

2.8 Chemicals

All chemicals were purchased from Sigma (Oakville, ON, Canada) unless indicated otherwise. H1152 was obtained from Calbiochem (San Diego, CA, USA). Tween 20, Coomassie Brilliant Blue-R250, TEMED, PVDF and nitrocellulose membranes were from Bio-Rad Laboratories. Rabbit polyclonal antibodies specific for MYPT1 phosphorylated at T697 (anti-MYPT1-T697), T855 (anti-MYPT1-T855), and FAK phosphorylated at Y397 (anti-FAK-Y397) were obtained from Millipore (Temecula, CA, USA). Polyclonal rabbit anti-LC_{20} and rabbit anti-GAPDH were from Santa Cruz Biotechnology (Santa Cruz, CA, USA). Polyclonal rabbit anti-ROK2 was from Cell Signalling (Danvers, MA, USA). Actin antibody was purchased from Cytoskeleton (Denver, CO, USA). SM22 antibody was from Novus (Oakville, ON, Canada). Biotin-conjugated goat anti-rabbit, secondary antibody was from Chemicon International and horseradish peroxidase-conjugated streptavidin was from Pierce Biotechnology (Rockford, CT, USA). HRP-conjugated goat anti-rabbit IgG secondary antibody was from Millipore (Billerica, MA, USA). Phos-tag™ ligand was obtained from NARD Institute Ltd (Amajasaki City, Hyogo Prefecture, Japan).

2.9 Statistical analysis

All values are presented as means ± SEM, with *n* values indicative of the number of vessels studied for each treatment. In general, vessels from one rat were employed to minimize variability between control and treatment groups. Statistical difference was determined using unpaired Student's *t* tests or repeated measures ANOVA followed by Bonferroni's *post hoc* test. *P value* <0.05 was considered statistically significant.

Chapter Three: The progressive dysfunction in the cerebral myogenic response of GK rats and the contribution of ROK in the regulation of cerebral arterial diameter

3.1. Hypothesis and objectives

We tested the hypothesis that the dysfunction in myogenic constriction of the cerebral resistance arteries from GK rats progresses with age and severity of the disease. Moreover, we investigated the contribution of ROK to the defective control of cerebral diameter in GK rats. The primary objectives of this part of the study were:

1. To detect changes in serum glucose and insulin levels in different age groups of GK rats compared to age-matched WR.

2. To evaluate the myogenic response of cerebral arteries from 8-10 and 18-20 week GK rats compared to age-matched WR.

3. To determine the role of ROK in the development of the dysfunctional control of GK cerebral diameter using the ROK inhibitor, H1152.

3.2. Results

3.2.1 Serum glucose and insulin levels in GK rats and age-matched WR

Figure 3.1 A & B show the mean ± SEM levels of serum glucose and insulin in three age groups of GK rats (8-9 week, 10-12 week and 18-20 week) and age-matched control WR that were employed in this study. Data were kindly shared by Dr. Mishra (A. Braun laboratory, University of Calgary) (Mishra et al., 2014). Glucose levels were not different between GK and age-matched WR up to the end of the 9^{th} week of age. However, blood glucose levels progressively increased after the beginning of the 10^{th} week of age to reach double the value of the age-matched WR by 18 weeks in GK rats (Figure 3.1A). It was also apparent that 18-20 week GK rats were urinating excessively compared to control WR and younger GK rats. As

described for glucose, no change in insulin level was detected prior to the end of the 9th week of age in GK rats compared to age-matched WR, but a progressive increase was apparent beginning at the 10th week such that the insulin level was 2-fold greater in 18-20 week GK rats compared to age-matched WR (Figure 3.1B). The hyperinsulinemia detected at the beginning of the 10th week in GK rats is likely due to insulin resistance encountered earlier in life (before 10 weeks) that triggers a compensatory increase in insulin release to match metabolic demands of insulin-sensitive tissues. The development of hyperinsulinemia by the age of 10 weeks after a state of insulin resistance at the age of 4-5 weeks in GK rats was previously reported (O'Rourke et al., 1997; Standaert et al., 2004; Cao et al., 2011; Gao et al., 2011).

Accordingly, the GK rats were divided into two age groups: the first group was studied at the age of 8-10 weeks representing an insulin-resistant, prediabetic stage having no detectable change in glucose or insulin levels. The second group was studied at the age of 18-20 weeks representing the diabetic stage with measurable hyperglycemia and hyperinsulinemia.

A

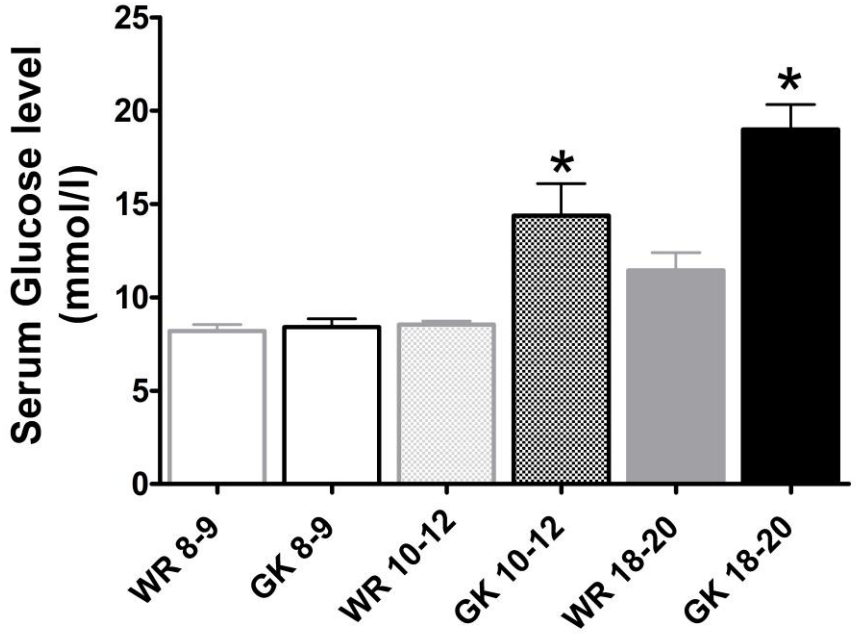
Serum Glucose level (mmol/l)
25
20
15
10
5
0
*
*
WR 8-9
GK 8-9
WR 10-12
GK 10-12
WR 18-20
GK 18-20

B

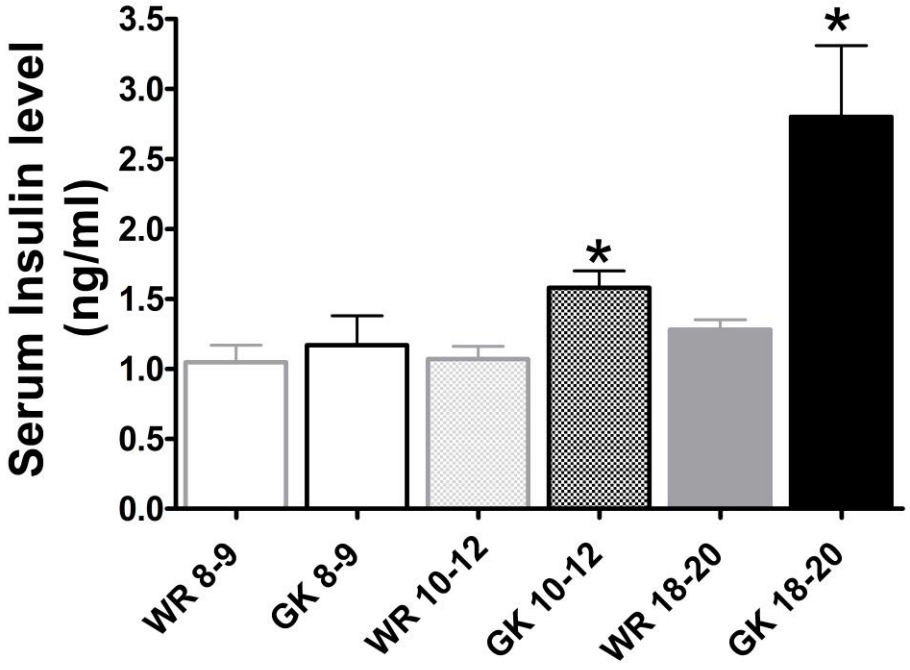
Serum Insulin level (ng/ml)
3.5
3.0
2.5
2.0
1.5
1.0
0.5
0.0
*
*
WR 8-9
GK 8-9
WR 10-12
GK 10-12
WR 18-20
GK 18-20

Figure 3.1: Serum glucose and insulin levels of GK rats and age-matched WR

Panel A: Mean serum glucose levels (± SEM) measured in 8-9 week-old GK, 10-12 week-old GK, 18-20 week-old GK and age-matched WR (n=5).

Panel B: Mean serum insulin levels (± SEM) measured in 8-9 week-old GK, 10-12 week-old GK, 18-20 week-old GK and age-matched WR (n=5). Note the progressive increase in blood glucose and serum insulin levels was detected after the beginning of the 10^{th} week in GK rats (data provided by Dr. Mishra, Braun laboratory, University of Calgary). * Significantly different ($p<0.05$) from corresponding age-matched WR values.

3.2.2 The myogenic response of cerebral arteries from 8-10 week WR

Figure 3.2 (left panels) shows the diameter-pressure relationships between 10 and 140 mmHg for posterior cerebral arteries from 8-10 week WR. In the presence of 2.5 mM Ca^{2+} in Krebs' saline, cerebral arteries of WR exhibited a passive increase in diameter with pressure elevation until 40 mmHg; above this pressure active myogenic constriction was detected and the vessels maintained a relatively constant diameter between 60 and 120 mmHg of intraluminal pressure (i.e. the myogenic reactivity phase; Osol et al. 2002). In the absence of Ca^{2+}, vessels dilated passively in response to pressure elevation implicating the importance of Ca^{2+} for development of the myogenic response. This pressure-dependent constriction between 60-120 mmHg is consistent with published reports from the Cole laboratory and others for the cerebral myogenic response in Sprague Dawley (SD) rats (Davis & Hill, 1999; Johnson et al., 2009; El-Yazbi et al., 2010; Cole & Welsh, 2011).

3.2.3 The myogenic response of cerebral arteries from 8-10 week GK

Figure 3.2 (right panels) depicts the diameter-pressure relationships between 10 and 140 mmHg of posterior cerebral arteries from 8-10 week GK rats. In 2.5 mM Ca^{2+} Krebs' saline, cerebral arteries of GK rats exhibited a smaller basal diameter between 10 and 40 mmHg, maintenance of diameter from 40 to 80 mmHg (i.e. loss of myogenic reactivity), and forced dilation at > 80 mmHg. In the absence of Ca^{2+}, the enhanced constriction at low pressure was abolished and vessels dilated passively upon pressure elevation from 20-140 mmHg.

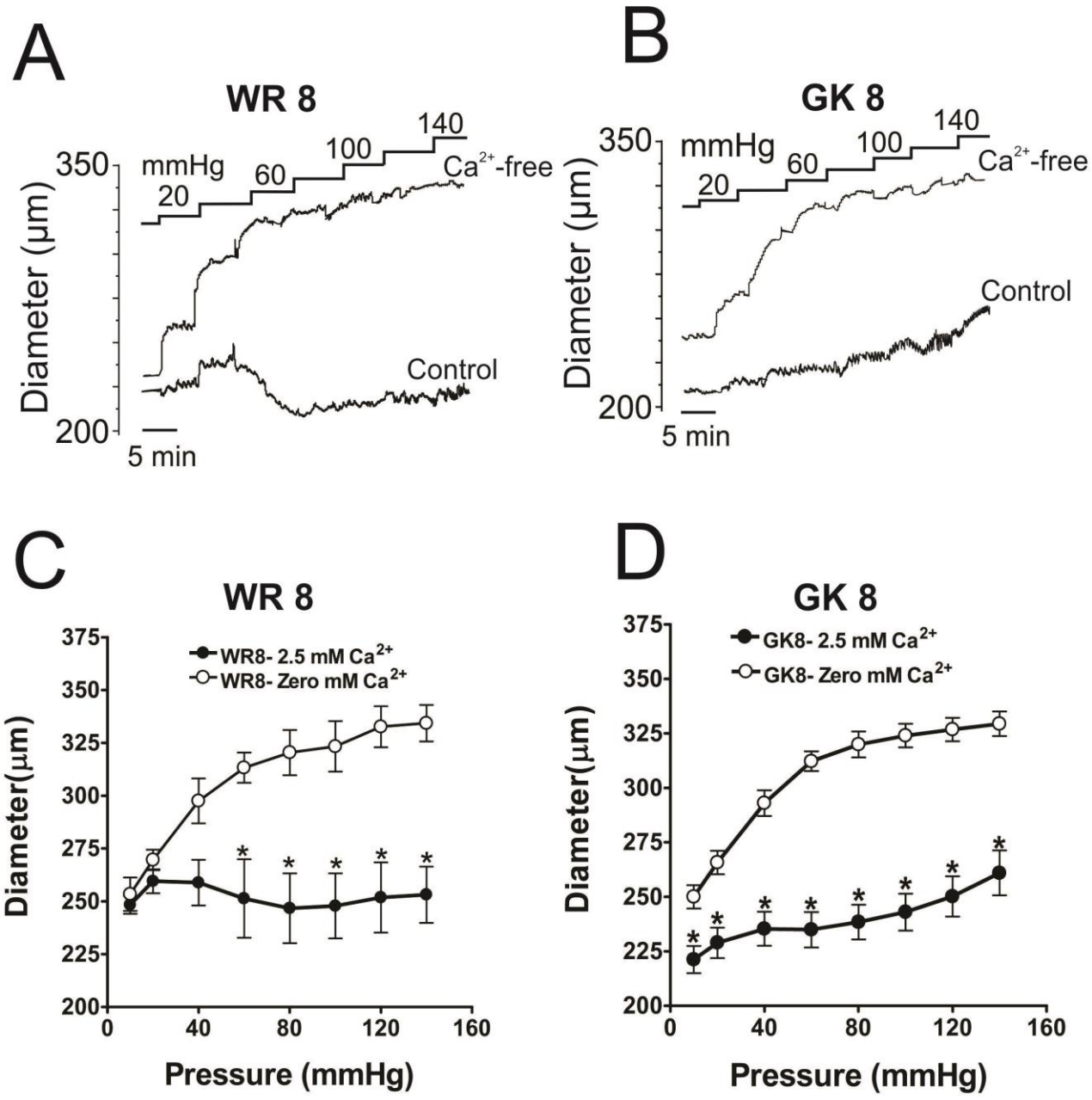
A
WR 8
Diameter (μm)
350
200
mmHg
20
60
100
140
Ca2+-free
Control
5 min
B
GK 8
Diameter (μm)
350
200
mmHg
20
60
100
140
Ca2+-free
Control
5 min
C
WR 8
WR8- 2.5 mM Ca2+
WR8- Zero mM Ca2+
Diameter(μm)
375
350
325
300
275
250
225
200
0
40
80
120
160
Pressure (mmHg)
D
GK 8
GK8- 2.5 mM Ca2+
GK8- Zero mM Ca2+
Diameter(μm)
375
350
325
300
275
250
225
200
0
40
80
120
160
Pressure (mmHg)

Figure 3.2: The myogenic response of cerebral arteries from 8-10 week GK and age-matched WR

Panel A,B: Representative recordings of outer diameter between 10 and 140 mmHg of posterior cerebral arteries from 8-10 week WR (panel A) and age-matched GK (panel B) in the presence (control) and absence of 2.5 mM Ca^{2+} (Ca^{2+}-free) in Krebs' saline.

Panel C,D: Mean outer diameter (± SEM)-pressure relationships between 10 and 140 mmHg of posterior cerebral arteries from 8-10 week WR (panel C) and age-matched GK (panel D) in normal (2.5 mM Ca^{2+}) and zero Ca^{2+} Krebs' saline (n=8). * Significantly different ($p<0.05$) from corresponding pressure in zero mM Ca^{2+}.

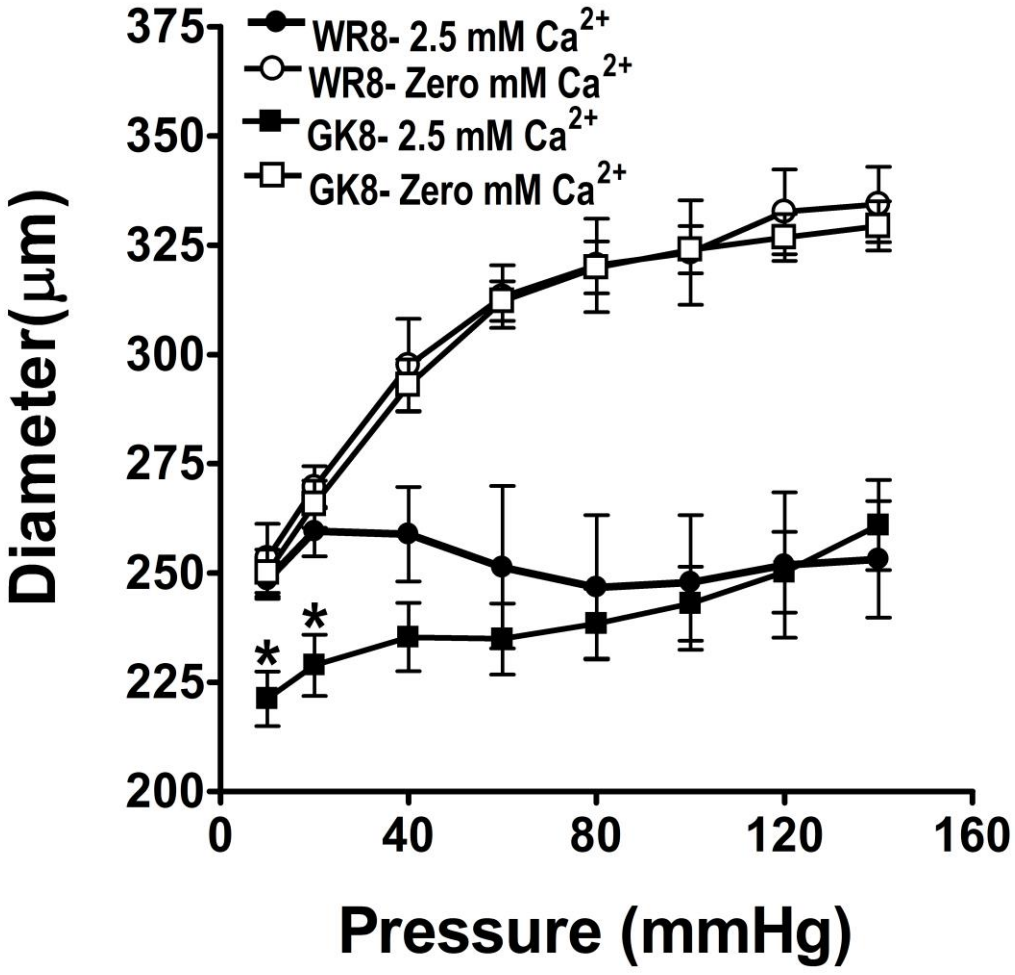

Figure 3.3: Comparison of the myogenic responses in cerebral arteries of 8-10 week GK and age-matched WR.

Mean outer diameter (± SEM)-pressure relationships between 10 and 140 mmHg of posterior cerebral arteries from 8-10 week GK and age-matched WR (n=8) in normal (2.5 mM Ca^{2+}) and zero Ca^{2+} Krebs' saline. * Significantly different ($p<0.05$) from corresponding value in WR at the same pressure.

3.2.4 Comparison of the myogenic responses in cerebral arteries of 8-10 week GK and age-matched WR

In figure 3.3, the pressure-diameter relationships between 10 and 140 mmHg of posterior cerebral arteries from 8-10 week GK rats and age-matched WR are compared (same data as presented in figure 3.2). No difference in passive diameter (Ca^{2+}-free curve) was detected at all pressures between GK and WR cerebral arteries. GK cerebral vessels exhibited a significantly smaller diameter at low pressure (10 & 20 mmHg) compared to WR vessels, but no significant difference was detected in diameter at other pressures (from 40-140 mmHg). Comparison of both pressure-diameter curves in the presence of Ca^{2+} illustrates that unlike WR cerebral vessels, GK vessels cannot maintain a constant diameter upon pressure elevation above ~80 mmHg.

3.2.5 Effect of H1152 on the cerebral myogenic response of 8-10 week GK and age-matched WR

To evaluate the role of ROK in the dysfunctional cerebral myogenic response of GK rats, the pressure-diameter relationships between 10 and 140 mmHg of posterior cerebral arteries from 8-10 week GK and age-matched WR were recorded in the presence of H1152 (0.5 µM) (Figure 3.4). In 8-10 week WR cerebral arteries, H1152 completely abolished the myogenic response and vessels passively dilated upon pressure increase from 60 to 140 mmHg to diameter values comparable to values in Ca^{2+} free condition. This result is consistent with previous reports implicating a key role for ROK in the development of the myogenic response (Johnson et al., 2009; Moreno-Domínguez et al., 2013). In cerebral arteries from GK rats, H1152 blocked the enhanced constriction detected at low pressure and vessels dilated passively upon pressure elevation between 10-140 mmHg to diameter values that were not significantly different from values in Ca^{2+}-free conditions at the corresponding pressure. These results suggest that ROK

contributed to the abnormal level of basal myogenic constriction of prediabetic GK cerebral arteries.

3.2.6 Comparison of the effects of H1152 on the cerebral myogenic response of 8-10 week GK and age-matched WR

Diameter-pressure relationships between 10 and 140 mmHg of posterior cerebral arteries from 8-10 week GK rats and WR in the presence and absence of H1152 (0.5 μM) are compared in figure 3.5 (same data as presented in figure 3.4). H1152 abolished all the differences in myogenic response of cerebral arteries from GK rats and WR; mean diameter values in the presence of H1152 were not different within the tested pressure range.

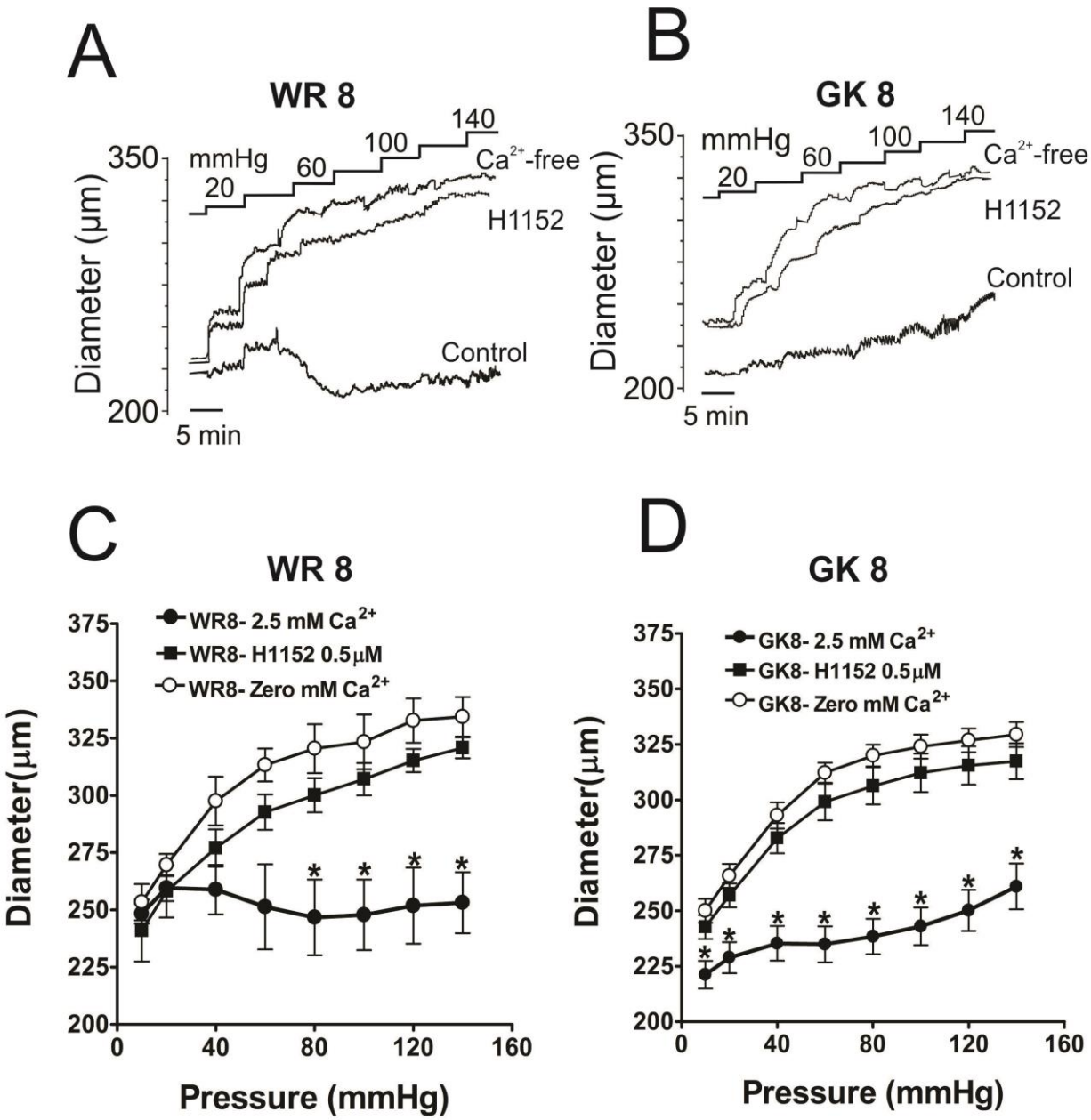
A
WR 8
350
200
Diameter (μm)
mmHg
20
60
100
140
Ca2+-free
H1152
Control
5 min
B
GK 8
350
200
Diameter (μm)
mmHg
20
60
100
140
Ca2+-free
H1152
Control
5 min
C
WR 8
WR8- 2.5 mM Ca2+
WR8- H1152 0.5μM
WR8- Zero mM Ca2+
Diameter(μm)
375
350
325
300
275
250
225
200
0
40
80
120
160
Pressure (mmHg)
D
GK 8
GK8- 2.5 mM Ca2+
GK8- H1152 0.5μM
GK8- Zero mM Ca2+
Diameter(μm)
375
350
325
300
275
250
225
200
0
40
80
120
160
Pressure (mmHg)

Figure 3.4: Effect of H1152 on the cerebral myogenic response of 8-10 week GK and age-matched WR.

Panel A,B: Representative recordings of outer diameter between 10 and 140 mmHg of posterior cerebral arteries from 8-10 week WR (panel A) and age-matched GK (panel B) in normal Krebs' saline (2.5 mM Ca^{2+}, control), 0.5 μM H1152, and zero Ca^{2+} saline (Ca^{2+}-free) .

Panel C,D: Mean outer diameter (± SEM)-pressure relationships between 10 and 140 mmHg of posterior cerebral arteries from 8-10 week WR (panel C) and age-matched GK (panel D) in normal Krebs' saline (2.5 mM Ca^{2+}, control), 0.5 μM H1152, and zero Ca^{2+} saline (n=8). * Significantly different ($p<0.05$) from corresponding pressure value in the presence of H1152.

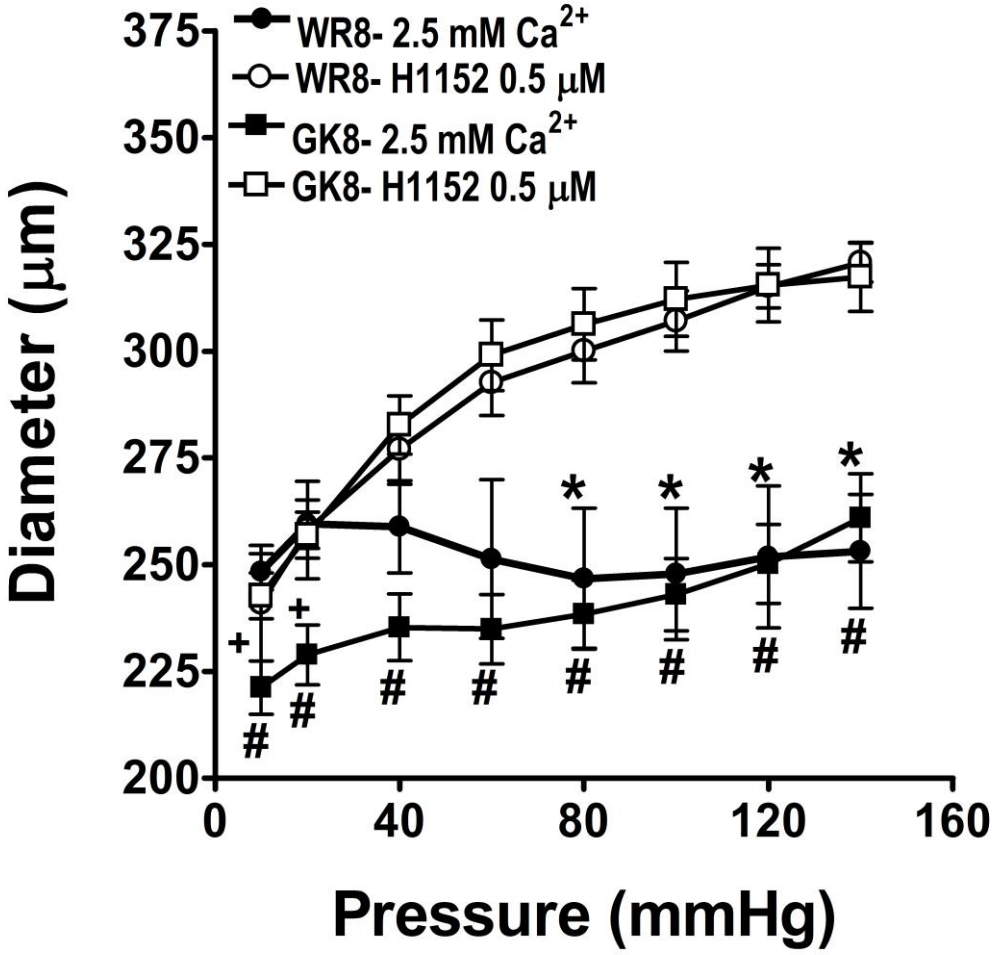

Figure 3.5: Comparison of the effects of H1152 on the cerebral myogenic response of 8-10 week GK and age-matched WR.

Mean outer diameter (± SEM)-pressure relationships between 10 and 140 mmHg of posterior cerebral arteries from 8-10 week GK and age-matched WR in normal Krebs' saline (2.5 mM Ca^{2+}) ± H1152 (0.5 μM) (n=8). * Significantly different ($p<0.05$) from corresponding value in WR in the presence of H1152. # Significantly different ($p<0.05$) from corresponding value in GK in the presence of H1152. + Significantly different ($p<0.05$) from corresponding WR value.

3.2.7 The myogenic response of cerebral arteries from 18-20 week WR

Figure 3.6 (left panels) shows the diameter-pressure relationships between 10 and 140 mmHg for posterior cerebral arteries from 18-20 week WR. In the presence of Ca^{2+} in the bathing solution, the myogenic response of 18-20 week WR cerebral arteries was similar to that of 8-10 week WR vessels. Vessels exhibited myogenic reactivity between 60 and 120 mmHg of intraluminal pressure. The myogenic constriction was completely abolished in the absence of Ca^{2+}.

3.2.8 The myogenic response of cerebral arteries from 18-20 week GK

Figure 3.6 (right panels) depicts the diameter-pressure relationships between 10 and 140 mmHg for posterior cerebral arteries from 18-20 week GK rats. Cerebral arteries from 18-20 week GK rats exhibited a proportional increase in diameter with pressure elevation within the tested pressure range in 2.5 mM Ca^{2+} Krebs' saline, similar to that observed for the Ca^{2+}-free conditions. However, a significant difference in mean diameter values was evident between 40-120 mmHg in normal compared to Ca^{2+}-free Krebs' saline suggesting that GK cerebral arteries still exhibit a residual myogenic force generation within the physiological range.

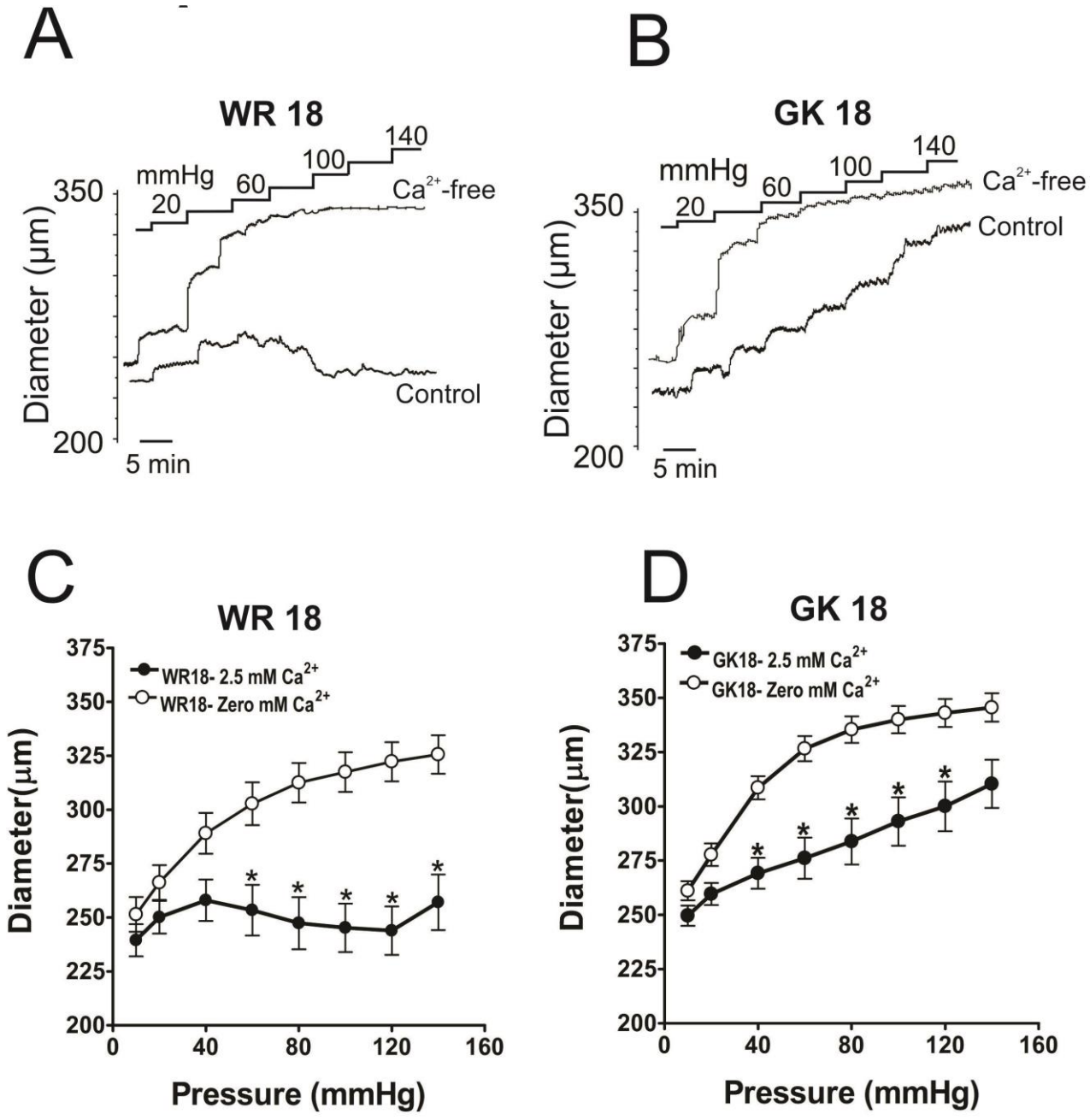
A
WR 18
mmHg
20
60
100
140
Ca2+-free
Control
Diameter (µm)
350
200
5 min
B
GK 18
mmHg
20
60
100
140
Ca2+-free
Control
Diameter (µm)
350
200
5 min
C
WR 18
WR18- 2.5 mM Ca2+
WR18- Zero mM Ca2+
Diameter(µm)
375
350
325
300
275
250
225
200
0
40
80
120
160
Pressure (mmHg)
D
GK 18
GK18- 2.5 mM Ca2+
GK18- Zero mM Ca2+
Diameter(µm)
375
350
325
300
275
250
225
200
0
40
80
120
160
Pressure (mmHg)

Figure 3.6: The myogenic response of cerebral arteries from 18-20 week GK and age-matched WR

Panel A,B: Representative recordings of outer diameter between 10 and 140 mmHg of posterior cerebral arteries from 18-20 week WR (panel A) and age-matched GK (panel B) in the presence (control) and absence of 2.5 mM Ca^{2+} (Ca^{2+}-free) in Krebs' saline.

Panel C,D: Mean outer diameter (± SEM)-pressure relationships between 10 and 140 mmHg of posterior cerebral arteries from 18-20 week WR (panel C) and age-matched GK (panel D) in normal Krebs' saline (2.5 mM Ca^{2+}) and zero Ca^{2+} (n=8). * Significantly different ($p<0.05$) from corresponding pressure value in the absence of Ca^{2+}.

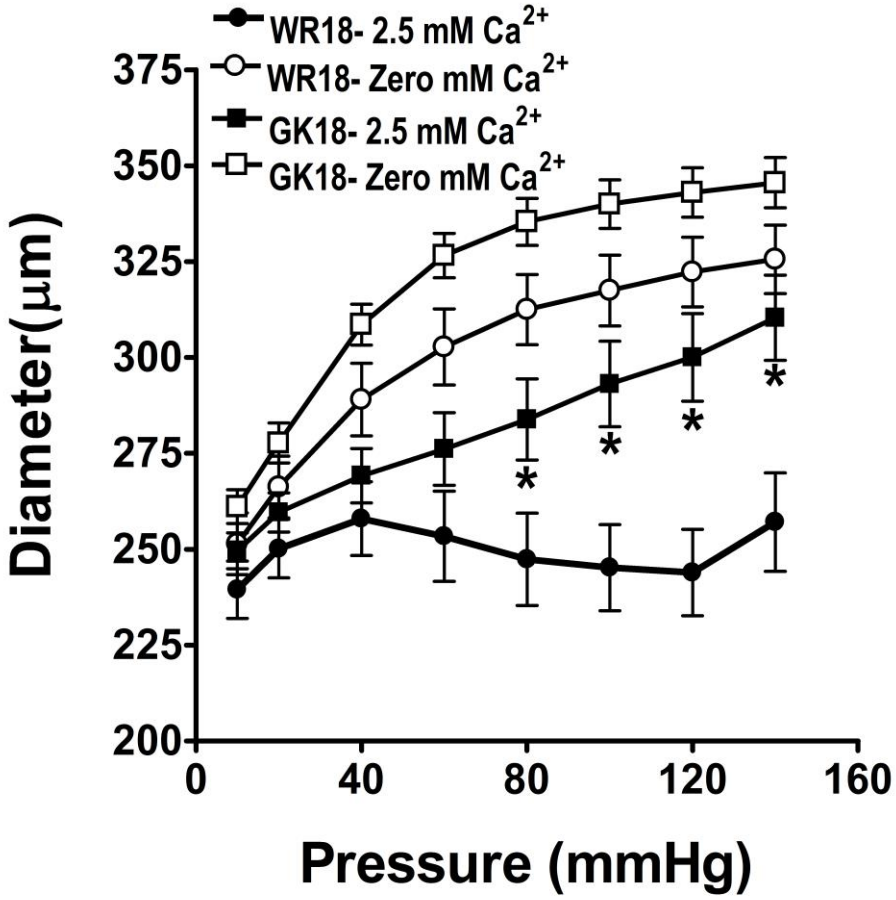

Figure 3.7: Comparison of the myogenic responses of cerebral arteries from 18-20 week GK and age-matched WR.

Mean outer diameter (± SEM)-pressure relationships between 10 and 140 mmHg of posterior cerebral arteries from 18-20 week GK and age-matched WR in normal Krebs' saline (2.5 mM Ca^{2+}) and zero Ca^{2+} Krebs' saline (n=8). * Significantly different ($p<0.05$) from corresponding value in WR at the same pressure.

3.2.9 Comparison of the myogenic responses of cerebral arteries from 18-20 week GK rats and age-matched WR

Figure 3.7 represents a comparison of the diameter-pressure relationships between 10 and 140 mmHg of posterior cerebral arteries from 18-20 week GK rats and age-matched WR (same data as presented in figure 3.6). No significant difference in passive diameter (Ca^{2+}-free curve) was detected within the tested pressure range between GK and WR cerebral vessels. The diameter of GK cerebral vessels was significantly larger between 80 and 140 mmHg compared to WR vessels. Although the diameters of both GK and WR cerebral arteries were not different at 10 mmHg, GK vessels did not exhibit an effective myogenic constriction and failed to maintain constant diameter between 60-140 mmHg compared to WR arteries that maintained diameter within the same pressure range.

3.2.10 Effect of H1152 on the cerebral myogenic response of 18-20 week GK and age-matched WR

Figure 3.8 shows the effect of H1152 (0.5 μM) on the diameter-pressure relationships between 10 and 140 mmHg of posterior cerebral arteries from 18-20 week WR and age-matched GK rats. As indicated with 8-10 week WR, cerebral vessels from 18-20 week WR did not show any evidence of myogenic response in the presence of H1152 and passively dilated upon pressure increase from 60 to 140 mmHg to diameter values comparable to values in Ca^{2+}-free conditions. In cerebral arteries from GK rats, H1152 blocked the residual tone and vessels dilated passively upon pressure elevation such that the change in diameter was not significantly different from that in the absence of Ca^{2+}.

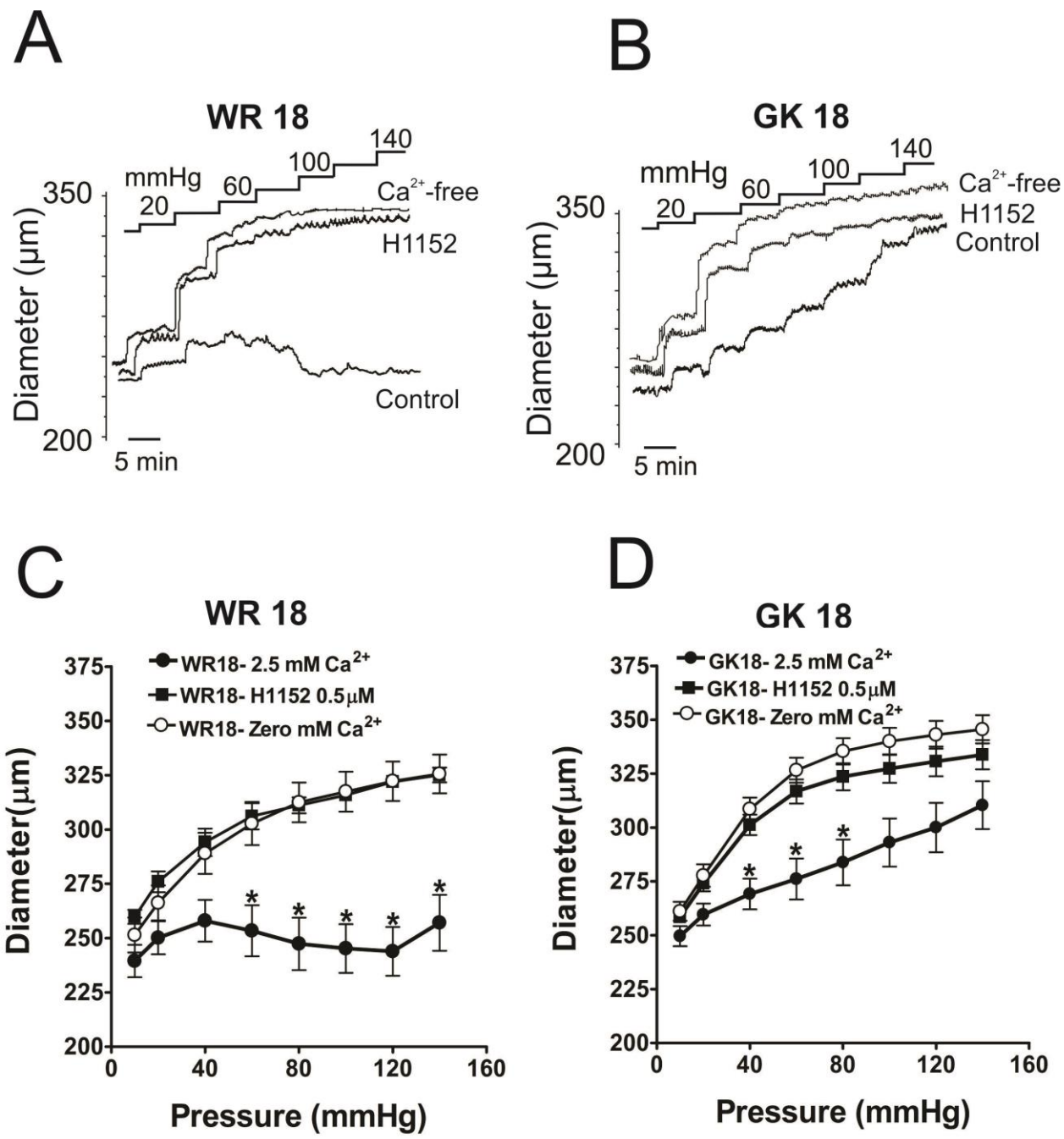
A
WR 18
mmHg
20
60
100
140
Ca2+-free
H1152
Control
Diameter (μm)
350
200
5 min
B
GK 18
mmHg
20
60
100
140
Ca2+-free
H1152
Control
Diameter (μm)
350
200
5 min
C
WR 18
WR18- 2.5 mM Ca2+
WR18- H1152 0.5μM
WR18- Zero mM Ca2+
Diameter(μm)
375
350
325
300
275
250
225
200
0
40
80
120
160
Pressure (mmHg)
D
GK 18
GK18- 2.5 mM Ca2+
GK18- H1152 0.5μM
GK18- Zero mM Ca2+
Diameter(μm)
375
350
325
300
275
250
225
200
0
40
80
120
160
Pressure (mmHg)

Figure 3.8: Effect of H1152 on the cerebral myogenic response of 18-20 week GK and age-matched WR.

Panel A,B: Representative recordings of outer diameter between 10 and 140 mmHg of posterior cerebral arteries from 18-20 week WR (panel A) and age-matched GK (panel B) in normal Krebs' saline (2.5 mM Ca^{2+}, control), 0.5 μM H1152, and zero Ca^{2+} saline (Ca^{2+}-free).

Panel C,D: Mean outer diameter (± SEM)-pressure relationship between 10 and 140 mmHg of posterior cerebral arteries from 18-20 week WR (panel C) and age-matched GK (panel D) in normal Krebs' saline (2.5 mM Ca^{2+}, control), 0.5 μM H1152, and zero Ca^{2+} saline (n=8). * Significantly different ($p<0.05$) from corresponding pressure value in the presence of H1152.

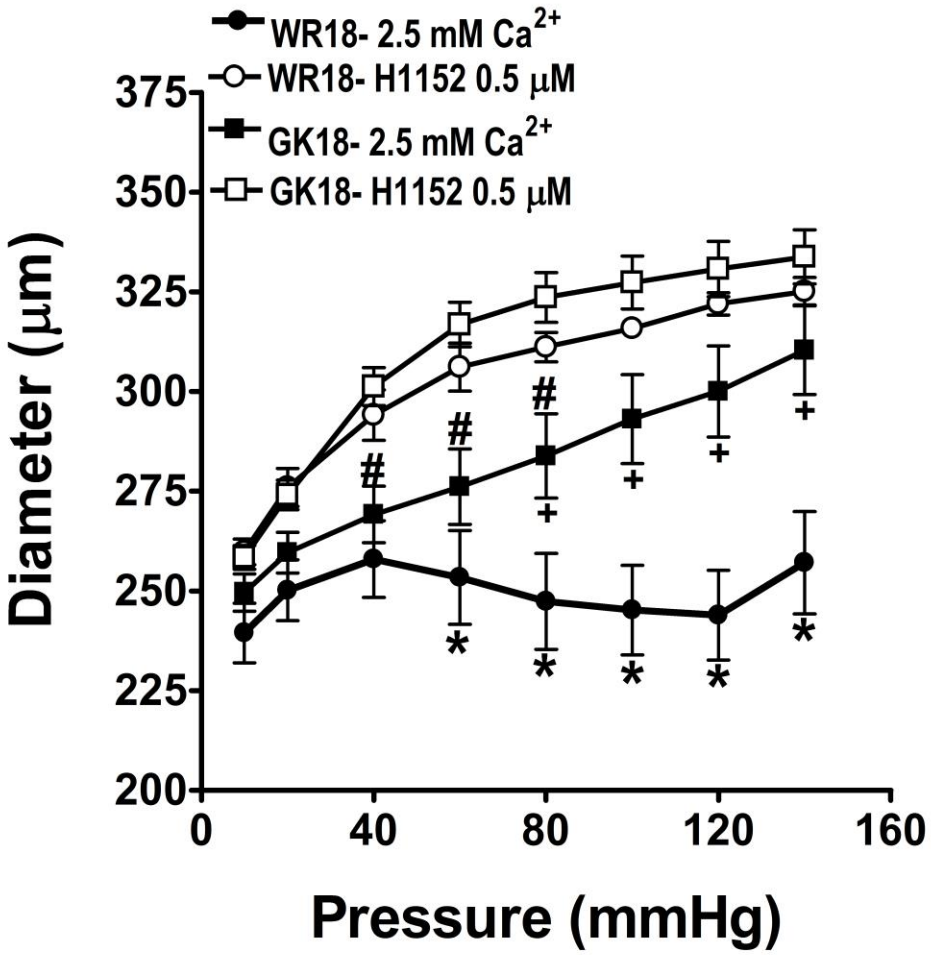

Figure 3.9: Comparison of the effects of H1152 on the cerebral myogenic response of 18-20 week GK and age-matched WR.

Mean outer diameter (± SEM)-pressure relationships between 10 and 140 mmHg of posterior cerebral arteries from 18-20 week GK and age-matched WR in normal Krebs' saline (2.5 mM Ca^{2+}) ± H1152 (n=8). * Significantly different ($p<0.05$) from corresponding WR value in the presence of H1152. # Significantly different ($p<0.05$) from corresponding GK value in the presence of H1152. + Significantly different ($p<0.05$) from corresponding WR value.

3.2.11 Comparison of the effects of H1152 on the cerebral myogenic response of 18-20 week GK and age-matched WR

Diameter-pressure relationships between 10 and 140 mmHg of posterior cerebral arteries from 18-20 week GK rats and age-matched WR in the presence and absence of H1152 (0.5 μM) are compared in figure 3.9 (same data presented in figure 3.8). H1152 abolished the myogenic response in cerebral arteries from both GK and WR; mean diameter values in the presence of H1152 were not different within the tested pressure range.

3.2.12 Cerebral myogenic response in 8-10 *versus* 18-20 week WR

Comparison of the diameter-pressure relationships between 10 and 140 mmHg of posterior cerebral arteries from 8-10 and 18-20 week WR indicated that the myogenic response in 2.5 mM Ca^{2+} Krebs' saline was identical at these two ages (figure 3.10). The passive diameter curves were also not different. These results indicate that the difference in age did not have any effect on the myogenic response in WR.

3.2.13 Cerebral myogenic response in 8-10 *versus* 18-20 week GK

In figure 3.11, the diameter-pressure relationships between 10-140 mmHg of posterior cerebral arteries from 8-10 and 18-20 week GK rats are compared. Cerebral arteries from 8-10 week GKs exhibited a significantly smaller mean diameter within the tested pressure range (10 – 140 mmHg) compared to 18-20 week GK vessels. Similar to WR control, no significant difference in the passive diameter was apparent over the entire pressure range in these groups.

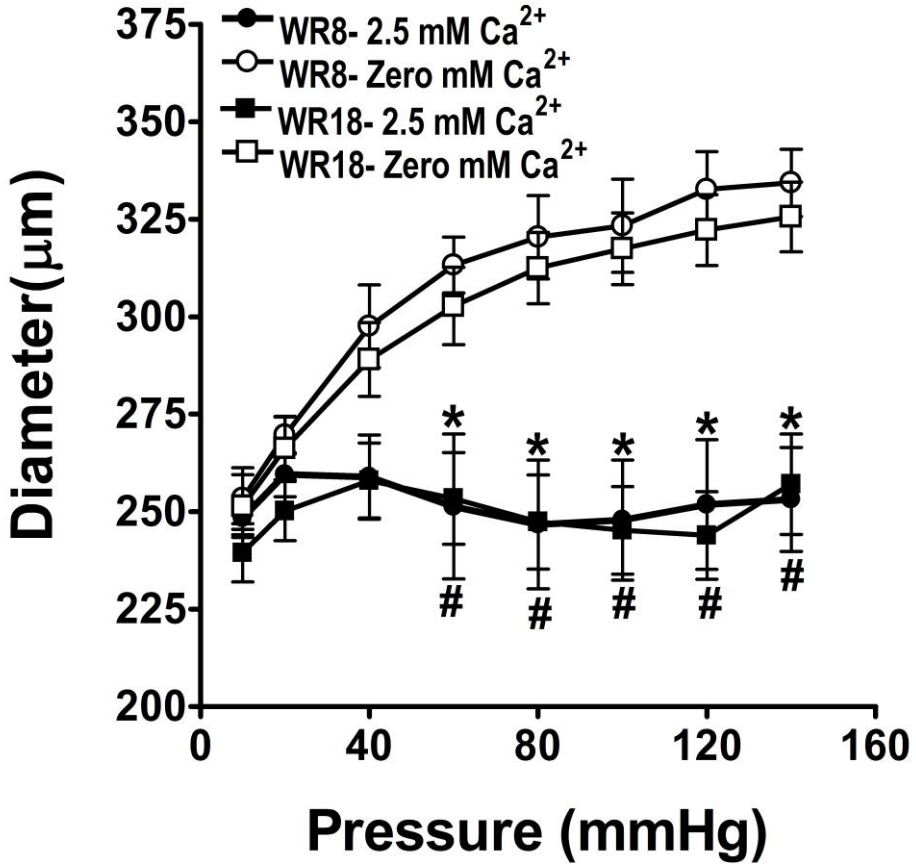

Figure 3.10: Cerebral myogenic response in 8-10 *versus* 18-20 week WR.

Mean outer diameter (± SEM)-pressure relationships between 10 and 140 mmHg of posterior cerebral arteries from 8-10 and 18-20 week WR in normal Krebs' saline (2.5 mM Ca^{2+}) and zero Ca^{2+} saline (n=8). * Significantly different ($p<0.05$) from corresponding value in 8-10 week WR in zero Ca^{2+}. $^{\#}$ Significantly different ($p<0.05$) from corresponding value in 18-20 week WR in zero Ca^{2+}.

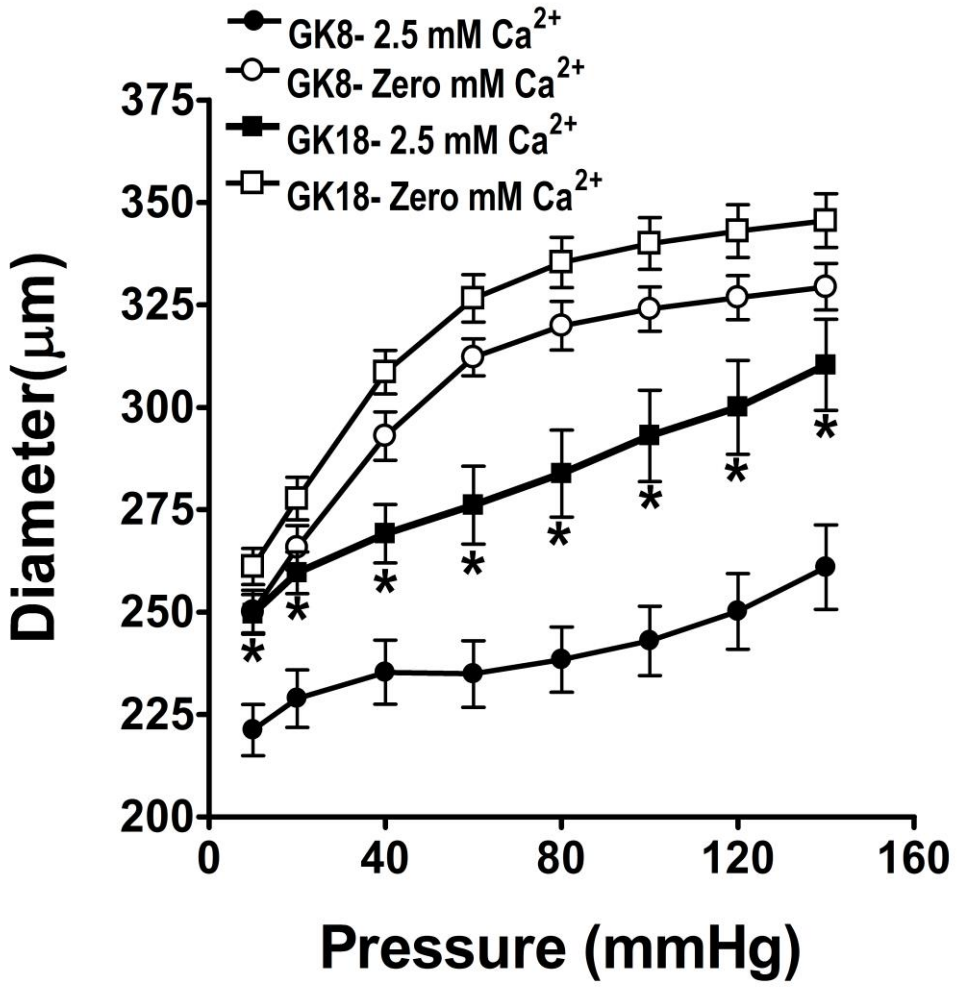

Figure 3.11: Cerebral myogenic response in 8-10 *versus* 18-20 week GK.

Mean outer diameter (± SEM)-pressure relationships between 10 and 140 mmHg of posterior cerebral arteries from 8-10 and 18-20 week GK in normal Krebs' saline (2.5 mM Ca^{2+}) and zero Ca^{2+} saline (n=8). * Significantly different ($p<0.05$) from corresponding value of 8-10 week GK values.

3.3. Summary of findings

In this section, we provide evidence that the myogenic response in GK rats is abnormal at two different disease stages. Specifically, we show that at 8-10 weeks, when the animals are likely insulin-resistant but have normal insulin and glucose levels, the cerebral arteries exhibited enhanced basal myogenic tone at low pressure (below 40 mmHg). Above 40 mmHg vessels maintained a relatively constant diameter with no evidence of myogenic reactivity; i.e. maintenance of diameter rather than pressure-evoked decrease in diameter. At intraluminal pressures higher than 80 mmHg the vessels were incapable of generating sufficient force to withstand pressure elevation to maintain diameter at the same level. This enhanced constriction was abolished following ROK inhibition with H1152 suggesting a crucial role for ROK as the cause of the abnormal myogenic tone. As GK rats grow older and exhibit signs of diabetes, such as hyperglycemia and hyperinsulinemia, by 18-20 weeks, the cerebral arteries are not truly myogenic; i.e. they failed to exhibit any signs of pressure-dependent constriction over the pressure range tested. In other words, vessels exhibited a loss of myogenic reactivity with no maintenance of diameter. Also, the passive diameters of the vessels in these groups were similar suggesting that vessel wall remodeling was not evident at least up to the 20^{th} week. These findings suggest that the dysfunctional myogenic response in type 2 diabetic GK rats begins as an enhanced constriction at the insulin resistance stage and develops to a loss of the myogenic response as the disease progresses to overt type 2 diabetes

Chapter Four: The biochemical basis of abnormal myogenic regulation of cerebral arterial diameter in GK rats

4.1 Hypothesis and objectives

In the experiments reported in this chapter we tested the hypothesis that the progressive dysfunction in myogenic constriction of the cerebral arteries from GK rats is due to abnormal regulation of Ca^{2+} sensitization (specifically, abnormal MLCP regulation) and actin polymerization pathways downstream of ROK. The primary objectives of this part of the study were:

1. To detect changes in the Ca^{2+} sensitization mechanism in cerebral arteries from 8-10 and 18-20 week GK rats compared to age-matched control WR.

2. To evaluate changes in the actin polymerization mechanism in cerebral arteries from 8-10 and 18-20 week GK rats compared to age-matched control WR.

3. To determine the upstream signaling mechanisms that could trigger defective regulation of Ca^{2+} sensitization and/or actin polymerization, specifically FAK phosphorylation and RhoA/ROK activation in prediabetic GK rats.

4.2 Results

4.2.1 Molecular changes in the Ca^{2+} sensitization mechanism in 8-10 week GK cerebral arteries

In the previous chapter (Chapter 3), evidence was provided that indicated the presence of an enhanced myogenic tone at low intraluminal pressure in 8-10 week GK rats and loss of the myogenic response in 18-20 week-old rats. Pressure-dependent constriction in resistance arteries is attributed to: (i) phosphorylation of LC_{20} that initiates actomyosin cross-bridge cycling; and (ii) dynamic actin cytoskeletal reorganization that is essential for transmitting the force generated

by the contractile apparatus to VSMC membrane and extracellular matrix (Walsh & Cole, 2013). Here we investigated whether the evolution of type 2 diabetes in GK rats was associated with a progressive dysfunction in LC_{20} phosphorylation that could explain, at least partially, the presence of abnormal myogenic constriction in GK rats compared to WR control animals.

4.2.1.1 Pressure-dependent phosphorylation of LC_{20} in cerebral arteries from 8-10 week WR

A pressure-dependent increase in LC_{20} phosphorylation was detected in the cerebral arteries of 8-10 week control WR as shown in Figure 4.1 (left blot in panel A and open bars in panel B). The two bands in panel A represent phosphorylated LC_{20} (1-P, upper) and unphosphorylated LC_{20} (0-P, lower) separated using Phos-tag™ gel electrophoresis (details in Chapter 2.6.1). LC_{20} phosphorylation increased with pressure elevation from 10 (26.3% ± 0.5) to 60 (38.0% ± 1.0) and 120 mmHg (49.6% ± 1.1) in 8-10 week WR cerebral arteries. These findings are in line with published reports from the Cole laboratory for cerebral and skeletal muscle resistance arteries from SD rats (Johnson et al., 2009; Moreno-Domínguez et al., 2013).

4.2.1.2 Changes in phosphorylation of LC_{20} with pressure in cerebral arteries from 8-10 week GK *vs* age-matched WR

Figure 4.1 compares the changes in LC_{20} phosphorylation with pressure in 8-10 week GK and age-matched WR cerebral arteries. Phospho-LC_{20} content was elevated at 10 mmHg in prediabetic GK compared to WR (35.4% ± 1.1 in GK and 26.3% ± 0.5 in WR) coincident with the enhanced basal myogenic tone in GK compared to WR. The extent of LC_{20} phosphorylation was not different at 60 mmHg between GK (40.1% ± 1.9) and WR (38.0% ± 1.0) coincident with impaired myogenic reactivity. Notably, LC_{20} phosphorylation at 120 mmHg was significantly lower in GK (31.0% ± 2.0) compared to WR arteries (49.6% ± 1.1).

A

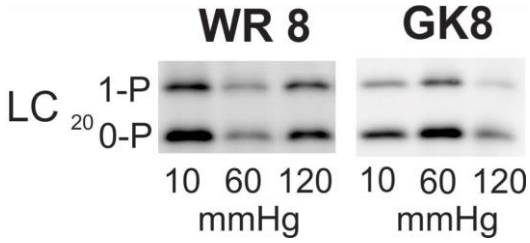

B

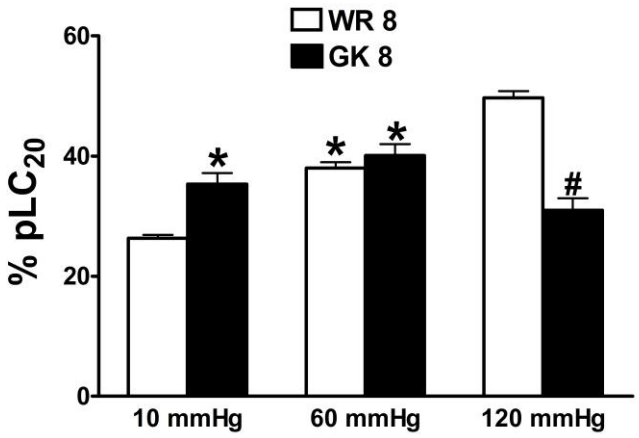

Figure 4.1: **Changes in LC_{20} phosphorylation with pressure in 8-10 week GK *vs* age-matched WR rats**

Representative western blots (panel A) and mean level ± SEM (panel B) of phosphorylated LC_{20} as a percentage of total LC_{20} at 10, 60 and 120 mmHg in 8-10 week GK cerebral arteries and age-matched WR (n=7). The unphosphorylated (0-P) and mono-phosphorylated (1-P) LC_{20} were separated by Phos-tag™ SDS-PAGE and visualized using pan-LC_{20} antibody.

* Significantly different ($p<0.05$) from corresponding WR at 10 mmHg. # Significantly different ($p<0.05$) from corresponding WR at 120 mmHg.

4.2.1.3 Effect of H1152 on LC_{20} phosphorylation in pressurized cerebral arteries from 8-10 week GK

LC_{20} phosphorylation level is dependent on the balance between MLCK and MLCP activities. One hypothesis to explain the elevated level of phospho-LC_{20} is the inhibition of MLCP activity through phosphorylation of MYPT1 by ROK. The two phosphorylation sites on MYPT1 that have been linked to MLCP inhibition by ROK are T855 and T697 (rat numbering) (Cole & Welsh, 2011). First we tested whether the elevated phospho-LC_{20} level detected at lower pressure was dependent on ROK activity by incubating pressurized vessels with 0.5 µM H1152 and quantifying the level of phosphorylation of LC_{20}. Figure 4.2 shows that ROK inhibition with H1152 (0.5 µM) abolished the increased level of phospho-LC_{20} in 8-10 week GK rats at 10 mmHg (36.7% ± 1.5; -H1152 *vs* 28.2% ± 1.5; +H1152) but did not have a significant effect on the phospho-LC_{20} level at 120 mmHg (29.17% ± 1.2; -H1152 *vs* 35.4% ± 2.2; +H1152). These findings suggest that the increase in LC_{20} phosphorylation level at 10 mmHg was likely due to enhanced ROK activity.

A

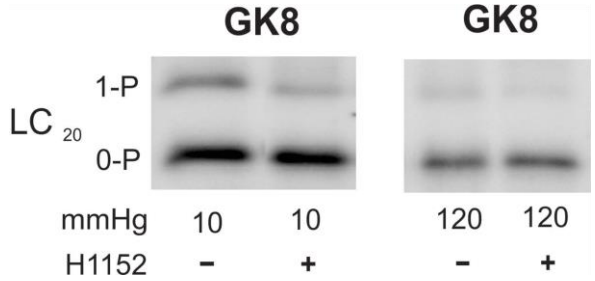

B

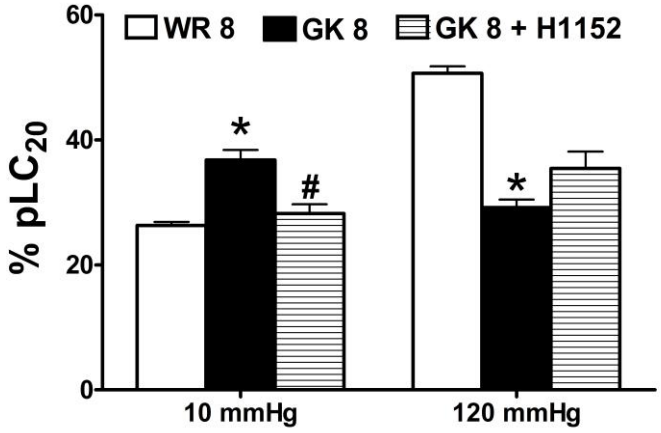

Figure 4.2: Effect of H1152 on LC_{20} phosphorylation in pressurized cerebral arteries from 8-10 week GK rats

Representative western blots **(panel A)** and mean levels ± SEM **(panel B)** of phosphorylated LC_{20} as a percentage of total LC_{20} at 10 and 120 mmHg in 8-10 week GK cerebral arteries ± H1152 (0.5 μM) compared to age-matched WR (n=5). The unphosphorylated (0-P) and mono-phosphorylated (1-P) LC_{20} were separated by Phos-tag™ SDS-PAGE and visualized using pan-LC_{20} antibody. * Significantly different ($p<0.05$) from corresponding WR value. # Significantly different ($p<0.05$) from corresponding GK value.

4.2.1.4 Pressure-dependent phosphorylation of MYPT1-T855 in cerebral arteries from 8-10 week WR

An increased level of ROK activity would be expected to result in a greater level of phosphorylation of MYPT1 at T855 and/or T697. Thus, we quantified phospho-MYPT1-T855 and T697 content in pressurized vessels from 8-10 week WR and GK rats (details in Chapter 2.6.2). A pressure-dependent increase in the phosphorylation of MYPT1-T855 was detected in 8-10 week WR as shown in figure 4.3 (left blot in panel A and open bars in panel B). Pressure elevation was associated with a two-fold increase in phospho-MYPT1-T855 content at 60 mmHg (2 ± 0.02) and an almost three-fold increase at 120 mmHg (2.8 ± 0.18) compared to 10 mmHg (set to a value of 1). These values are consistent with published reports for phospho-MYPT1-T855 content in cerebral and gracilis arteries of SD rats (Johnson et al., 2009; Moreno-Domínguez et al., 2013).

4.2.1.5 Changes in phosphorylation of MYPT1-T855 with pressure in cerebral arteries from 8-10 week GK rats *vs* age-matched WR

Figure 4.3 compares the changes in phospho-MYPT1-T855 with pressure in cerebral arteries of 8-10 week GK and age-matched WR. A significant elevation in phospho-MYPT1-T855 level was detected at 10 mmHg in vessels of GK rats (1.4 ± 0.04) compared to WR. No further change in phosphoprotein content was detected on pressurization to 60 and 120 mmHg such that the levels in GK arteries (2.8 ± 0.18) were significantly lower than those of WR arteries (1.4 ± 0.12) at 120 mmHg coincident with impaired myogenic reactivity in GK.

A

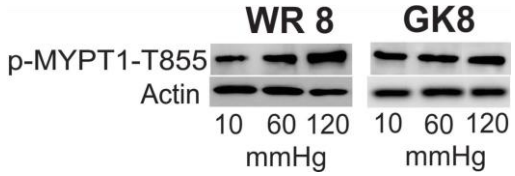

B

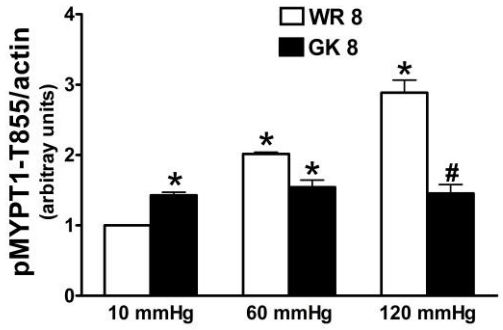

Figure 4.3: Changes in phosphorylation of MYPT1-T855 with pressure in 8-10 week GK *vs* age-matched WR

Panel A: Representative western blots for phospho-MYPT1-T855 and corresponding actin in each lane for cerebral arteries at 10, 60 and 120 mmHg from 8-10 week GK and age-matched WR.

Panel B: Mean levels ± SEM of phospho-MYPT1-T855 normalized to the corresponding actin level in each lane for samples from 8-10 week GK cerebral arteries and age-matched WR at 10, 60 and 120 mmHg with WR value at 10 mmHg set to 1 (n=8). * Significantly different ($p<0.05$) from WR value at 10 mmHg. # Significantly different ($p<0.05$) from WR value at 120 mmHg.

4.2.1.6 Effect of H1152 on MYPT1-T855 phosphorylation in pressurized cerebral arteries from 8-10 week GK

To determine whether the increased phosphorylation of MYPT1-T855 was due to enhanced ROK activity, pressurized cerebral arteries were incubated with H1152 (0.5 μM), flash-frozen and phospho-MYPT1-T855 content was quantified. Figure 4.4 shows that ROK inhibition with H1152 abolished the elevated phosphorylation of MYPT1-T855 at all pressures in cerebral vessels of 8-10 week GK rats. At 10 mmHg, H1152 reduced the phosphorylation of MYPT1-T855 in GK vessels (from 1.4 ± 0.04 to 0.45 ± 0.03) to a level that was lower than that detected in age-matched WR. These findings support the view that enhanced ROK activity contributes to the augmented basal myogenic tone in 8-10 week GK cerebral arteries. It also highlights the crucial role that ROK plays in the maintenance of appropriate myogenic tone at all pressures in control WR, as was previously demonstrated in cerebral and skeletal muscle resistance arteries from SD rats (Johnson et al., 2009; Moreno-Domínguez et al., 2013).

A

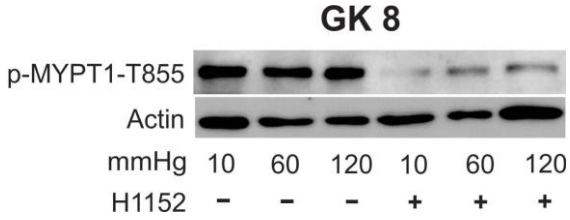

B

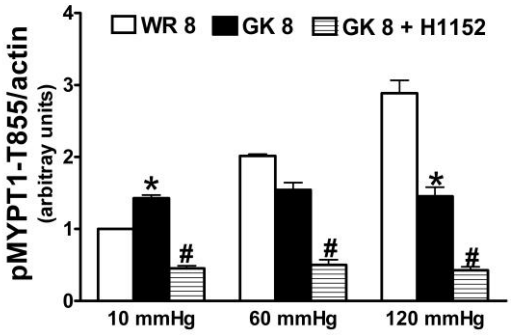

Figure 4.4: Effect of H1152 on the phosphorylation of MYPT1-T855 in pressurized cerebral arteries from 8-10 week GK

Panel A: Representative western blots for phospho-MYPT1-T855 and corresponding actin in each lane for cerebral arteries at 10, 60 and 120 mmHg from 8-10 week GK rats ± H1152 (0.5 µM).

Panel B: Mean level ± SEM of phospho-MYPT1-T855 normalized to the corresponding actin level in each lane for samples of cerebral arteries at 10, 60 and 120 mmHg from 8-10 week GK rats ± H1152 (0.5 µM) and age-matched WR with WR value at 10 mmHg set to 1 (n=5). * Significantly different ($p<0.05$) from corresponding WR value. # Significantly different ($p<0.05$) from corresponding value in GK and WR.

4.2.1.7 Changes in phosphorylation of MYPT1-T697 with pressure in cerebral arteries from 8-10 week WR

T697 is the other site on MYPT1 that was reported to be phosphorylated by ROK and associated with an inhibition of MLCP activity (Feng et al., 1999). No significant pressure-dependent increase in phospho-MYPT1-T697 was detected at 60 mmHg (0.96 ± 0.07) or 120 mmHg (1.2 ± 0.11) compared to the 10 mmHg value (Figure 4.5 left blot in panel A and open bars in panel B). These findings suggest that the myogenic response in WR cerebral arteries is not dependent on the pressure-dependent increase in phosphorylation of MYPT1-T697, similar to the findings for SD rats (Johnson et al., 2009; El-Yazbi et al., 2010).

4.2.1.8 Changes in phosphorylation of MYPT1-T697 with pressure in cerebral arteries from 8-10 week GK *vs* age-matched WR

Figure 4.5 compares the change in phospho-MYPT1-T697 in cerebral arteries of 8-10 week GK and age-matched WR. Phospho-MYPT1-T697 was significantly elevated at 10 mmHg (1.4 ± 0.1 *vs* 1 ± 0) and 60 mmHg (1.4 ± 0.09 *vs* 0.91 ± 0.07) in GK *vs* WR vessels suggesting that elevated phosphorylation at T697 could also play a role in development of enhanced basal myogenic tone detected in 8-10 week GK cerebral arteries.

4.2.1.9 Effect of H1152 on MYPT1-T697 phosphorylation in pressurized cerebral arteries from 8-10 week GK rats

In this experiment, the ROK inhibitor H1152 was used to determine whether the elevated phospho-MYPT1-T697 detected in GK rats was dependent on ROK activity. Elevated levels of phospho-MYPT1-T697 in 8-10 week GK cerebral arteries were not affected by H1152 treatment at 10 (1.4 ± 0.1 *vs* 1.4 ± 0.13) or 60 mmHg (1.42 ± 0.09 *vs* 1.2 ± 0.09) as shown in figure 4.6.

These data suggest that the enhanced phosphorylation of MYPT1-T697 is not due to ROK activity.

4.2.1.10 MYPT1 mRNA and protein levels in cerebral arteries from 8-10 week GK and age-matched WR

To determine whether the change in MYPT1 phosphorylation may be attributed to differences in MYPT1 expression between the two strains, MYPT1 mRNA and protein content were quantified by real-time PCR and western blotting, respectively, in WR and GK rats (details in Chapter 2, sections 2.4 & 2.6). In figure 4.7, MYPT1 transcript levels relative to ß-actin (panel A) and protein levels of MYPT1 normalized to actin (panel B) or GAPDH (panel C) were compared using cerebral arteries from 8-10 week GK and age-matched WR. No differences were detected in MYPT1 expression at the mRNA or protein level. This suggests that the changes detected in MYPT1 phosphorylation between GK and age-matched WR cannot be attributed to a difference in the MYPT1 content.

A

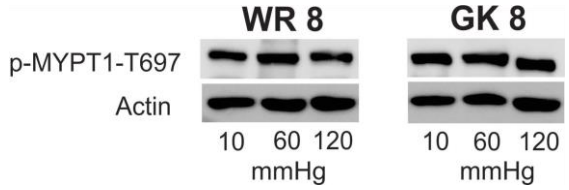

B

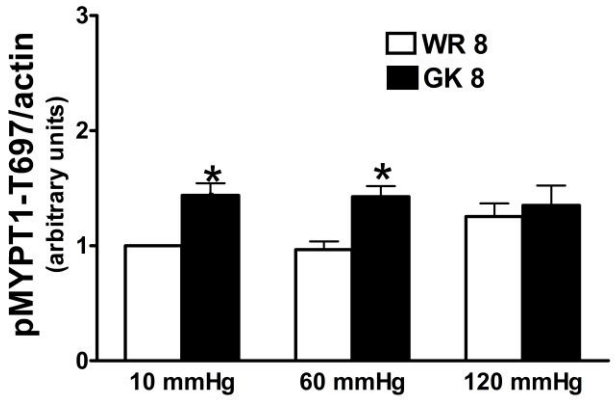

Figure 4.5: Changes in phosphorylation of MYPT1-T697 with pressure in 8-10 week GK *vs* age-matched WR

Panel A: Representative western blots for phospho-MYPT-T697 and corresponding actin in each lane for cerebral arteries from 8-10 week GK rats and age-matched WR at 10, 60 and 120 mmHg.

Panel B: Mean levels ± SEM of phospho-MYPT-T697 normalized to the corresponding actin level in each lane for samples of cerebral arteries at 10, 60 and 120 mmHg from 8-10 week GK rats and age-matched WR with the value for WR at 10 mmHg set to 1 (n=5). * Significantly different ($p<0.05$) from corresponding WR value at 10 mmHg.

A

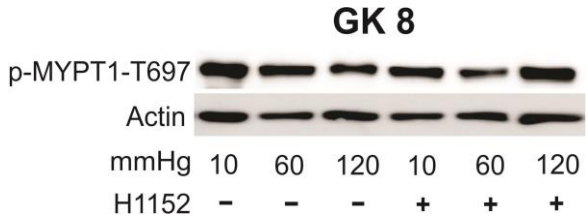

B

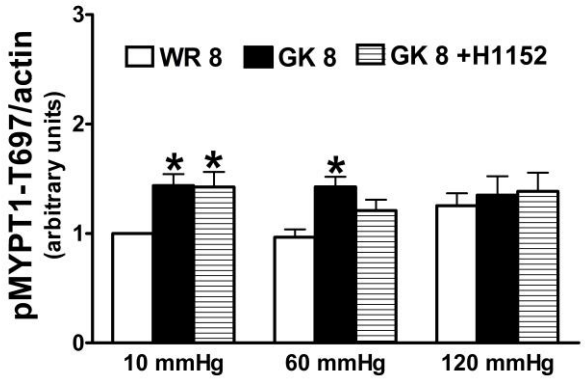

Figure 4.6: Effect of H1152 on the phosphorylation of MYPT1-T697 in pressurized cerebral arteries from 8-10 week GK

Panel A: Representative western blots for phospho-T697-MYPT1 and corresponding actin in each lane for cerebral arteries from 8-10 week GK rats at 10, 60 and 120 mmHg ± H1152 (0.5 μM).

Panel B: Mean level ± SEM of phospho-T697-MYPT1 normalized to corresponding actin level in each lane for samples of cerebral arteries at 10, 60 and 120 mmHg ± H1152 (0.5 μM) from 8-10 week GK rats and age-matched WR with WR value at 10 mmHg set to 1 (n=4). *Significantly different ($p<0.05$) from corresponding WR value at 10 mmHg.

A

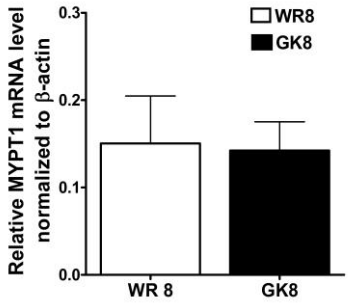

B

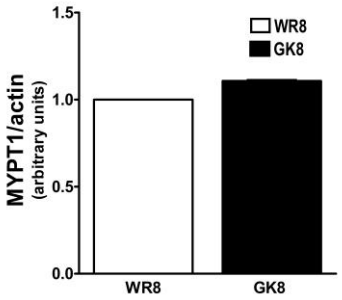

C

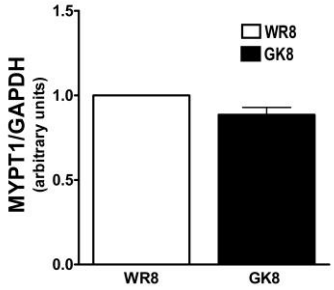

Figure 4.7: MYPT1 mRNA and protein expression in cerebral arteries from 8-10 week GK *vs* age-matched WR

Panel A: Mean levels ± SEM of MYPT1 transcript expression relative to ß-actin determined by real-time PCR using mRNA derived from cerebral arteries of 8-10 week GK rats and age-matched WR. Relative transcript levels were determined using the $2^{-\Delta\Delta Ct}$ method (n=5).

Panel B,C: Mean levels ± SEM of MYPT1 protein normalized to actin (panel B) & GAPDH (panel C) in cerebral arteries from 8-10 week GK and age-matched WR with the value of WR set to 1 (n=10). Note: no significant difference in MYPT1 mRNA/protein between GK and WR was detected.

4.2.2 Molecular changes in the Ca^{2+} sensitization mechanism in 18-20 week GK cerebral arteries

4.2.2.1 Pressure-dependent phosphorylation of LC_{20} in cerebral arteries from 18-20 week WR

As discussed in the previous chapter (Chapter 3), we observed a impaired myogenic constriction in vessels from 18-20 week GK rats. Here we investigated whether changes in LC_{20} and MYPT1 phosphorylation could explain, at least in part, this impairment in the myogenic response. We first confirmed that the pressure-evoked LC_{20} phosphorylation detected in cerebral arteries from 8-10 week WR was present in 18-20 week-old animals. Similar to 8-10 week WR, a pressure-dependent increase in the phosphorylation of LC_{20} was detected on pressurization from 10 (36.5% ± 0.5) to 60 (46.4% ± 0.8) and 120 mmHg (52.9% ± 0.9) in 18-20 week WR cerebral arteries (Figure 4.8, left blot in panel A and open bars in panel B).

4.2.2.2 Changes in LC_{20} phosphorylation with pressure in cerebral arteries from 18-20 week GK rats *vs* age-matched WR

Figure 4.8 compares the changes in LC_{20} phosphorylation with pressure in 18-20 week GK and age-matched WR cerebral arteries. No pressure-dependent change in the phosphorylation of LC_{20} was detected in cerebral arteries from 18-20 week GK rats. Phospho-LC_{20} content was not different at 10 mmHg in GK (30.2% ± 2.2) compared to WR (36.6% ± 0.5), but the levels were significantly lower at 60 and 120 mmHg in GK (33.3% ± 2.5 and 31% ± 2) compared to vessels of WR (46.4% ± 0.8 and 52.9% ± 0.9). Notably, these reduced levels of LC_{20} phosphorylation are coincident with the loss of the ability of 18-20 week GK vessels to develop pressure-dependent constriction within the physiological range (60-120 mmHg).

4.2.2.3 Pressure-dependent phosphorylation of MYPT1-T855 in cerebral arteries from 18-20 week WR

We investigated whether the loss of pressure-dependent LC_{20} phosphorylation is due to abnormal MYPT1-T855 phosphorylation in 18-20 week GK rats. First, we confirmed that there was a pressure-dependent change in MYPT1 phosphorylation at T855 with myogenic constriction in 18-20 week WR cerebral arteries. Similar to 8-10 week WR, pressure elevation from 10 to 60 (2.3 ± 0.24) and 120 mmHg (3 ± 0.07) was associated with an increase in phospho-MYPT1-T855 content in cerebral arteries of 18-20 week WR arteries as depicted in figure 4.9 (left blot in panel A and open bars in panel B).

4.2.2.4 Changes in phosphorylation of MYPT1-T855 with pressure in cerebral arteries from 18-20 week GK *vs* age-matched WR

Figure 4.9 compares the changes in MYPT1-T855 phosphorylation with pressure in 18-20 week GK and age-matched WR cerebral arteries. Consistent with the LC_{20} results, no significant change in phospho-MYPT1-T855 content was detected on pressure elevation from 10 (1 ± 0.12) to 60 (1.13 ± 0.2) and 120 mmHg (1.19 ± 0.18). These findings along with the LC_{20} phosphorylation data are consistent with the idea that an abnormal level of Ca^{2+} sensitization via MYPT1 phosphorylation and MLCP inhibition contributes to the impaired the myogenic response in 18-20 week GK cerebral arteries.

A

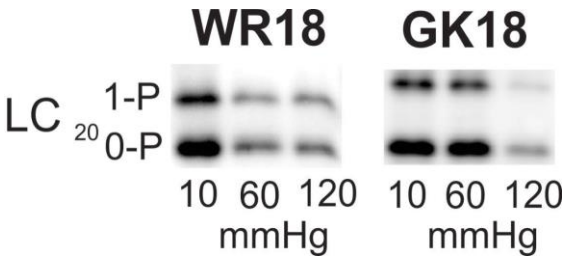

B

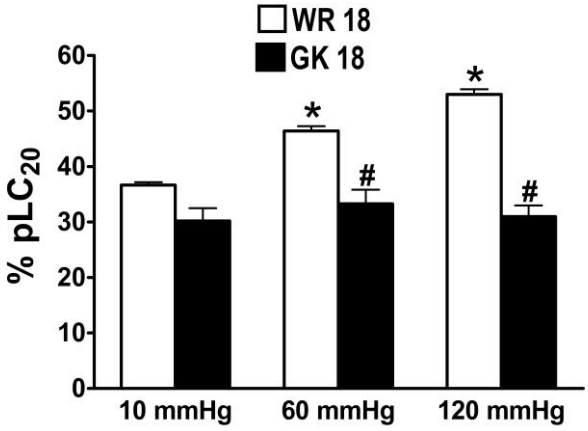

Figure 4.8: **Changes in LC_{20} phosphorylation with pressure in cerebral arteries from 18-20 week GK *vs* age-matched WR**

Representative western blots **(panel A)** and mean levels ± SEM **(panel B)** of phosphorylated LC_{20} as a percentage of total LC_{20} at 10, 60 and 120 mmHg in cerebral arteries from 18-20 week GK and age-matched WR (n=7). The unphosphorylated (0-P) and mono-phosphorylated (1-P) LC_{20} were separated by Phos-tag™ SDS-PAGE and visualized using pan-LC_{20} antibody.

* Significantly different ($p<0.05$) from WR at 10 mmHg. # Significantly different ($p<0.05$) from corresponding WR value.

A

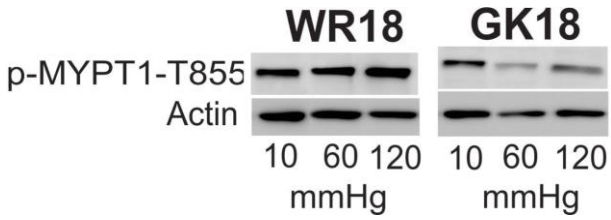

B

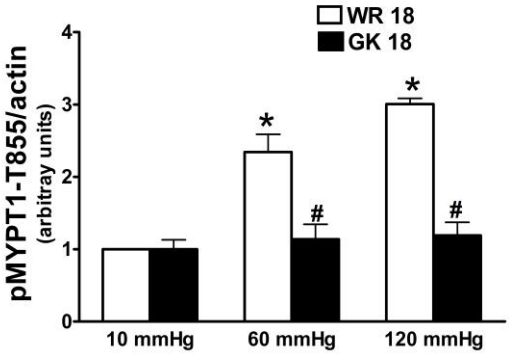

Figure 4.9: Changes in phosphorylation of MYPT1-T855 with pressure in cerebral arteries from 18-20 week GK *vs* age-matched WR

Panel A: Representative immunoblots for phospho-MYPT1-T855 and corresponding actin in each lane at 10, 60 and 120 mmHg in 18-20 week GK cerebral arteries and age-matched WR.

Panel B: Mean levels ± SEM of phospho-MYPT1-T855 normalized to the corresponding actin level in each lane for samples of cerebral arteries at 10, 60 and 120 mmHg from 18-20 week GK and age-matched WR with WR value at 10 mmHg set to 1 (n=8). * Significantly different ($p<0.05$) from WR value at 10 mmHg. # Significantly different ($p<0.05$) from corresponding WR value.

4.2.2.5 MYPT1 mRNA and protein levels in cerebral arteries from 18-20 week GK and age-matched WR

Figure 4.10 shows a comparison of MYPT1 transcript (relative to ß-actin; panel A) and protein levels (normalized to actin (panel B) and GAPDH (panel C)) in cerebral arteries from 18-20 week GK and age-matched WR. No difference was detected in the MYPT1 expression suggesting that the loss of pressure-dependent phosphorylation of MYPT1 is not due to differences in the level of expression of MYPT1 in the two groups.

4.2.2.6 Comparison of MYPT1 mRNA levels between GK and WR cerebral arteries

Expression levels of MYPT1 transcripts in cerebral arteries of 8-10 and 18-20 week GK rats and age-matched WR were quantified using real-time PCR; no differences in expression were apparent in the four groups. This suggested that neither age, strain or disease state affects the expression of MYPT1 mRNA in cerebral arteries of GK rats (Figure 4.11, panel A; same data as presented in figures 4.7 and 4.10).

4.2.2.7 Comparison of MYPT1 protein levels between GK and WR cerebral arteries

A comparison of the expression of MYPT1 protein in cerebral arteries of 8-10 and 18-20 week GK and age-matched WR did not show any significant differences between the four groups in the MYPT1 protein content normalized to actin (figure 4.11, panel B; same data as presented in figure 4.7. and 4.10) and GAPDH (figure 4.11, panel C; same data as presented in figure 4.7 and 4.10). This result along with the mRNA data presented in 4.2.2.6 supports the view that the changes in phosphorylation of MYPT1 in cerebral arteries of prediabetic and diabetic GK rats are due to differences in ROK activity rather than a change in the level of MYPT1 expression.

A

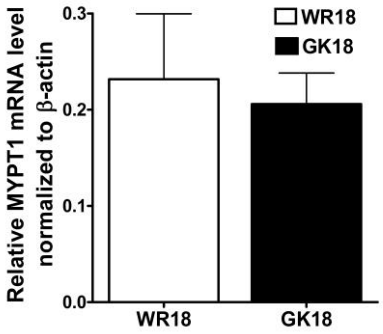

B

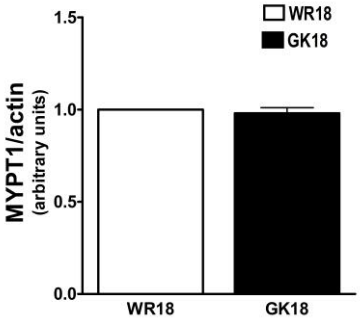

C

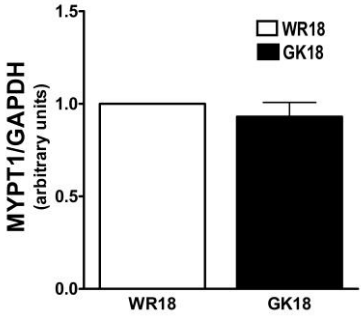

Figure 4.10: MYPT1 mRNA and protein expression in 18-20 week GK *vs* age-matched WR

Panel A: Mean levels ± SEM of MYPT1 transcripts relative to ß-actin determined by real-time PCR using mRNA derived from cerebral arteries of 18-20 week GK rats and age-matched WR. Relative transcript levels were determined using the $2^{-\Delta\Delta Ct}$ method (n=5).

Panel B,C: Mean levels ± SEM of MYPT1 protein normalized to actin (panel B) and GAPDH (panel C) in cerebral arteries from 18-20 week GK and age-matched WR with the value of WR set to 1 (n=10). Note the lack of significant difference in MYPT1 mRNA/protein between GK and WR vessels.

A

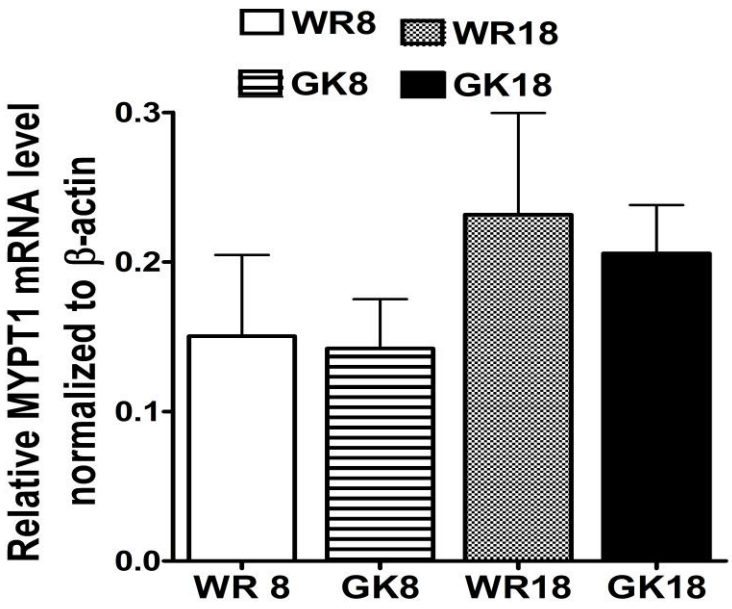
WR8
WR18
GK8
GK18
Relative MYPT1 mRNA level
normalized to β-actin
0.3
0.2
0.1
0.0
WR 8
GK8
WR18
GK18

B

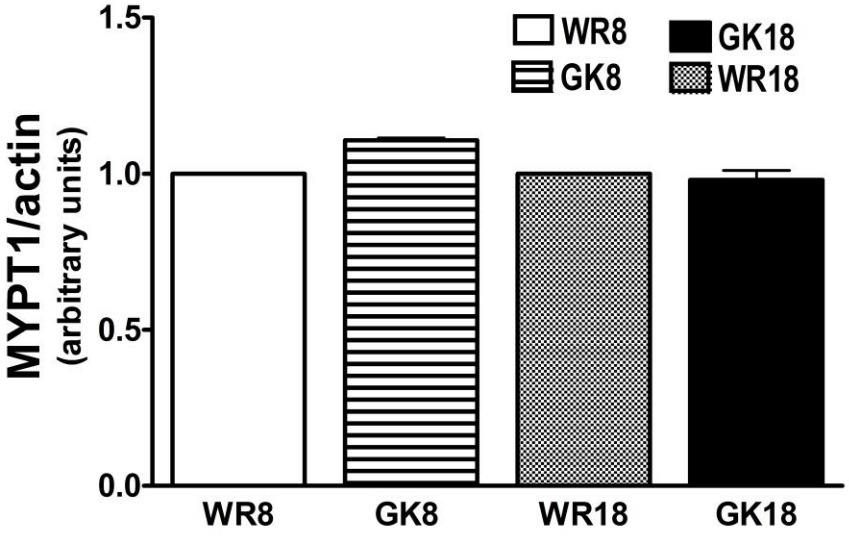
WR8
GK18
GK8
WR18
MYPT1/actin
(arbitrary units)
1.5
1.0
0.5
0.0
WR8
GK8
WR18
GK18

C

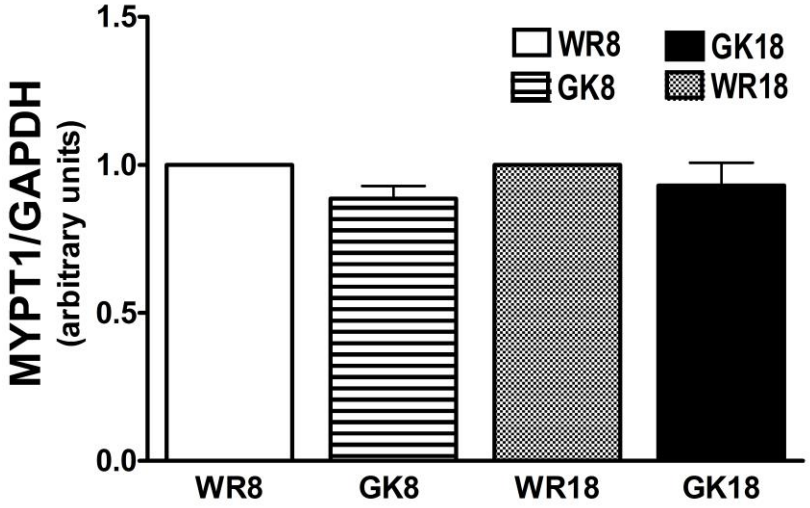

Figure 4.11: Comparison of MYPT1 mRNA and protein levels in GK *vs* WR cerebral arteries

Panel A: Mean levels ± SEM of MYPT1 transcripts relative to ß-actin determined by real-time PCR using mRNA derived from cerebral arteries of 8-10 and 18-20 week GK rats and age-matched WR. Relative transcript levels were determined by the $2^{-\Delta\Delta Ct}$ method (n=5).

Panel B,C: Mean levels ± SEM of MYPT1 protein normalized to actin (panel B) or GAPDH (panel C) in cerebral arteries from 8-10 and 18-20 week GK and age-matched WR with the value of WR at the corresponding age group set to 1 (n=10). Note the lack of significant difference in MYPT1 mRNA/protein between GK and WR vessels at both ages.

4.2.3 Summary of molecular changes in the Ca^{2+} sensitization mechanism in GK cerebral arteries

Here we have provided evidence for a role of dysfunctional regulation of the Ca^{2+} sensitization mechanism in GK cerebral arteries that is associated with impairment in the myogenic response as described in Chapter 3. The key findings of this first section of Chapter 4 are:

1. Elevated phosphorylation of LC_{20}, MYPT1-T855, and MYPT1-T697 were detected at low intraluminal pressure in cerebral arteries of 8-10 week GK rats. The enhanced phosphorylation of LC_{20} and MYPT1-T855, but not MYPT1-T697 was completely abolished by ROK inhibition with H1152.
2. Pressure elevation evoked an increase in the phosphorylation of MYPT1-T855 and consequently LC_{20} in WR, but not cerebral arteries of 8-10 or 18-20 week GK rats.
3. No differences in the mRNA or protein levels of MYPT1 in cerebral arteries were detected between the WR and GK rats supporting the view that detected changes in MYPT1 phosphorylation were not due to variations in MYPT1 expression between the two groups.

4.2.4 Molecular changes in the actin polymerization mechanism in GK cerebral arteries

As discussed in Chapter 1, dynamic actin cytoskeleton reorganization is now considered crucial for appropriate tone development in the myogenic response. The cortical actin cytoskeleton forms a subsarcolemmal network to transmit force generated by the contractile apparatus across the smooth muscle membrane and to the extracellular matrix within the vessel wall. This view is supported by findings from our laboratory and others that pressure elevation evokes a concomitant decrease in G-actin content and increase in active myogenic constriction (Mehta & Gunst, 1999; Cipolla et al., 2002; Moreno-Domínguez et al., 2013; Moreno-Domínguez et al., 2014). In this section, we investigated whether the progression of type 2 diabetes affected the process of actin polymerization and consequently the development of pressure-dependent constriction in GK cerebral arteries. G-actin content in the samples was normalized to SM22, a cytosolic smooth muscle specific protein that is retained exclusively in the supernatant following high-speed centrifugation, and the ratios were then compared (Walsh et al., 2011; Moreno-Domínguez et al., 2014).

4.2.4.1 Pressure-dependent changes in G-actin content in cerebral arteries from 8-10 week WR

A pressure-evoked decline in G-actin content was detected in cerebral arteries of 8-10 week WR (Figure 4.12, left blot in panel A and open bars in panel B). As reported earlier for cerebral and skeletal muscle resistance vessels from SD rats, pressure elevation from 10 mmHg was associated with a decrease in G-actin/SM22 ratio at 60 (0.44 ± 0.03) and 120 mmHg (0.32 ± 0.07). These findings confirm the presence of increased actin polymerization in the cerebral myogenic response of WR.

4.2.4.2 Changes in G-actin content with pressure in cerebral arteries from 8-10 week GK rats *vs* age-matched WR

Figure 4.12 compares the changes in G-actin content with pressurization in 8-10 week GK and age-matched WR cerebral arteries. The G-actin/SM22 ratio at 10 mmHg in GK cerebral arteries (0.58 ± 0.06) was significantly lower than that of WR vessels. No further change was detected upon pressurization to 60 (0.49 ± 0.02) or 120 mmHg (0.45 ± 0.05). This result suggests that actin polymerization is enhanced at low pressure, but not altered by further pressurization in GK cerebral vessels. This result is also consistent with the presence of elevated basalmyogenic tone observed in GK rats at 10 mmHg. (Chapter 3).

4.2.4.3 Pressure-dependent changes in G-actin content in cerebral arteries from 18-20 week WR

A similar pressure-dependent decrease in G-actin/SM22 ratio was detected in vessels of 18-20 week compared to 8-10 week WR (figure 4.13, left blot in panel A and open bars in panel B). This suggests that the actin polymerization mechanism was not affected by the age difference between the two groups of control animals.

4.2.4.4 Changes in G-actin content with pressure in cerebral arteries from 18-20 week GK rats *vs* age-matched WR

Figure 4.13 compares the changes in G-actin content with pressure in 18-20 week GK and age-matched WR cerebral arteries. Contrary to age-matched WR, pressurization did not evoke a change in the G-actin/SM22 ratio at 10 (0.87 ± 0.05), 60 (1.05 ± 0.04), and 120 mmHg (1.03 ± 0.12) in vessels from GK rats. The inability of pressurization to elicit increased actin polymerization within the cortical actin cytoskeleton would also be expected to contribute to the observed impairment of the cerebral myogenic constriction in 18-20 week GK rats.

4.2.5 Summary of molecular changes in the actin polymerization mechanism in GK cerebral arteries

As previously mentioned, dynamic actin cytoskeleton polymerization is increasingly viewed as a crucial mechanism for the development of myogenic constriction in cerebral arteries. In this section of Chapter 4, evidence was provided for the inappropriate regulation of actin polymerization in GK rats. Key findings of this section include:

1. Pressure elevation was associated with a decline in the G-actin pool in cerebral arteries from both age groups of WR employed.
2. In prediabetic 8-10 week GK cerebral arteries, the G-actin content was lower than WR control animals at basal intraluminal pressure.
3. No pressure-dependent change in the G-actin content was detected within the physiological range in either prediabetic or diabetic GK cerebral arteries.

A

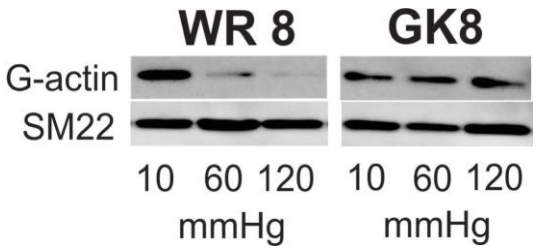

B

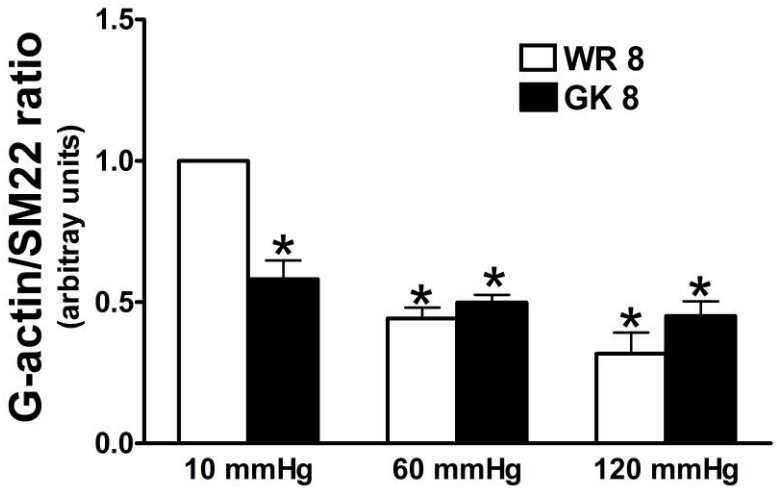

Figure 4.12: Changes in G-actin content with pressure in cerebral arteries from 8-10 week GK *vs* age-matched WR

Panel A: Representative western blots for G-actin and corresponding SM22 in each lane at 10, 60 and 120 mmHg for 8-10 week GK cerebral arteries and age-matched WR.

Panel B: Mean levels ± SEM of G-actin content normalized to the corresponding SM22 level in each lane at 10, 60 and 120 mmHg for 8-10 week GK cerebral arteries and age-matched WR with the value for WR at 10 mmHg set to 1 (n=6). * Significantly different ($p<0.05$) from WR value at 10 mmHg.

A

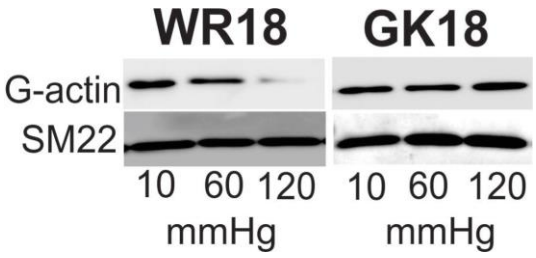

B

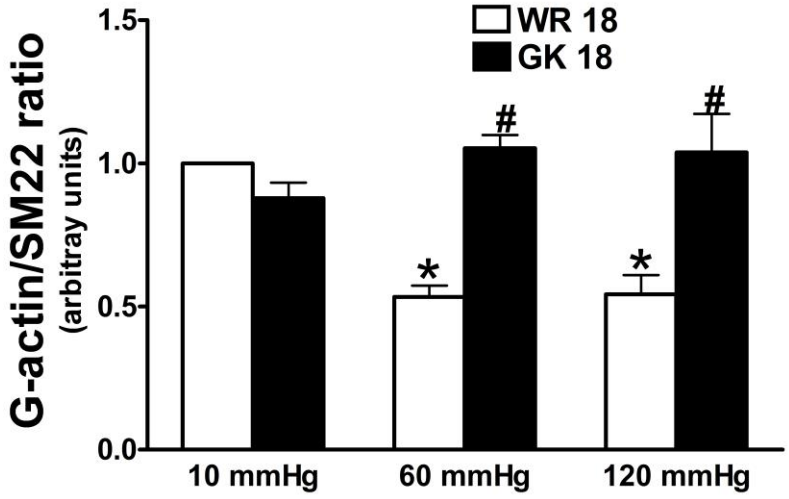

Figure 4.13: Changes in G-actin content with pressure in cerebral arteries from 18-20 week GK *vs* age-matched WR

Panel A: Representative western blots for G-actin and corresponding SM22 in each lane at 10, 60 and 120 mmHg for 18-20 week GK cerebral arteries and age-matched WR.

Panel B: Mean levels ± SEM of G-actin content normalized to the corresponding SM22 level in each lane at 10, 60 and 120 mmHg for 18-20 week GK cerebral arteries and age-matched WR with the value for WR at 10 mmHg set to 1 (n=6). * Significantly different ($p<0.05$) from WR value at 10 mmHg. # Significantly different ($p<0.05$) from corresponding WR value.

4.2.6 Defects in upstream signaling pathway that could underlie the abnormal regulation of Ca^{2+} sensitization and actin polymerization mechanisms in prediabetic GK rats

We detected an increase in the phosphorylation of LC_{20} and MYPT1-T855, and in actin polymerization at low intraluminal pressure, with the former being abolished by ROK inhibition with H1152 in 8-10 week GK cerebral arteries. We concluded that an elevated basal level of ROK activity was responsible for these changes and the resulting augmented constriction at low pressure. ROK has two different isoforms, ROK1 (or ROK-β) and ROK2 (or ROK-α), that are both activated by the small GTPase, RhoA. Both isoforms are ubiquitously expressed in invertebrates and vertebrates, with ROK1 abundant in circulating inflammatory cells and ROK2 abundant in VSMCs (Satoh et al., 2011). Here we focused on ROK2 because of its high expression levels in VSMCs, and employed real-time PCR and western blotting to detect any differences in its expression in vessels from 8-10 week GK and WR. We also investigated whether abnormal integrin signaling contributes to the loss in pressure-evoked change of phosphoproteins in prediabetic GK vessels.

4.2.6.1 ROK mRNA/protein expression in cerebral arteries from 8-10 week GK *vs* age-matched WR

The levels of ROK2 mRNA and protein were quantified using real-time PCR and western blotting, respectively, in cerebral arteries of 8-10 week GK rats and age-matched WR (figure 4.14). No significant difference was detected in ROK2 mRNA or protein content in GK *vs* age-matched WR cerebral arteries. For this reason, we attributed the change in the ROK-mediated responses in GK cerebral arteries to a change in the activation of ROK, rather than an increased level of its expression.

4.2.6.2 RhoA mRNA levels in cerebral arteries from 8-10 week GK *vs* age-matched WR

It is possible that the increased MYPT1-T855 phosphorylation and altered actin dynamics in prediabetic GK cerebral arteries is due to an enhanced activation and/or expression of RhoA, the upstream activator of ROK2. We excluded the possibility of a change in the expression of RhoA by comparing the level of RhoA transcripts relative to ß-actin in cerebral arteries of 8-10 week GK and age-matched WR using real-time PCR (figure 4.15). The expression of RhoA mRNA was not different between the two strains suggesting that a greater level of RhoA activation rather than expression was responsible for the enhanced ROK2-mediated phosphorylation of MYPT1-T855 in cerebral arteries of 8-10 week GK rats.

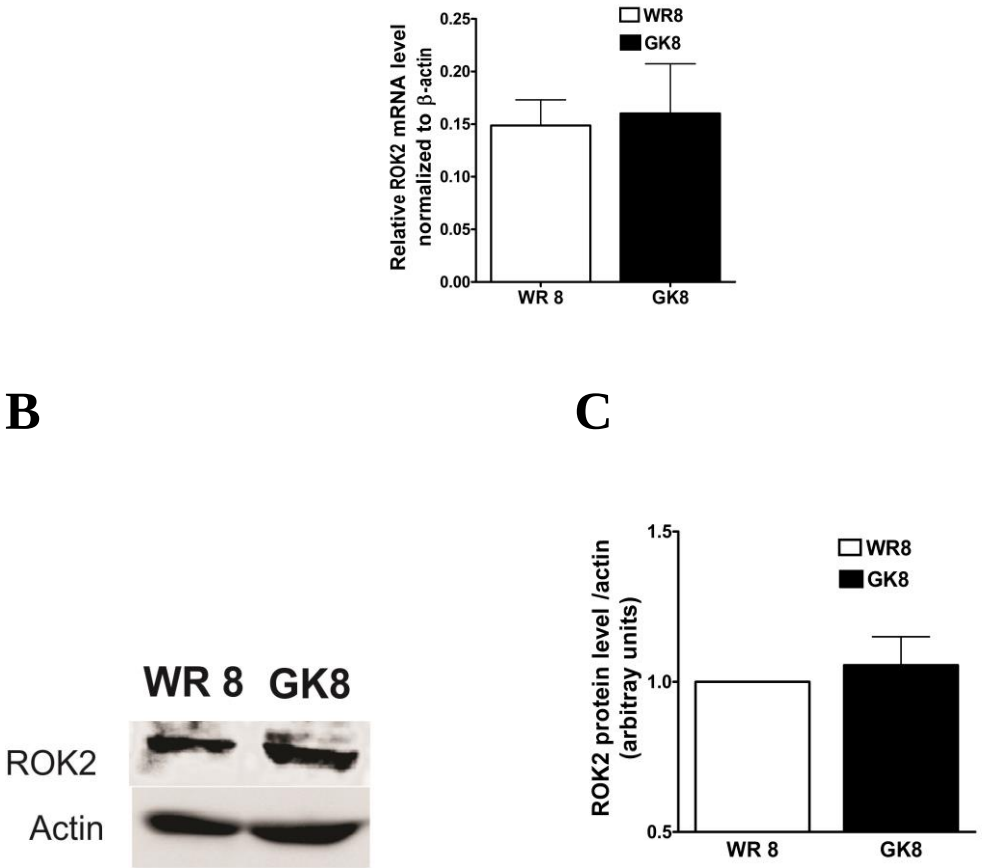

Figure 4.14: ROK2 mRNA and protein levels in cerebral arteries from 8-10 week GK *vs* age-matched WR

Panel A: Mean values ± SEM for level of ROK2 transcript expression relative to ß-actin determined by real-time PCR using mRNA derived from cerebral arteries of 8-10 week GK and age-matched WR. Relative transcript levels were determined by the $2^{-\Delta\Delta Ct}$ method (n=5).

Panel B,C: Representative immunoblots (panel B) and mean levels ± SEM (panel C) of ROK2 protein normalized to actin in cerebral arteries from 8-10 week GK and age-matched WR with the value of WR set to 1 (n=4). Note: no significant differences in mRNA or protein levels of ROK2 between GK and WR vessels were detected.

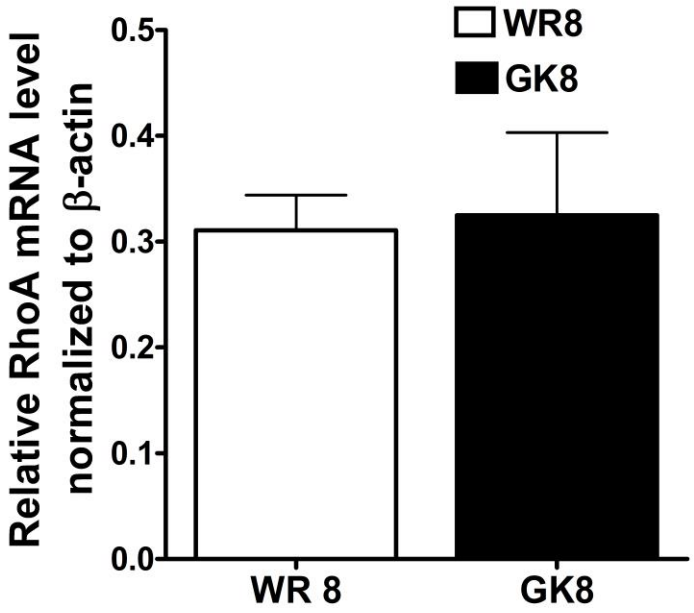

Figure 4.15: RhoA mRNA level in cerebral arteries from 8-10 week GK *vs* age-matched WR

Mean levels ± SEM of RhoA transcript relative to ß-actin determined by real-time PCR from mRNA derived from cerebral arteries of 8-10 week GK rats and age-matched WR. Relative transcript levels were determined using the $2^{-\Delta\Delta Ct}$ method (n=5). Note: no significant difference in mRNA level of RhoA between GK and WR vessels was detected.

4.2.6.3 Integrins, FAK phosphorylation and the myogenic response

4.2.6.3.1 Integrins and the myogenic response

A mechanotransduction mechanism is essential to detect changes in intraluminal pressure and transduce this signal into a contractile response. As discussed in Chapter 1, several candidate mechanosensors have been described to date. Stimulation of integrin adhesions is known to initiate cellular signaling responsible for VSMC contractility via Ca^{2+}-dependent activation of MLCK, and/or RhoA/ROK-, Cdc42- and PKC-dependent signaling to inhibit MLCP and activate actin cytoskeleton polymerization in many cell types (DeMali et al., 2003; Legate et al., 2009) and it was postulated that similar mechanisms contribute to the development of pressure-dependent myogenic constriction in resistance arteries (Davis et al., 2001; Wu et al., 2001; Martinez-Lemus et al., 2005; Walsh & Cole, 2013; Colinas et al., 2015).

4.2.6.3.2 Integrins and FAK phosphorylation

Mechanical activation of integrin adhesions evokes an increase in tyrosine autophosphorylation of adhesion proteins, FAK and SFK, that is considered to be an essential initial event in integrin signaling (Clark & Brugge, 1995; Thomas & Brugge, 1997). A pressure-induced FAK-Y397 phosphorylation was detected in mesenteric resistance arteries in the context of structural remodeling of vessels due to hypertension (Rice et al., 2002). Recently, Colinas et al. (2015) have provided direct evidence of a pressure-dependent increase in FAK-Y397 and SFK-Y416 phosphorylation in rat cerebral arteries. Anti-α5 integrin blocking antibodies, FAK inhibitor, and selective SFK inhibitor abolished the myogenic response within the physiological range in cerebral arteries and reduced the pressure-evoked autophosphorylation of FAK-Y397 and SFK-Y416. This inhibition of pressure-dependent autophosphorylation of FAK and SFK was also associated with reduced phosphorylation of LC_{20} and MYPYT1-T855 and inhibition of the

pressure-evoked decline in G-actin. These findings support the view that FAK and SFK autophosphorylation downstream of integrin activation is crucial for development of the myogenic response within the physiological pressure range (Colinas et al., 2015). Based on the observed loss of pressure-evoked phosphorylation of LC_{20}, MYPT1-T855 and actin polymerization in prediabetic GK cerebral arteries, we investigated whether inappropriate FAK autophosphorylation in response to intraluminal pressure elevation may contribute to the abnormal pressure-evoked responses in prediabetic GK cerebral arteries.

4.2.6.3.3 Pressure-dependent phosphorylation of FAK-Y397 in cerebral arteries from 8-10 week WR

The effect of pressure elevation on phosphorylation of FAK-Y397 in cerebral arteries of 8-10 week WR is shown in figure 4.16 (left blot in panel A and open bars in panel B). Pressurization from 10 to 80 mmHg was accompanied by an ~3-fold (2.8 ± 0.3) increase in the autophosphorylation of FAK at Y397, but no further change was detected at 120 mmHg (2.3 ± 0.28). These results are consistent with data from our laboratory employing SD cerebral arteries that showed an increase in FAK-Y397 phosphorylation at 80 mmHg with no further change at 120 mmHg (Colinas et al., 2015).

4.2.6.3.4 Changes in phosphorylation of FAK-Y397 with pressure in cerebral arteries from 8-10 week GK *vs* age-matched WR

Figure 4.16 compares the effect of pressure elevation on FAK-Y397 phosphorylation in cerebral arteries of 8-10 week GK and age-matched WR. Contrary to WR cerebral arteries, no pressure-dependent change in the phosphorylation of FAK-Y397 was detected in cerebral vessels from GK rats. This result is consistent with the lack of pressure-evoked change in the

phosphorylation of LC_{20} and MYPT1-T855, and G-actin content within the physiological pressure range described earlier in this Chapter.

4.2.6.4 Summary of molecular changes in the upstream signaling mechanisms that could underlie the dysfunctional myogenic response in cerebral arteries of prediabetic GK rats

In the final section of the results, we focused on exploring the upstream signaling defects that may explain the dysfunctional control of cerebral arterial diameter in response to pressure elevation in prediabetic GK rats. We separated the molecular defects of prediabetic cerebral arteries into two components, the first being the enhanced basal myogenic tone associated with augmented MYPT1 and LC_{20} phosphorylation, and actin polymerization at low intraluminal pressure that is ROK-mediated, and the second being the impaired myogenic reactivity associated with lack of pressure-evoked MYPT1 and LC_{20} phosphorylation, and actin polymerization.

No change in RhoA or ROK2 expression at both mRNA and protein levels was detected in 8-10 week GK cerebral arteries compared to age-matched WR. This finding indicates that an enhanced activation of RhoA and/or ROK2 activity may contribute to the enhanced level of basal myogenic tone in prediabetic GK cerebral arteries at low intraluminal pressure. A lack of pressure-dependent FAK autophosphorylation, an important initial step in integrin signaling, was also detected. This indicates a possible role for abnormal integrin signaling as the cause of the loss of pressure-evoked regulation of the contractile mechanism and actin dynamics observed in cerebral arteries of prediabetic GK rats between 60 and 120 mmHg and consequently impaired myogenic reactivity.

A

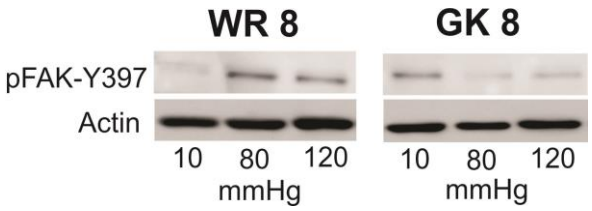

B

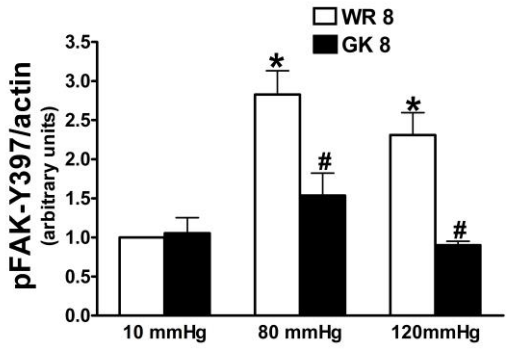

Figure 4.16: Changes in phosphorylation of FAK-Y397 with pressure in cerebral arteries from 8-10 week GK *vs* age-matched WR

Panel A: Representative western blots for phospho-FAK-Y397 and corresponding actin in each lane for cerebral arteries at 10, 80 and 120 mmHg from 8-10 week GK rats and age-matched WR.

Panel B: Mean levels ± SEM of phospho-FAK-Y397 normalized to the corresponding actin level in each lane for samples of cerebral arteries at 10, 80 and 120 mmHg from 8-10 week GK and age-matched WR with the value for WR at 10 mmHg set to 1 (n=5). * Significantly different ($p<0.05$) from WR value at 10 mmHg. # Significantly different ($p<0.05$) from corresponding WR value.

Chapter Five: Discussion

5.1 Overview and summary of the results

Sir William Bayliss discovered the myogenic response more than a hundred years ago (Bayliss 1902) and concluded that it is a crucial mechanism for the control of blood flow to body organs in response to changes in intravascular pressure. Since then the molecular mechanisms of cerebral blood flow autoregulation have been extensively studied by many researchers specifically addressing the role of myogenic control in the cerebral circulation. A detailed understanding of the molecular basis for the development of myogenic tone in cerebral arteries was greatly improved after the development of an ultra-sensitive western blotting technique capable of detecting differences in phosphoprotein and G-actin content in small segments of pressurized resistance arteries (Takeya et al., 2008). Utilization of this technique in the present investigation allowed us to quantify small amounts of ROK, phosphorylated MYTP1 and LC_{20}, and G-actin in single pressurized resistance arteries from GK rats at different stages in the development of type 2 diabetes. Taken together, the present results combined with previous findings provide major advances in our understanding of the role of Ca^{2+} sensitization and actin polymerization in the cerebral myogenic response, and that defects in the activation of these mechanisms can contribute to impairment of this fundamental physiological mechanism in disease.

Impaired myogenic constriction has been detected in multiple vascular beds of type 2 diabetic animals and patients, including the cerebral vasculature (Schofield et al., 2002; Didion et al., 2007; Kelly-Cobbs et al., 2011; Kold-Petersen et al., 2012). Why this fundamental mechanism of blood flow autoregulation is defective in type 2 diabetes is unknown. Much attention has been devoted to the well-characterized loss of endothelium-dependent vasodilation

in diabetes (Muris et al., 2013). However, it is now clear that the contractile function of VSMC is also affected by the disease independent of endothelial dysfunction (Abd-Elrahman et al., 2015).

The experiments described in this thesis were designed to detect molecular changes in the contractile mechanisms of VSMCs that could underlie the abnormal pressure-dependent control of cerebral arterial diameter in a rat model of type 2 diabetes, the GK rat. Given the crucial role played by the myogenic response in normal functioning of the cerebral circulation (Faraci & Heistad, 1990), delineating the molecular basis of impaired cerebral myogenic constriction is an important step forward in understanding the causes of abnormal cerebrovascular autoregulation and the increased incidence of ischemic and hemorrhagic stroke in diabetic patients (Giorda et al., 2007). Moreover, it provides new insights that may eventually lead to alternative therapeutic options that could be used to prevent or retard the progression of cerebrovascular disease associated with type 2 diabetes.

The findings presented in this thesis provide evidence for an abnormal myogenic response in prediabetic GK cerebral arteries and indicate that the extent of dysfunction increases with the severity of the diabetic condition, resulting in a complete loss of cerebral myogenic regulation in animals with established type 2 diabetes. Our biochemical evidence shows that there are parallel, progressive alterations in MYPT1 and LC_{20} phosphorylation, as well as G-actin content that are consistent with the evolution of dysfunction in the myogenic response. Focusing on the prediabetic GK cerebral arteries, the abnormal myogenic response was separated into two components: (i) an enhanced basal myogenic tone at low intraluminal pressure (below 40 mmHg), and (ii) an impaired myogenic reactivity; i.e. impaired pressure-evoked change in diameter within the physiological range (60-120 mmHg). Our biochemical results indicate that the enhanced myogenic tone detected at low intraluminal pressure may be attributed to an

enhanced activation of ROK rather than a change in its level of the expression. Moreover, the loss of myogenic reactivity was associated with a lack of a pressure-evoked change in MYPT1 and LC_{20} phosphorylation as well as G-actin content and may be the result of abnormal FAK phosphorylation downstream of integrin activation by intraluminal pressure increase.

5.2 GK rats as a model for type 2 diabetes

The GK rat is a non-obese Wistar substrain that exhibits spontaneous onset of diabetes early in life (4-5 weeks of age) due to polygenic factors. Although type 2 diabetes is usually associated with obesity in Western societies, about 60 % of type 2 diabetic individuals in Asian populations are non-obese (Brunetti, 2007). The GK rat model also permits the study of diabetes-related characteristics without the influence of confounding hyperlipidemia and/or obesity-related factors (Nie et al., 2011). We did not detect a change in blood glucose or insulin levels up to the end of the 9^{th} week of age. However, at the beginning of the 10^{th} week, blood glucose and insulin levels started to progressively increase suggesting that by the 8^{th} week insulin resistance is evident and the subsequent rise in insulin is a compensatory response to the preexisting resistance to insulin action in tissues. This view is consistent with previous reports indicating that insulin resistance is evident in GK rats as early as 4 to 5 weeks and leads to hyperinsulinemia in older animals (O'Rourke et al., 1997; Gao et al., 2011). These differences in young versus older GK rats were exploited here to document the progressive changes in the myogenic response by comparing 8-10 week prediabetic, insulin resistant and 18-20 week established diabetic rats.

5.3 The myogenic response of WR cerebral arteries

The myogenic response of cerebral arteries from control WR was evaluated to replicate the reported results obtained using the same vascular bed in SD rats (Johnson et al., 2009; El-

Yazbi et al., 2010; Moreno-Domínguez et al., 2013). Pressure-dependent constriction within the physiological range was associated with a parallel pressure-evoked increase in the phosphorylation of LC_{20} & MYPT1-T855 and pressure-evoked decline in G-actin content. No differences in the behaviour were detected in 8-10 and 18-20 week WR indicating that aging within this range does not affect myogenic control of cerebral arterial diameter. This result also implies that any differences detected between the prediabetic and diabetic GK cerebral arteries may be attributed to the progression of diabetes rather than aging. Also, our data for the myogenic response of WR cerebral arteries emphasize the crucial role of ROK in the myogenic response as treatment with H1152 completely abolished the myogenic constriction within the physiological range.

5.4 The myogenic response of GK cerebral arteries

GK cerebral arteries show a compromised myogenic response at 8-10 weeks of age (enhanced basal myogenic tone and impaired myogenic reactivity) that progress to an impaired pressure-evoked constriction within the physiological range by 18-20 weeks of age. These findings are consistent with previous reports describing an enhanced myogenic response in 10 week GK cerebral arteries progressing to a loss of the myogenic response in 18-22 week animals (Li et al., 2010; Kelly-Cobbs et al., 2011; Kold-Petersen et al., 2012). These results are also consistent with the initial development of higher blood pressure values in GK animals beginning at the 8^{th} week of age (Kelly-Cobbs et al., 2011; Rao et al., 2013). However, Kelly-Cobbs et al. (2011) detected an enhanced myogenic constriction at high pressures (between 80 and 140 mmHg), but not at low pressure in 10 week GK cerebral arteries. Moreover, the loss of myogenic constriction in 18 week GK cerebral arteries was attributed to vascular remodeling. Cerebrovascular remodeling was not evident in our study at least up to the age of 20 weeks since

no change in the passive diameter was detected between 18-20 week GK and age-matched WR. The slight variations in myogenic behaviour reported in this thesis and by Kelly-Cobbs and colleagues may be due to the difference in the GK rat colonies employed. Here we used rats from a commercially available GK colony that was transferred to Canada from Charles River laboratories in Japan. In contrast, Kelly-Cobbs et al. (2011) employed animals from a colony that was initiated by breeding pairs in Aarhus, Denmark and subsequently transferred to Taconic Laboratories, USA. The slight differences in the myogenic response at similar ages may thus reflect variations in the age-dependent progression of the disorder and/or severity of the condition between these different colonies.

Given the fact that there was no change in blood glucose and insulin level, the enhanced basal myogenic tone of prediabetic 8-10 week GK cerebral arteries may be linked to the presence of insulin resistance. As discussed earlier, vascular resistance to the actions of insulin results in a selective impairment of the PI3K pathway that maintains a vasodilatory influence of insulin on VSMC (Muniyappa & Quon, 2007; Muniyappa et al., 2007; Lee et al., 2009). It is possible that the lack of insulin action due to the presence of insulin resistance is the trigger responsible for the enhanced basal tone in GK cerebral arteries. On the other hand, the MAPK pathway remains unaffected by insulin resistance, but it is over-activated by the compensatory hyperinsulinemia encountered in older GK animals. The consequences of MAPK pathway over-activation include VSMC proliferation and endothelin-1 release (Lee et al., 2009; Muniyappa & Quon, 2007; Muniyappa et al., 2007). These factors may provoke a switch in cerebral VSMCs to a proliferative, non-contractile phenotype in older GK animals and contribute to the loss of the myogenic response at this age.

It is worth noting that although we detected changes in the myogenic response of prediabetic and diabetic GK cerebral arteries, we focused on identifying the molecular defects at the early disease stage (prediabetic). This approach was taken based on the view that understanding the basis for dysfunction at this stage may provide better insights concerning novel therapeutic targets that could be exploited to delay the evolution of defects with the disease progression. Our focus for the prediabetic GK rats was to understand the mechanisms that contribute to the enhanced myogenic tone between 10 and 40 mmHg. Although there was no significant change in cerebral artery diameter between GK and WR with in the physiological range, impaired myogenic reactivity compromises the ability of the vessels to dilate in response to pressure decline and is expected to have major consequences on flow autoregulation.

To understand the molecular basis for this abnormal myogenic behavior of the GK rats, we investigated two major mechanisms involved in the myogenic response, specifically Ca^{2+} sensitization and dynamic actin cytoskeletal reorganization. The calcium-dependent activation of MLCK as a mechanism for the myogenic response was not directly addressed in this thesis. Although its possible contribution to the abnormal myogenic response in GK rats cannot be ruled out, previous studies detected no difference in the pressure-evoked $[Ca^{2+}]_i$ increase in cerebral arteries of 20 week GK rats compared to WR control (Kold-Petersen et al., 2012). It therefore seemed prudent for us to focus on the Ca^{2+} sensitization and dynamic actin cytoskeleton remodeling mechanisms as a cause of the myogenic dysfunction observed in this study.

5.5 Ca^{2+} sensitization and the abnormal myogenic constriction of prediabetic GK cerebral arteries

To investigate the role of Ca^{2+} sensitization in the abnormal myogenic response detected in GK cerebral arteries, we measured phosphorylation of MYPT1-T855 and T697 as the two

major sites for phosphorylation of MYPT1 by ROK that are known to inhibit MLCP activity (Feng et al., 1999; Cole & Welsh, 2011). LC_{20} phosphorylation was also quantified to confirm the downstream consequences of any changes in MLCP activity of GK cerebral arteries.

5.5.1 Role of MYPT1–T855 and LC_{20} phosphorylation downstream of ROK in the abnormal myogenic response of prediabetic GK cerebral arteries

We detected an increase in MYPT1-T855 and LC_{20} phosphorylation in 8-10 week GK cerebral arteries at low intraluminal pressure and a loss of pressure-dependent increase in the phosphorylation of LC_{20} and MYPT1-T855 over the physiological range of pressure. These findings suggest that an increase in MYPT1-T855 leading to greater inhibition of MLCP and an enhanced phosphorylation of LC_{20} contributes to the augmented myogenic constriction at low intraluminal pressure in cerebral arteries of prediabetic GK rats. This view is based on the finding that treatment with ROK inhibitor reversed the augmented constriction between 10 to 80 mmHg and completely abolished the increase in MYPT1-T855 and LC_{20} phosphorylation at low pressure. We did not detect any change in the protein expression of ROK2 (ubiquitously expressed in VSMCs) in cerebral arteries from 8-10 week GK compared to age-matched WR. Moreover, the level of RhoA mRNA was also not different. For this reason, we postulate that the enhanced basal tone in prediabetic GK cerebral arteries results from an increase in ROK2 activation owing to greater RhoA activity, or due to an as yet unidentified alternative mechanism as discussed below.

This scenario is supported by previous reports implicating the RhoA/ROK pathway in abnormal VSMC contraction in different diabetic models. For instance, contractions induced by serotonin, angiotensin II, phenylephrine and high $[K^+]$ were significantly greater in aortic and mesenteric artery smooth muscle strips isolated from *db/db* diabetic mice compared to control

mice due to higher ROK activity in the former compared to the latter (Guo et al., 2005). Enhanced activation of the RhoA/ROK pathway was also detected in another study employing cultured vascular tissue from type 2 diabetic *db/db* mice with no significant change in ROK expression (Xie et al., 2006). The activated ROK in mesenteric arteries from *db/db* diabetic mice caused inhibition of MLCP activity resulting in an increase in the phosphorylation of LC_{20} and augmented VSMC contraction, contributing to an enhanced contractile response to phenylephrine (Nobe et al., 2009). A RhoA/ROK mechanism was also suggested to contribute to the development of diabetes-associated hypertension and the enhanced contractile response of mesenteric resistance arteries to agonist stimulation with no apparent change in RhoA, ROK1 or ROK2 protein expression (Rao et al., 2013). Serotonin-induced contractions were also augmented in carotid arteries of GK rats apparently as a result of enhanced ROK activation rather than an increase in expression level (Matsumoto et al., 2010; Matsumoto et al., 2014).

The mechanism(s) responsible for the enhanced ROK activity in VSMC of type 2 diabetes has not been identified with certainty. However, the mechanisms suggested to date include: increased oxidative stress that is known to stimulate the kinase activity of ROK (Didion et al., 2007), loss of endothelium-derived NO that normally functions to suppress ROK activity (Sauzeau et al., 2000), and/or defective insulin- and insulin receptor-signaling (Begum, 2003). We did not detect a significant difference in the acetylcholine-induced vasorelaxation of pressurized, endothelium-intact prediabetic GK cerebral arteries compared to WR control (preliminary observations). This suggested that the cause of the enhanced activity of ROK in prediabetic GK cerebral arteries may be traced to abnormalities in the VSMC rather than endothelial cells. There is considerable evidence for interplay between the RhoA/ROK pathway and insulin receptor signaling in VSMCs in the literature as discussed in the following section.

5.5.2 Crosstalk between defective insulin signaling and the RhoA/ROK pathway in diabetic VSMCs in the context of Ca^{2+} sensitization

Cultured aortic VSMCs from 7-8 week-old GK rats have been employed to demonstrate the presence of crosstalk between insulin signaling and ROK activity in the context of the control of VSMC contractility (Begum et al., 2000; Sandu et al., 2000; Lee et al., 2009). Insulin was found to activate MLCP by decreasing MYPT1 phosphorylation in control VSMCs from WR via two different signaling mechanisms. First, insulin inactivates ROK by blocking RhoA activation and translocation to the membrane fraction. Second, insulin induces iNOS expression via PI3K signaling leading to generation of NO/cGMP that elicits vasorelaxation through several mechanisms including suppression of RhoA activation (Begum, 2003; Moncada & Higgs, 2006). Diabetes in GK was accompanied by a lack of an insulin-mediated decrease in MYPT1 phosphorylation in cultured VSMCs due to impaired inhibition of ROK. Moreover, studies have shown a marked reduction in insulin-stimulated IRS-1 tyrosine phosphorylation, PI3K activity and iNOS-mediated vasorelaxation in VSMCs of GK rats compared to WR control; i.e. preferential inactivation of PI3K/NO/cGMP signaling in response to insulin receptor activation. Thus, the authors concluded that insulin resistance of GK VSMCs is accompanied by defective insulin-mediated ROK inhibition and PI3K/Akt/iNOS/cGMP signaling, the two major mechanisms participating in insulin-evoked MYPT1 activation and vasorelaxation (Sandu et al., 2000; Begum et al., 2002).

Although the above-discussed studies were conducted in cultured VSMCs that do not necessarily mimic the myocytes present in intact vessels, they indicate the potential mechanisms of crosstalk between insulin resistance and RhoA/ROK signaling. It is thus possible that insulin resistance may directly result in elevated ROK activity owing to the loss of a basal inhibitory

action of insulin on ROK activity via the PI3K pathway. Alternatively, insulin evokes geranylgeranylation and activation of RhoA via the MAPK pathway (Wang et al., 2004). Thus, an increase in MAPK activity as a consequence of insulin resistance could also be responsible for activation of ROK signaling detected here. The balance between ROK inhibition and activation evoked by the PI3K and MAPK pathways, respectively, will determine the overall effect of insulin on vessel diameter and is dominated by the vasodilatory influence on the PI3K pathway in physiological situations (Anfossi et al., 2009). Thus, a preferential inactivation of PI3K/NO/cGMP due to insulin resistance (Begum, 2003; Muniyappa et al., 2007; Anfossi et al., 2009) would be accompanied by unopposed MAPK signaling and enhanced ROK activation in type 2 diabetes. Unfortunately, to the best of our knowledge, no previous studies of the molecular basis of insulin-evoked signaling or how this signaling is affected in type 2 diabetes have been conducted using intact resistance arteries. Possible suggestions for future experiments to address this lack of information are discussed in detail in Chapter 7.

Interestingly, chronic inhibition of ROK in insulin-resistant Zucker obese rats prevented the development of insulin resistance, hypertension, dyslipidemia, and obesity. These beneficial actions of ROK inhibition were attributed mainly to the restoration of insulin signaling. This finding suggests that enhanced ROK activity may actually contribute to the development of insulin resistance via serine phosphorylation of a critical protein in insulin signaling, possibly IRS-1, causing a feed-forward suppression of PI3K signaling (Begum et al., 2002; Kanda et al., 2006). Taken together, these findings suggest that there is a mutual interaction between RhoA/ROK and insulin signaling that exists to properly regulate the hemodynamic and metabolic actions of insulin. Defects in insulin signaling would influence RhoA/ROK signaling causing metabolic abnormalities to be associated with vascular dysfunction.

5.5.3 Role of MYPT1-T697 phosphorylation in the abnormal myogenic response of prediabetic GK cerebral arteries

The other phosphorylation site on MYPT1 that is known to inhibit the activity of MLCP when phosphorylated by ROK is T697 (Feng et al., 1999). We have previously shown that the phosphorylation of MYPT1-T697 does not play a role in development of the myogenic response within the physiological pressure range (60-120 mmHg), but increased MYPT1-T697 phosphorylation was observed at non-physiological high pressure, 140 mmHg, or in the presence of both pressure and agonist, 80 mmHg and serotonin (El-Yazbi et al., 2010).

MYPT1-T697 phosphorylation was elevated in 8-10 week GK cerebral arteries at all pressures and was not sensitive to the ROK inhibitor, H1152. The elevated phosphorylation of MYPT1-T697 in prediabetic GK cerebral arteries may contribute to the enhanced basal myogenic tone observed in these vessels by causing a further inhibition of MLCP activity. Begum et al. (2002) showed that insulin via an NO/cGMP-mediated mechanism inhibits ROK activity and reduced MYPT1-T697 phosphorylation in cultured aortic VSMCs which would be expected to elicit vasorelaxation. Contrary to this report, ROK inhibition did not affect the enhanced MYPT1-T697 phosphorylation in our experiments suggesting that the increased phospho-MYPT1-T697 in GK cerebral arteries was not due to ROK. It is significant that reported changes in MTPT1-T697 phosphorylation in response to insulin reported by Begum et al. (2002) were detected in cultured VSMCs from control animals; no data were presented for VSMCs from GK rats. However, these observations imply that insulin can influence the phosphorylation of MYPT1-T697 and that this signal may be altered in insulin resistance that would explain altered MYPT1-T697 phosphorylation in prediabetic GK cerebral arteries.

Although ROK is known to phosphorylate MYPT1 at the T697 site, several additional protein kinases are known to mediate phosphorylation of the same site, including zipper interacting protein kinase (ZIPK) (Ihara & MacDonald, 2007), myotonic dystrophy protein kinase (DMPK) (Murányi et al., 2001), integrin-linked kinase (ILK) (Murányi et al., 2002), and p21-activated protein kinase (Takizawa et al., 2002). This might suggest a possible role of any of these kinases in the abnormal control of cerebral arterial diameter in GK rats. This view is supported by published reports; for example, ILK was found to be over-expressed in the retina of streptozotocin-induced diabetic rats and postulated to be the cause of diabetes-induced damage and/or alterations of neural and microvascular structures in the retina (Li et al., 2007). In another study, changes in DMPK expression were found to directly influence insulin signaling, glucose homeostasis and the onset of insulin resistance in diabetic patients (Llagostera et al., 2007). Thus, further studies are required to determine the role of ZIPK, ILK and DMPK in the dysfunctional pressure-dependent control of diameter and their link to the effects of insulin resistance on GK cerebral arteries.

5.5.4 MYPT1 mRNA and protein expression are not different between cerebral arteries of GK and control rats

MYPT1 protein expression was not different between GK and WR rats in the two age groups employed in this study. This conclusion was confirmed at the mRNA level by real-time PCR and at the protein level by western blotting. This result ruled out the possibility of a change in MYPT1 expression secondary to aging or disease progression. Moreover, the data provide evidence that changes in MYPT1 phosphorylation detected in GK cerebral arteries compared to WR control are due to a difference in regulation of MYPT1 phosphorylation by ROK rather than a difference in MYPT1 protein content between the two rat strains.

5.5.5 The possible role of CPI-17 in the abnormal myogenic response of prediabetic GK cerebral arteries

As a potent inhibitor of MLCP at the catalytic site (Eto, 2009), higher phospho-CPI-17 may contribute to the increased LC_{20} phosphorylation in prediabetic GK cerebral arteries. Experiments from our laboratory did not detect an obligatory role for CPI-17 phosphorylation in pressure-evoked constriction of rat cerebral and skeletal muscle arteries (Johnson et al., 2009; Moreno-Domínguez et al., 2013). However, determining whether enhanced CPI-17 expression and/or phosphorylation causing a higher inhibition of MLCP activity contributes to the increase in basal tone in cerebral arteries of type 2 diabetic animals would be a worthwhile goal for future experiments (Chapter 7). This view is supported by several studies that have implicated a role of higher CPI-17 phosphorylation in abnormal VSMC contractility in diabetes. For instance, exposing VSMCs from *db/db* mouse mesenteric arteries to high glucose increased the phosphorylation of CPI-17 via a PKC-dependent mechanism (Xie et al., 2006). The enhanced contractile response to noradrenaline in mesenteric arteries from streptozotocin-induced diabetic rats was also associated with an increased activation of PKC (Mueed et al., 2005).

5.6 Actin polymerization and the abnormal myogenic constriction of prediabetic GK cerebral arteries

Our laboratory among others has demonstrated an obligatory role for dynamic cytoskeletal reorganization, involving increased actin polymerization evoked by ROK- and PKC-mediated signaling pathways, to the myogenic response of cerebral resistance arteries (Cipolla et al., 2002; Moreno-Domínguez et al., 2014). We investigated whether augmented actin polymerization contributes to the enhanced tone detected at low intraluminal pressure in cerebral arteries from prediabetic GK rats. G-actin content was quantified in pressurized cerebral arteries

after homogenization in F-actin stabilization buffer and centrifugation to separate F- and G-actin (Walsh et al., 2011). This actin polymerization mechanism was activated at basal intraluminal pressure in 8-10 week GK cerebral arteries (G-actin content was lower than in WR vessels at 10 mmHg). These results suggest that actin polymerization could play an important role, in addition to Ca^{2+} sensitization, in the enhanced basal myogenic tone of 8-10 week GK cerebral arteries. Interestingly, enhanced actin polymerization due to activation of the RhoA/ROK pathway was reported for cardiac myocytes from streptozotocin-diabetic rats (Lin et al., 2007). In endothelial cells, exposure to hyperglycemia triggers the production of oxygen free radicals that in turn activates endothelial SFK. The enhanced tyrosine kinase activity initiates actin polymerization leading to dysfunctional Ca^{2+} signaling and endothelial dysfunction (Schaeffer et al., 2003). Here, for the first time we report that abnormal activation of actin polymerization could contribute to the defective pressure-evoked constriction in VSMCs from a type 2 diabetic animal model.

5.6.1 Role of actin polymerization downstream of ROK in the abnormal myogenic constriction of prediabetic GK cerebral arteries

Similar to Ca^{2+} sensitization, our results suggest that the enhanced actin polymerization detected in prediabetic GK cerebral arteries is likely due to a higher level of ROK activity. This claim is supported by the view that: (i) enhanced basal tone in GK arteries was associated with augmented MYPT1-T855 phosphorylation and a higher decline in G-actin content compared to control, and (ii) the enhanced constriction in GK cerebral vessels was fully reversed by ROK inhibition. These results indicate that enhanced ROK activity in prediabetic GK cerebral arteries likely alters the pressure-dependent control of diameter through both mechanisms, Ca^{2+} sensitization and actin polymerization, but direct evidence of this should be obtained in the

future by quantification of the G-actin content of vessels treated with H1152. The role of ROK in the initiation of actin polymerization in the context of the myogenic response was indicated by previous work from our laboratory in which a reduction in the decline in G-actin content following pressurization was detected in the presence of H1152 and accompanied by a lower level of cofilin phosphorylation in rat cerebral arteries (Moreno-Domínguez et al., 2014). Cofilin contributes to actin dynamics by binding to and severing actin filaments favoring depolymerization (Moriyama et al., 1996; Ichetovkin et al., 2002). Cofilin activity is suppressed following phosphorylation at S3 by LIM kinase, and LIM kinase activity is dependent on phosphorylation by ROK (Bernard 2007; Walsh & Cole, 2013). The current view holds that ROK downstream of RhoA plays a crucial role in development of the myogenic response through phosphorylation of MYPT1 and LIM kinase, thus initiating Ca^{2+} sensitization and actin polymerization mechanisms, respectively.

5.6.2 Crosstalk between defective insulin signaling and the RhoA/ROK pathway in diabetic VSMCs in the context of actin polymerization

Begum et al. (2002) reported a role for actin cytoskeletal reorganization in the vasodilatory action of insulin in cultured VSMCs. Insulin, via NO/cGMP, inactivates RhoA inhibiting ROK activity leading to inhibition of actin polymerization, which may contribute to the vasodilator actions of insulin. Thus, similar to what has been discussed under the Ca^{2+} sensitization mechanism (section 5.3.2), we can postulate that insulin resistance in diabetic vessels would be associated with augmented actin polymerization due to loss of the inhibitory action of insulin on the RhoA/ROK pathway. However, more experiments are needed to test this hypothesis in intact resistance arteries from diabetic animals, as are proposed in Chapter 7.

5.7 Role of FAK-Y397 autophosphorylation in the abnormal myogenic response of prediabetic GK cerebral arteries

Consistent with the impaired myogenic reactivity detected in prediabetic GK cerebral arteries, no significant change in the molecular determinants of Ca^{2+} sensitization and actin polymerization (LC_{20}, MYPT1-T855, and G-actin content) were apparent following pressure elevation to 60 and 120 mmHg. The levels of LC_{20} and MYPT1-T855 phosphorylation were also significantly lower than corresponding values at 120 mmHg and can explain, at least in part, the inability of prediabetic GK cerebral arteries to maintain a constant diameter or constrict further on pressurization to above 80 mmHg. This finding differs markedly from the pressure-evoked increase in phosphorylation of LC_{20} & MYPT1-T855 and decline in G-actin content that was evident in vessels of WR, and reported previously for SD rats (Johnson et al., 2009; Moreno-Domínguez et al., 2013; Moreno-Domínguez et al., 2014). It is worth noting that no significant change in arterial diameter was detected between 8-10 week GK and age-matched WR control within the physiological range (60-120 mmHg). This could be attributed to the actin polymerization mechanism that was functional up to 120 mmHg (no difference in G-actin content between GK and WR at 120 mmHg) and could provide stiffness to the vessel and, thereby, hinder major changes in vessel diameter. Thus it was appropriate to test for defects in the mechanotransduction mechanism that might lead to this loss of pressure-dependent regulation in prediabetic GK cerebral arteries.

5.7.1 Integrin activation, FAK phosphorylation and pressure-evoked constriction

As discussed earlier, results from our laboratory have provided direct evidence for a role of integrin adhesions as a mechanotransduction mechanism in the myogenic response. As such, a pressure-dependent increase in FAK-Y397 and SFK-Y416 phosphorylation in the myogenic

response of rat cerebral arteries was apparent (Colinas et al., 2015), consistent with previous observations of increased levels of tyrosine phosphorylation following elevation of intraluminal pressure in cremaster arterioles (Spurrell et al., 2000; Murphy et al., 2002). The role of tyrosine phosphorylation of FAK and SFK in the myogenic response downstream of integrins was supported using anti-α5 integrin blocking antibodies, FAK inhibitor, and selective SFK inhibitor that abolished the myogenic response, reduced the pressure-evoked autophosphorylation of FAK-Y397 and SFK-Y416, and blocked phosphorylation of LC_{20}, MYPYT1-T855 and the decline in G-actin in cerebral arteries (Colinas et al., 2015).

Integrin activation is known to evoke RhoA/ROK signaling in several cell types including VSMCs (Burridge & Chrzanowska-Wodnicka, 1996; Juliano, 2002; Colinas et al., 2015); specifically, stimulation of integrins activates RhoA through RhoGEFs that catalyze the exchange of GTP for GDP leading to RhoGTPase activation (Lessey et al., 2012). Thus, the tyrosine phosphorylation of RhoGEF by FAK/SFKs downstream of integrins may be an essential mechanism for the regulation of RhoA in the myogenic response. Based on this reasoning, inappropriate FAK tyrosine phosphorylation would be expected to result in dysfunctional pressure-evoked RhoA activation and loss of the pressure-evoked constriction.

5.7.2 Inappropriate pressure-evoked FAK-Y397 phosphorylation in prediabetic GK cerebral arteries

We tested the hypothesis that the impaired pressure-evoked activation of Ca^{2+} sensitization and actin polymerization mechanisms in prediabetic GK cerebral arteries may be the result of dysfunction in the regulation of FAK signaling. Indeed, here we report the absence of a pressure-dependent change in FAK-Y397 autophosphorylation in prediabetic GK cerebral arteries. Thus, we anticipate that the loss of pressure-evoked change in LC_{20} and MYPT1-T855

phosphorylation and G-actin is likely due to inappropriate FAK phosphorylation downstream of integrins leading to dysfunctional pressure-evoked RhoA/ROK activation and constriction in GK cerebral arteries. The possible contribution of insulin resistance to defective integrin signaling will be addressed in the next section.

5.7.3 Crosstalk between integrins, FAK phosphorylation and insulin signaling

It was previously reported that integrin engagement is essential to stimulate both IRS-1-associated PI3K activity and Akt activity and that these are important steps in insulin-mediated glucose transport and glycogen synthesis (Guilherme & Czech 1998). Integrin $\alpha_5\beta_1$ signaling also potentiates insulin receptor kinase activity and formation of complexes containing IRS-1 and PI3K in response to insulin stimulation to promote cell adhesion (Guilherme et al.,1998). FAK phosphorylation was shown to associate with both insulin receptors and IRS proteins following insulin stimulation (Lebrun et al., 2000). In hepatocytes, the focal adhesion-targeting property and tyrosine kinase activity of FAK were found to be essential for insulin-mediated stimulation of glycogen synthesis, and FAK acts to promote insulin action downstream of PI3K by a specific interaction with Akt (Huang et al., 2002). In skeletal muscle cells, FAK signaling appeared to be essential for normal insulin-stimulated glucose transport and glycogen synthesis by maintaining actin cytoskeletal integrity possibly through changes in a FAK/RhoA signaling pathway (Huang et al., 2006). Thus, it is now clear that both integrin activation and downstream FAK phosphorylation are crucial for insulin- and insulin receptor-mediated signaling in the regulation of glucose homeostasis. Inappropriate FAK signaling was postulated to be associated with insulin resistance in skeletal muscle and liver cells, the two most important target tissues of insulin for the regulation of glucose homeostasis (Huang et al., 2006). Taken together, the cross talk between insulin and integrin/FAK signaling in different cell types, and the above-discussed

reports suggesting that insulin resistance can lead to inappropriate integrin signaling through FAK, permits us to postulate that insulin resistance might be associated with dysfunctional FAK phosphorylation downstream of integrin activation, and that this may underlie the loss of pressure-evoked activation of the RhoA/ROK pathway. The loss of pressure-mediated activation of ROK subsequently contributes to the inappropriate regulation of Ca^{2+} sensitization, actin polymerization pathways and myogenic constriction.

Another possibility that we did not explore here is that there might be a change in integrin expression associated with insulin resistance in GK rats. Previous reports have suggested that insulin regulates the expression of cell surface integrin that may contribute to the mechanisms whereby insulin regulates cell growth (Wertheimer et al., 1998). It is possible that insulin resistance could affect integrin expression and consequently pressure-evoked constriction. Alternatively, insulin receptor signaling triggers extracellular matrix protein synthesis (Anfossi et al., 2009) and it is possible that insulin resistance could evoke remodeling of the extracellular matrix environment and alter the activation of specific integrins resulting in a loss of mechanotransduction. Further studies will be required to test these possibilities as discussed in Chapter 7.

5.8 Defects in Ca^{2+} sensitization and actin polymerization mechanisms associated with loss of myogenic constriction in diabetic GK cerebral arteries

By the age of 18-20 weeks, GK rats are very ill as indicated by high serum insulin and glucose levels, and a high frequency of urination. In the cerebral arteries, there was obvious impairment of the myogenic response due to a failure to appropriately regulate MLCP activity and actin cytoskeleton reorganization. Specifically, no pressure-dependent increase in MYPT1-T855 and LC_{20} phosphorylation was detected, nor was there any decline in G-actin content.

The loss of pressure-dependent regulation of arterial diameter has been reported in multiple vascular beds, including cerebral arteries, isolated from diabetic animals or models with an established diabetic phenotype. For example, a loss of pressure-dependent constriction was reported for afferent arterioles of streptozotocin-diabetic rats (Hayashi et al., 1992). Kelly-Cobbs et al. (2011) showed that in the cerebral arteries of 18 week-old GK rats there was a loss of the myogenic response due to vascular remodeling; and an impaired myogenic response of both cerebral and coronary arteries was evident in 22 week-old GK rats (Kold-Petersen et al., 2012). A similar loss of myogenic response was also reported for retinal arterioles of type 1 diabetic patients (Lorenzi et al., 2010) and subcutaneous gluteal vessels isolated from type 2 diabetic patients when compared to the arteries of healthy individuals (Schofield et al., 2002).

We attribute the loss of myogenic constriction to a lack of pressure-evoked Ca^{2+} sensitization and actin dynamics. This view is consistent with recent studies using 22 week-old GK rats that demonstrated a reduction in myogenic constriction of cerebral and coronary arteries with no apparent change in the pressure-dependent increase in $[Ca^{2+}]_i$ (measured by Fura-2) between 20-100 mmHg. It was concluded that the attenuated myogenic tone development resulted from a reduction in the Ca^{2+} sensitivity of the contractile apparatus due to defective ROK signaling, but no direct evidence of this was reported (Kold-Petersen et al., 2012). The findings presented here indicate that the interpretation of Kold-Petersen et al. (2012) was correct, but also that abnormal actin dynamics are also involved.

It is worth noting that varied findings have been reported concerning the myogenic control of arterial diameter in different animal models of diabetes and even within the same animal model. This suggests that the defects in the myogenic response may be dependent on the vascular bed, type of diabetes and duration of the disorder. The severity of the disease condition

and accompanying differences in the extent of insulin resistance, hyperinsulinemia and hyperglycemia, and/or the presence of co-incident risk factors for cardiovascular disease, such as hyperlipidemia, obesity and hypertension, may also be relevant to understanding the variability in the reported changes in the myogenic response in type 2 diabetes.

5.9 Hyperinsulinemia and/or hyperglycemia and defective RhoA/ROK signaling

It is possible that hyperinsulinema and/or hyperglycemia detected in diabetic GK rats might contribute to the defective pressure-evoked RhoA/ROK activation. This view is supported by studies in mesenteric arteries from *ob/ob* mice which show that, under hyperglycemic conditions, phenylephrine-induced contraction was suppressed due to defective receptor-coupled RhoA activation and reduced ROK expression (Nobe et al., 2012). However, further studies are needed to delineate the specific contributions of hyperinsulinemia and hyperglycemia to the defective regulation of the RhoA/ROK pathway in type 2 diabetes. One potential mechanism whereby hyperinsulinemia and/or hyperglycemia could evoke defective ROK signaling is through initiating a change in the VSMC phenotype thus affecting the contractile behavior of the VSMC in a phenomenon known as plasticity. This mechanism will be discussed in detail in the following section.

5.10 VSMC plasticity secondary to hyperinsulinemia and/or hyperglycemia

5.10.1 VSCM plasticity at a glance

VSMCs in blood vessels exhibit remarkable plasticity, switching between differentiated (contractile) and dedifferentiated (synthetic) phenotypes in response to changes in the local environment (Owens et al., 2004). Differentiated VSMCs maintain a highly organized cytoskeleton, express various contractile proteins and play an important role in regulating vessel tone and blood pressure. However, VSMC dedifferentiation to a synthetic, non-contractile

phenotype results in a loss of fibers and a loose F-actin network with a concomitant reduction in some contractile proteins. A switch to the synthetic phenotype is thought to be an early event in numerous cardiovascular diseases such as atherosclerosis, restenosis, and hypertension. The ability of VSMCs to maintain plasticity and respond appropriately to external factors is therefore critical in maintaining appropriate proportions between the two cellular phenotypes and thereby maintain healthy vessel function (Gomez & Owens, 2012; Porter & Riches, 2013). It is possible, therefore, that the lack of pressure-dependent constriction in VSMCs from GK rats with established diabetes is reflecting a switch to the synthetic phenotype, as would be expected based on the previously discussed activation of the MAPK pathway in the presence of hyperinsulinemia. Additional experiments are required to validate this idea.

5.10.2 Role of the RhoA/ROK pathway in VSMC plasticity

The loss of contractility in the synthetic VSMC appears to be due, at least partly, to dysregulation of the RhoA/ROK pathway. This view is supported by studies showing that the loss of RhoA expression in pulmonary arteries from rats with chronic pulmonary hypertension could be responsible for pulmonary artery VSMC dedifferentiation and pulmonary artery remodeling (Sauzeau et al., 2003; Chen et al., 2006). Similarly, coronary VSMC differentiation from proepicardial cells also requires RhoA-mediated actin reorganization and ROK activity (Lu et al., 2001).

5.10.3 Role of hyperinsulinemia in VSMC plasticity

Hyperglycemia and hyperinsulinemia were found to exert direct effects on VSMCs and cause potentially detrimental changes in phenotype and function that accelerates cardiovascular complications in type 2 diabetes (Porter & Riches, 2013). Specifically, insulin induces a concentration-dependent proliferative effect on primate and human aortic VSMCs in culture

(Pfeifle & Ditschuneit, 1981; Porter & Riches, 2013). In bovine aortic VSMCs, insulin induced proliferation and migration via MAPK pathway (Wang et al., 2003). Thus as discussed previously, it is possible that insulin resistance impairs the beneficial effects of insulin signaling via PI3K, whereas the 'detrimental' pathways may predominate via preservation, or even over-activation of MAPK signaling in response to hyperinsulinemia. This may, therefore, lead to a predominance of the synthetic phenotype of the VSMC at later stages of type 2 diabetes progression.

5.10.4 Role of hyperglycemia in VSMC plasticity

In contrast to insulin, hyperglycemia has variable effects on VSMC plasticity. Some studies reported that glucose increases proliferation and growth of VSMCs from human aorta, human umbilical artery, and rat aorta in a manner that is synergistic to insulin (Nakamura et al., 2001; Kobayashi et al., 2005; Cifarelli et al., 2008). On the other hand, other studies have not detected any effect of high glucose levels on VSMC phenotype. For example, in porcine and human VSMCs, high levels of glucose did not modulate proliferation, either alone or in the presence of other VSMC mitogens such as platelet-derived growth factor (PDGF) (Suzuki et al., 2001). Whether hyperglycemia evokes a phenotypic switching in VSMCs towards the synthetic form, synergistic to insulin or not, the combination of hyperglycemia and hyperinsulinemia would result in a relative increase in the synthetic over the contractile phenotype.

5.10.5 Role of inflammation associated with type 2 diabetes in VSMC plasticity

It is worth noting that chronic inflammation is a hallmark of type 2 diabetes. Pro-inflammatory cytokines such as interleukins, MCP-1 (monocyte chemoattractant protein-1) and TNF-α (tumour necrosis factor-α) were detected at elevated circulating levels in diabetic individuals. These inflammatory cytokines are known to induce VSMC dedifferentiation,

proliferation and migration and exacerbate vascular dysfunction in diabetic states (Dandona et al., 2004; Porter & Riches, 2013). Thus it is also possible that the inflammatory burden that the diabetic vessels encounter would evoke VSMC dedifferentiation and result in a loss of the contractile properties of VSMC later in the progression of type 2 diabetes.

5.10.6 VSMC plasticity in GK rats

A few studies have indirectly reported VSMC plasticity in GK VSMCs. In cultured VSMCs isolated from GK rats exhibiting hyperglycemia, hyperinsulinemia, enhanced VSMC proliferation and migration was attributable to increased MAPK activation (Jacob et al., 2004; Ragolia et al., 2004). Similarly, both basal and interleukin-1β-stimulated levels of MAPK activity were significantly higher in VSMCs from GK rats compared to WR rats (Wakabayashi et al., 2010). These reports collectively suggest that enhanced VSMC proliferation and migration in GK rats may be associated with hyperinsulinemia and hyperglycemia and that MAPK signaling contributes to this process.

Given the fact that the severity of the 'type 2 diabetes phenotype' was found to be influenced by the degree of insulin resistance, duration of type 2 diabetes and effectiveness of glycemic control (Porter & Riches, 2013), it is possible that 18-20 week GK rats would be more affected by dysfunctional VSMC plasticity causing a loss of the contractile phenotype secondary to hyperglycemia, hyperinsulinemia and MAPK activation. This switch in the phenotype could elicit a proliferative response in the wall of diabetic vessels and possibly be responsible for the loss of VSMC contractility through impaired regulation of RhoA/ROK signaling.

5.11 Significance of findings

Figure 5.1 summarizes our proposed view of how type 2 diabetes affects insulin signaling and VSMC contractility based on a contemporary understanding of insulin action and the data presented in this thesis. Briefly, insulin resistance present at the earliest stage of the disease may lead to preferential inactivation of the P13K pathway (Anfossi et al., 2009). Impaired basal PI3K signaling will result in RhoA/ROK pathway activation, greater inhibition of MLCP, and augmented actin cytoskeleton remodeling (Begum, 2003) and, thereby, enhanced basal tone. Moreover, the enhanced ROK activity may cause an inhibitory phosphorylation of IRS that can intensify the impairment in PI3K signaling (Kanda et al., 2006). Disease progression is associated with hyperinsulinemia that may amplify the preserved MAPK signaling downstream of insulin receptor activation in VSMCs (Anfossi et al., 2009). MAPK activation may cause phenotypic switching of VSMC from the contractile to the synthetic phenotype (Ragolia et al., 2004). The synthetic phenotype is characterized by defective RhoA/ROK signaling (Sauzeau et al., 2003; Chen et al., 2006) and may underlie the loss of myogenic constriction in later stages of type 2 diabetes.

5.12 Summary

In summary, this study indicates that Ca^{2+} sensitization leading to increased LC_{20} phosphorylation, and actin dynamics leading to increased actin polymerization, are augmented at low intraluminal pressure due to increased H1152-sensitive ROK activity, and that these two defects contribute to the enhanced cerebral myogenic tone in early type 2 diabetes. As the disease progresses, the myogenic response is impaired due to suppression of mechanisms for pressure-dependent regulation of Ca^{2+} sensitization and actin polymerization in VSMCs; i.e. diabetes progression is associated with loss of the mechanisms responsible for the development

of the myogenic response. These findings can provide clues to understanding the propensity of ischemic and hemorrhagic stroke in type 2 diabetic patients. Specifically, restricted cerebral blood flow at lower systemic pressure in early type 2 diabetes could contribute to cerebral ischemic events, and the loss of myogenic constriction and excessive blood flow may predispose to an increased incidence of hemorrhagic stroke in the later stages of the disease, particularly in individuals with hypertension.

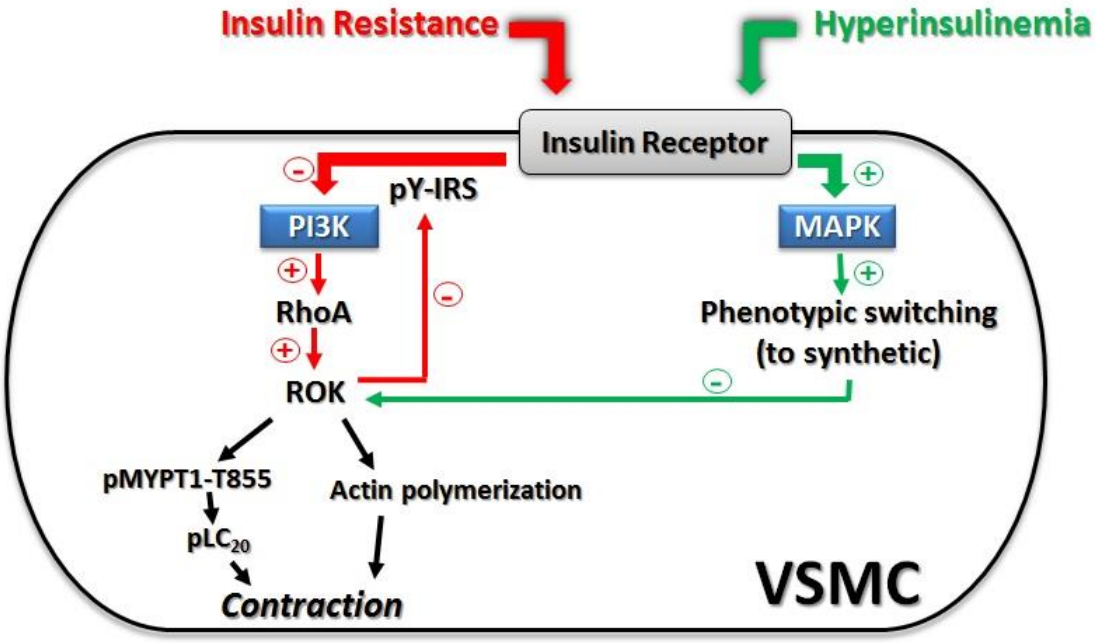

Figure 5.1: Proposed model for altered VSMC contraction during different stages of type 2 diabetes

Schematic representation of how insulin resistance and hyperinsulinemia encountered in the early and late stages of type 2 diabetes, respectively, may differently affect insulin signaling in VSMC. Insulin resistance causes a preferential inactivation of PI3K signaling leading to greater Rho/ROK activation. ROK phosphorylates MYPT1-T855 (p-MYPT1-T855) leading to inhibition of MLCP and increase of phospho-LC_{20} (pLC_{20}) content. ROK also enhances the polymerization of actin and inhibits the tyrosine phosphorylation of IRS (pY-IRS) leading to a feed-forward impairment in PI3K signaling. The inhibition of MLCP and the activation of actin polymerization elicit enhanced VSMC contraction. Hyperinsulinemia amplifies the preserved MAPK signaling leading to phenotypic switching to the synthetic phenotype. This phenotype is characterized by inactive RhoA/ROK signaling and loss of VSMC contractility.

Chapter Six: Limitations

In this chapter some limitations of the work presented in this thesis will be discussed. Three pressure steps (10, 60 and 120 mmHg) were employed in this study to explore the pressure-evoked change in phospho-MYPT1, phospho-LC_{20} and G-actin in GK rats. The operating physiological range of rat cerebral arteries is between 60 and 120 mmHg. The quantification of phosphoprotein content and G-actin at other test pressures (between 60 and 120 mmHg) would provide a better understanding of the changes in myogenic behaviour of GK cerebral arteries within the operating physiological range.

We attempted to relate the abnormal myogenic response to dysfunctional cerebral blood flow autoregulation and high incidence of stroke in type 2 diabetes. Longitudinal studies in GK rats and human patients are required to determine whether cerebral blood flow is actually affected by abnormal myogenic behaviour using non-invasive brain imaging techniques such as transcranial Doppler ultrasonography or magnetic resonance imaging. These studies will also help delineate how extrinsic factors released from the endothelium and surrounding nerve terminals can either mitigate or intensify the impairment in myogenic response to modulate cerebral blood flow *in vivo*.

The protein content of LC_{20} quantified was not normalized here to at least two reference proteins, similar to MYPT1, to exclude the possibility of a difference in expression of LC_{20} protein between GK and WR. Differences in LC_{20} protein content between the two strains could play a role along with the identified alteration in phosphorylation as a cause of the abnormal pressure-evoked constriction in GK *vs* WR. Similarly, we detected a difference in the pressure-dependent phosphorylation of FAK-Y397 in GK compared to WR cerebral arteries. However, possible differences in FAK protein content between the two strains were not addressed.

However, the change in phosphorylation level was sufficient to indicate inappropriate regulation of the signaling mechanisms involving these proteins that was the main focus of the study.

Alternative mRNA splicing of the MYPT1 gene produces two MYPT1 isoforms that differ by the presence (+) or absence (-) of a C-terminal leucine zipper (LZ) domain. LZ+ MYPT1 isoform is essential for PKG-mediated phosphorylation of MYPT1 that activates MLCP (Yuen et al., 2011). Changes in MYPT1 isoform expression result in changes in the sensitivity of smooth muscle to NO-mediated relaxation (Yuen et al., 2014). We have not explored the possible differential expression of these isoforms in GK cerebral arteries that might affect the overall activity of MLCP.

Fasudil, another ROK inhibitor, has been shown to inhibit intracellular Ca^{2+} dynamics (calcium release from IP3 receptors) along with ROK inhibition in rat hippocampal neurons (Huang et al., 2009). It is important to consider the potential inhibition of intracellular Ca^{2+} dynamics in VSMCs by H1152 based on the structure similarity between the two compounds.

Although we postulate that augmented actin polymerization downstream of ROK contributes to the enhanced basal myogenic tone in prediabetic GK cerebral arteries, no measurements of G-actin content were performed in the presence of H1152 in these vessels at low intraluminal pressure (10 mmHg). However, H1152 completely blocked the enhanced myogenic tone consistent with our claim that ROK is responsible for the augmented actin cytoskeleton dynamics detected in prediabetic GK cerebral arteries. We also assumed that H1152 would inhibit MYPT1-T855 and LC_{20} phosphorylation in WR cerebral arteries, similar to SD rats, but no actual measurement was performed to support this assumption. We felt that such H1152 experiments were not essential as the myogenic behaviour of cerebral vessels from WR was identical to that previously described for arteries from SD rats.

We suggested that a difference in RhoA expression does not play a role in the augmented ROK activity in prediabetic GK cerebral arteries. Our assumption was based on quantification of RhoA mRNA levels only; measurement of RhoA protein content would provide additional, essential support for this conclusion.

We concluded that there is no evidence for arterial wall remodeling in the GK since we did not detect a significant difference in the passive diameter of cerebral arteries from GK and WR within the tested pressure range. Morphometric measurements of inner diameter, wall thickness and circumferential dimensions would provide direct evidence in support of this conclusion.

Chapter Seven: Future directions

7.1 Most intriguing research areas for future study

The work presented in this thesis involved a characterization of the dysfunctional pressure-dependent control of cerebral arterial diameter in a type 2 diabetic rat model. It also included direct quantification of the molecular entities that might play a role in this dysfunction. Some of the directions for future study that are intriguing will be discussed in the following final section of the thesis. Specifically, we will discuss some future experiments to delineate the other plausible molecular mechanisms that could contribute to the abnormal myogenic response in GK rats. We will also discuss some future experiments to explore whether insulin resistance can trigger the dysfunctional myogenic response in GK rats and to test one therapeutic option that could be employed to mitigate this dysfunction.

7.2. Activation of the RhoA/ROK pathway in GK cerebral arteries

The experiments in this thesis provide evidence of an enhanced level of ROK activity in the cerebral arteries of prediabetic GK rats. The transcript expression of the upstream activator of ROK, RhoA, was not different in these vessels compared to control. Thus, it would be interesting to quantify the active form of RhoA, RhoA-GTP, which would directly indicate the activation status of RhoA and consequently ROK. New commercial assays are now available for quantification of RhoA-GTP with good sensitivity. The assay uses the Rho-binding domain (RBD) of the Rho effector protein, Rhotekin. The RBD motif binds specifically to the GTP-bound form of RhoA. The fact that the RBD region of Rhotekin has a high affinity for GTP-RhoA and that Rhotekin binding results in a significantly reduced intrinsic and catalytic rate of GTP hydrolysis make it an ideal tool for affinity purification of GTP-RhoA from cell lysates that

will permit direct quantification of active RhoA (Xie et al., 2013). Elevated levels of RhoA-GTP could be the cause of the enhanced ROK activity detected in prediabetic GK cerebral arteries.

It would also be interesting to quantify ROK and RhoA expression and the level of active RhoA in diabetic (18-20 week) GK rats. Although we speculate that progression of diabetes may be associated with a concomitant inappropriate regulation of the RhoA/ROK pathway, direct quantification of the expression levels and activities of RhoA and ROK of diabetic GK rats is essential to delineate how hyperglycemia and/or hyperinsulinemia would alter pressure-dependent constriction in the late stages of type 2 diabetes.

7.3 The PKC pathway and the cerebral myogenic response of GK rats

Several studies have implicated a contribution of PKC to the regulation of force in the myogenic response, but the mechanism(s) involved has not been well established (Hill et al., 1990; Osol et al., 1991; Dessy et al., 2000; Massett et al., 2002). Previous studies postulated that PKC might phosphorylate CPI-17 and/or MYPT1, leading to an inhibition of MLCP activity and increased LC_{20} phosphorylation (Somlyo & Somlyo, 2003; Dimopoulos et al., 2007). However, this is unlikely because we detected no evidence of a pressure-dependent increase in the level of phospho-CPI-17 or PKC-dependent MYPT1 phosphorylation in the myogenic response of rat cerebral or gracilis arteries (Johnson et al., 2009; El-Yazbi et al., 2010; Moreno-Domínguez et al., 2013). Some studies have reported evidence of an enhanced phosphorylation of CPI-17 via a PKC-dependent mechanism in the mesenteric arteries of two different diabetic animal models (Mueed et al., 2005; Xie et al., 2006). Thus in the future, the role that enhanced CPI-17 expression and/or phosphorylation downstream of PKC and its contribution to dysfunctional regulation of MLCP activity and the myogenic response in GK rats should be explored.

On the other hand, PKC-dependent activation of actin polymerization has been suggested to provide the link between PKC activation and myogenic constriction within the physiological range. PKC was found to phosphorylate HSP27 in a pressure-dependent manner in rat cerebral arteries. Phosphorylated HSP27 hinders the actin filament capping activity of HSP27 thus promoting actin polymerization and myogenic constriction (Moreno-Domínguez et al., 2014). Inappropriate regulation of PKC-mediated phosphorylation of HSP27 might play a role in the abnormal regulation of actin polymerization in GK cerebral arteries. Thus, it would be interesting to quantify HSP27 phosphorylation in the presence and absence of PKC inhibitor to delineate the role of PKC in the dysfunctional regulation of the actin polymerization mechanism in GK cerebral arteries.

7.4 Integrin signaling and the cerebral myogenic response of GK rats

As discussed earlier, the role of integrins as a mechanotransduction mechanism in the myogenic response has been supported by several studies in rat resistance arteries (Davis et al., 2001; Martinez-Lemus et al., 2005; Jackson et al., 2010; Colinas et al., 2015). Pressure-evoked FAK-Y397 autophosphorylation downstream of integrin adhesion stimulation was found to be essential for activation of the contractile machinery in the myogenic response (Colinas et al., 2015). A loss of pressure-evoked constriction, phosphorylation of contractile proteins and actin polymerization has been demonstrated in GK cerebral arteries (Chapter 3 & 4). We also provided preliminary evidence for inappropriate integrin adhesion signaling via FAK-Y397 phosphorylation in prediabetic GK cerebral arteries. Thus it would be interesting to explore the upstream molecular changes responsible for this loss of pressure-evoked FAK-Y397 phosphorylation and constriction in GK cerebral arteries. One possibility would be a decline in

the expression of integrin proteins in GK cerebral arteries that could be responsible for the loss of pressure-evoked changes in the myogenic response.

Another possibility would be a change in extracellular matrix protein expression resulting in altered integrin activation. Extracellular matrix proteins such as elastin, fibronectin, laminin and collagen interact with and activate integrins in response to increased intraluminal pressure to transmit the signal through the smooth muscle membrane to the contractile apparatus (Lessey et al., 2012). Differences in the expression of extracellular matrix proteins between GK and WR would lead to a change in the extracellular environment sensed by integrin adhesions and could result in defective integrin signaling in response to intraluminal pressure. A difference in extracellular matrix protein expression could involve a global change, or a change in the relative proportion of some proteins versus others.

It has been shown that SFK phosphorylation at Y416 is also important for proper integrin signaling in response to pressure in rat cerebral arteries (Colinas et al., 2015). It would be interesting to investigate whether abnormal phosphorylation of SFK plays a role in the inappropriate pressure-evoked myogenic constriction in GK cerebral arteries. Inappropriate integrin expression, activation and/or signaling would affect the mechanosensory and mechanotransduction functions of integrin adhesions and contribute to the dysfunctional pressure-evoked responses.

7.5 Insulin signaling and resistance to insulin action in cerebral arteries

In this section we will discuss some of the future experiments that could delineate the crosstalk between insulin resistance and abnormal regulation of the RhoA/ROK pathway that could affect VSMC contractility.

7.5.1 What is reported in the literature about insulin signaling?

Most of the reports that described the molecular mechanisms for the vascular actions of insulin in the endothelium and VSMCs were conducted using cultured cells that do not necessarily mimic the mechanisms present in myocytes of intact tissues. Several studies have suggested that insulin induces vasodilation in VSMC via two intertwined mechanisms that are both dependent on the production of NO either from the endothelium (via eNOS) or from VSMC (via iNOS) generated downstream of insulin and PI3K/Akt signaling (Begum et al., 2000; Begum et al., 2002; Begum, 2003; Muniyappa et al., 2007). NO generated in the endothelium or VSMCs blocks RhoA activation and translocation to the membrane through RhoA phosphorylation at S188 and decreased geranylgeranylation via a cGMP/PKG-mediated mechanism (Begum et al., 2002; Muniyappa et al., 2007). Inhibition of the RhoA/ROK pathway leads to decreased phosphorylation of MYPT1-T855 and activation of MLCP and also inhibits actin polymerization (Begum, 2003). NO may also act via a PKG-dependent mechanism in which the kinase directly interacts with, and activates MLCP (Kimura et al., 1996; Surks et al., 1999). Activation of MLCP induces LC_{20} dephosphorylation and VSMC relaxation.

Begum (2003) suggested that, during insulin resistance, the enhanced ROK activity detected in various models of diabetes impairs insulin-induced IRS-1 tyrosine phosphorylation. This impairment is mainly due to increased association of active ROK with IRS-1 leading to increased IRS-1 serine phosphorylation thus interrupting downstream insulin signaling via PI3K/Akt. According to Begum and coworkers, defective IRS-1/PI3K/Akt activation underlies the resistance to the vascular action of insulin in type 2 diabetes (Begum et al., 2002; Begum, 2003). Along the same lines, the experiments described in this thesis show that enhanced ROK

activation during insulin resistance results in dysfunctional regulation of MLCP activity and actin polymerization leading to abnormal myogenic constriction.

7.5.2 Why it is important to study insulin signaling in intact vessels?

Whether or not the molecular mechanisms for the vascular actions of insulin differ between intact arteries and cultured cells has not been explored. It would be of great interest, therefore, to delineate the molecular mechanisms of the vascular actions of insulin in isolated resistance arteries as opposed to cultured cells to determine whether the mechanisms are similar or different from those operable in intact tissues. This might provide clues for the possible link between defective insulin signaling and inappropriate control of arterial diameter during states of insulin resistance and, possibly, provide new avenues for the development of novel therapeutic interventions in the future.

7.5.3 Future experiments suggested to delineate the molecular mechanisms of insulin signaling in cerebral arteries

It would be interesting to determine whether the effect of insulin on the diameter of pressurized cerebral arteries is different in the presence and absence of functional endothelium. Selective NOS inhibitors (e.g. of iNOS) could be employed to confirm the contribution of different isoforms to the vascular actions of insulin in VSMC, as claimed in cultured cells, in pressurized cerebral arteries after removal of the endothelium. We could also use inhibitors of PKG and cGMP-mimetic molecules to validate that the vasodilatory signaling cascade of insulin is NO-mediated in VSMC. We can also employ our expertise to quantify the phosphorylation status of multiple proteins from isolated pressurized endothelium-denuded cerebral arteries that would offer a better understanding of the signaling pathway for insulin action in VSMC. Specifically, we would employ three-step western blotting to measure the phosphorylation of

IRS (tyrosine phosphorylation), Akt-T308/S473 (phosphorylation at both sites is required for maximal activity; Copps & White 2012), RhoA-S188 (phosphorylation at this site inhibits RhoA translocation and activation), LC_{20} & MYPT1-T855 phosphorylation and G-actin content after insulin stimulation in the presence and absence of PI3K inhibitor. These measurements would indicate whether insulin evokes phosphorylation of RhoA, inhibits ROK and blocks phosphorylation of MYPT1-T855 and inhibits actin polymerization via a signaling cascade involving IRS tyrosine phosphorylation and PI3K-Akt activation downstream of insulin receptor activation.

After delineating the signaling pathway of insulin action in VSMC, we can then pursue experiments to determine how type 2 diabetes would impair the vascular actions of insulin in GK rats. Specifically we would first detect the resistance to the vascular actions of insulin in pressurized arteries in the presence and absence of endothelium to investigate whether the defects in vascular actions of insulin occur at the level of the endothelium, VSMC or both. Then we would quantify the phosphorylation of IRS (at the tyrosine residues), Akt-T308/S473 and RhoA- S188. If this signaling cascade is dysfunctional, then it would provide a plausible explanation for the augmented ROK activity detected in prediabetic GK rats. Finally, it would be very interesting to explore whether the enhanced ROK activity will feedback to phosphorylate IRS at serine residues thus inhibiting the tyrosine phosphorylation of IRS downstream of insulin activation and contribute to the augmentation of insulin resistance.

7.6 Remodeling in diabetic GK cerebral arteries

As shown in Chapter 3, we did not detect a significant difference in the passive diameter of cerebral arteries of 18-20 week GK rats compared to control WR, but it is possible that a change would be evident in older animals. Thus, it would be interesting to investigate if there is a

progressive change in the passive diameter after 20 weeks of age that could contribute to the abnormal control of cerebral arterial diameter in more advanced stages of type 2 diabetes. Moreover, it would be important to perform morphometric measurements of arterial wall thickness and histological examination of the cerebral artery wall to detect any change in the VSMC layer proliferation and extracellular matrix composition that might imply an augmented activation of the MAPK pathway due to hyperinsulinemia, as discussed in Chapter 5.

7.7 Additional research areas for the future

7.7.1 Calcium, MLCK activation and the cerebral myogenic response of GK rats

In this thesis we have described molecular defects in the Ca^{2+} sensitization and actin polymerization mechanisms that could contribute to the dysfunctional myogenic response in GK rats. As discussed earlier, Ca^{2+} influx and MLCK activation also play a crucial role in the phosphorylation of LC_{20} and myogenic constriction (Brayden & Nelson, 1992; Knot & Nelson, 1998; Cole & Welsh, 2011). It would be interesting to explore whether impaired Ca^{2+} handling and Ca^{2+}-dependent activation of MLCK in VSMCs contribute to the abnormal myogenic response in prediabetic GK cerebral arteries. The defects can be at different levels, for instance: (i) increased VGCCs expression and/or activation that would result in enhanced Ca^{2+} influx and eventually augmented MLCK activation; (ii) decreased K_v and BK_{Ca} channel expression and/or activation that would lead to VSMC membrane depolarization, voltage-gated Ca^{2+} channel activation, Ca^{2+} influx, and augmented MLCK activation (Cole & Welsh 2011); (iii) increased expression of MLCK could also be explored as a potential mechanism involved in the enhanced phosphorylation of LC_{20} in prediabetic GK rats; and (iv) changes in the release of Ca^{2+} from intracellular stores in the form of propagating Ca^{2+} waves could be investigated as a potential cause for defective activation of MLCK and abnormal myogenic constriction.

7.7.2 Insulin sensitizers and the cerebral myogenic response of GK rats

We postulated that the dysfunctional control of myogenic response mechanisms may be attributed to insulin resistance and the secondary hyperinsulinemia as the disease progresses. Thus, it would be interesting to therapeutically intervene to improve the insulin sensitivity of VSMCs at the early stage of the disease to suppress or at least delay the progressive dysregulation in cerebral arterial diameter of GK rats. One potential therapeutic candidate that could be used is peroxisome proliferator activated receptor γ (PPARγ) agonists, known as thiazolidinediones, which are insulin sensitizer agents. PPAR*γ* belongs to the nuclear receptor superfamily that function as transcription factors to regulate various physiological and pathophysiological events, including adipocyte differentiation and insulin sensitivity (Tontonoz et al., 1994). PPAR*γ* activation enhances the lipid storage capacity of the adipose mass, and also increases the number of small, insulin-sensitive adipocytes, leading to improved insulin sensitivity (Rosen & Spiegelman, 2001). In addition to a regulatory function in glucose and lipid metabolism, PPAR*γ* is expressed in endothelial cells and VSMCs and has been shown to play a crucial role in facilitating proper functioning of the cardiovascular system (Touyz & Schiffrin, 2006; Takano & Komuro, 2009). PPAR*γ* activation inhibits VSMC proliferation and migration through several mechanisms, including direct inhibition of the production of growth factors and proinflammatory cytokines. PPARγ may also play a role in the induction of a differentiated phenotype in proliferating VSMCs that is important in vascular pathology (Touyz & Schiffrin, 2006; Takano & Komuro, 2009). Moreover, PPARγ ligands inhibit the RhoA/ROK pathway via inhibition of RhoA translocation to the cell membrane (Wakino et al., 2004). PPARγ also regulates the activity of PKC to provide tight control of myogenic tone in mouse mesenteric arteries (Ketsawatsomkron et al., 2012). In endothelial cells, PPAR*γ* modulates vascular tone

through antagonizing the production or activation of vasoconstrictors, such as angiotensin II and endothelin-1, while promoting vasodilation, mainly by increasing the production of vasodilating NO (Polikandriotis et al., 2005).

The available evidence suggests that treatment with thiazolidinediones improves vascular function in diabetic mice and humans (Touyz & Schiffrin, 2006; Takano & Komuro, 2009). For instance, treatment with the PPARγ agonist pioglitazone was reported to increase eNOS activity and enhance the vasodilatory response to acetylcholine in diabetic mice indicating an improvement in endothelial function (Huang et al., 2008). Also subjects treated for 26 weeks with rosiglitazone, another PPARγ agonist, exhibited reductions in markers of systemic inflammation and insulin resistance indicating potentially beneficial effects on overall cardiovascular risk in this patient population (Haffner et al., 2002).

Based on these findings for thiazolidinediones, it would be interesting to treat GK rats at early stage, such as at the onset of insulin resistance at 4-5 weeks of age, with daily thiazolidinedione and monitor the changes in the myogenic response and changes in the regulation of MLCP and actin polymerization downstream of ROK and PKC, as well as insulin signaling in cerebral arterial VSMCs. We postulate that thiazolidinedione treatment would improve the pressure-dependent control of cerebral arterial diameter in GK rats and delay the progression of the dysfunctional myogenic constriction. Moreover, these experiments would provide a better understanding of the molecular basis for the improvement in cardiovascular function upon treatment with thiazolidinediones in type 2 diabetes, specifically at the VSMC level. It is worth noting that most of the studies that have explored the pleiotropic effects of PPARγ agonists in vascular disease have focused on the endothelium. Our current understanding of some of the defects in VSMCs secondary to insulin resistance would offer a powerful tool in

pursing the research to understand the molecular mechanisms by which some of the commercially available antidiabetics improve vascular function at the VSMC level. The identification of novel therapeutic targets that can be employed to delay the progression of cerebrovascular deterioration may be utilized in the future to improve the prognosis of cerebrovascular disease in type 2 diabetic patients.

References

Abd-Elrahman, K. S., Walsh, M. P., & Cole, W. C. (2015). Abnormal Rho-associated kinase activity contributes to the dysfunctional myrteries in type 2 diabetes. Canadian Journal of Physiology and Pharmacology, 93(3), 177–84. doi:10.1139

Abdelsaid, M., Ma, H., Coucha, M., & Ergul, A. (2014). Late dual endothelin receptor blockade with bosentan restores impaired cerebrovascular function in diabetes. Life Sciences, 118(2):263-7. doi:10.1016/j.lfs.2013.12.231

Akash, M. S. H., Rehman, K., Sun, H., & Chen, S. (2013). Interleukin-1 receptor antagonist improves normoglycemia and insulin sensitivity in diabetic Goto-Kakizaki-rats. European Journal of Pharmacology, 701(1-3), 87–95. doi:10.1016/j.ejphar.2013.01.008

Alpers, B. J., Berry, R. G., & Paddison, R. M. (1959). Anatomical studies of the circle of Willis in normal brain. A.M.A. Archives of Neurology and Psychiatry, 81(4), 409–18.

Anfossi, G., Russo, I., Doronzo, G., & Trovati, M. (2009). Contribution of insulin resistance to vascular dysfunction. Archives of Physiology and Biochemistry, 115(4), 199–217. doi:10.1080/13813450903136791

Bárány, M., Barron, J. T., Gu, L., & Bárány, K. (2001). Exchange of the actin-bound nucleotide in intact arterial smooth muscle. The Journal of Biological Chemistry, 276(51), 48398–403. doi:10.1074/jbc.M106227200

Bayliss, W. M. (1902). On the local reactions of the arterial wall to changes of internal pressure. The Journal of Physiology, 28(3), 220–31.

Bear, J. E., & Gertler, F. B. (2009). Ena/VASP: towards resolving a pointed controversy at the barbed end. Journal of Cell Science, 122(Pt 12), 1947–53. doi:10.1242/jcs.038125

Begum, N. (2003). Insulin signaling in the vasculature. Frontiers in Bioscience : A Journal and Virtual Library, 8, s796–804.

Begum, N., Duddy, N., Sandu, O., Reinzie, J., & Ragolia, L. (2000). Regulation of myosin-bound protein phosphatase by insulin in vascular smooth muscle cells: evaluation of the role of Rho kinase and phosphatidylinositol-3-kinase-dependent signaling pathways. Molecular Endocrinology (Baltimore, Md.), 14(9), 1365–76. doi:10.1210/mend.14.9.0522

Begum, N., Sandu, O. A., & Duddy, N. (2002). Negative regulation of rho signaling by insulin and its impact on actin cytoskeleton organization in vascular smooth muscle cells: role of nitric oxide and cyclic guanosine monophosphate signaling pathways. Diabetes, 51(7), 2256–63.

Begum, N., Sandu, O. A., Ito, M., Lohmann, S. M., & Smolenski, A. (2002). Active Rho kinase (ROK-alpha) associates with insulin receptor substrate-1 and inhibits insulin signaling in vascular smooth muscle cells. The Journal of Biological Chemistry, 277(8), 6214–22. doi:10.1074/jbc.M110508200

Bernard, O. (2007). Lim kinases, regulators of actin dynamics. The International Journal of Biochemistry & Cell Biology, 39(6), 1071–6. doi:10.1016/j.biocel.2006.11.011

Blum, M., Brändel, C., & Müller, U. A. (2005). Myogenic response reduction by high blood glucose levels in human retinal arterioles. European Journal of Ophthalmology, 15(1), 56–61.

Brayden, J. E., Earley, S., Nelson, M. T., & Reading, S. (2008). Transient receptor potential (TRP) channels, vascular tone and autoregulation of cerebral blood flow. Clinical and Experimental Pharmacology & Physiology, 35(9), 1116–20. doi:10.1111/j.1440-1681.2007.04855.x

Brayden, J. E., & Nelson, M. T. (1992). Regulation of arterial tone by activation of calcium-dependent potassium channels. Science (New York, N.Y.), 256(5056), 532–5.

Brunetti, P. (2007). The lean patient with type 2 diabetes: characteristics and therapy challenge. International Journal of Clinical Practice. Supplement, (153), 3–9. doi:10.1111/j.1742-1241.2007.01359.x

Burridge, K., & Chrzanowska-Wodnicka, M. (1996). Focal adhesions, contractility, and signaling. Annual Review of Cell and Developmental Biology, 12, 463–518. doi:10.1146/annurev.cellbio.12.1.463

Cao, Y., Dubois, D. C., Sun, H., Almon, R. R., & Jusko, W. J. (2011). Modeling Diabetes Disease Progression and Salsalate Intervention in Goto-Kakizaki Rats. J Pharmacol Exp Ther., 339(3), 896–904. doi:10.1124/jpet.111.185686.environmental

Carlson, B. E., & Beard, D. A. (2011). Mechanical control of cation channels in the myogenic response. American Journal of Physiology. Heart and Circulatory Physiology, 301(2), H331–43. doi:10.1152/ajpheart.00131.2011

Cavarape, A., Bauer, J., Bartoli, E., Endlich, K., & Parekh, N. (2003). Effects of angiotensin II, arginine vasopressin and tromboxane A2 in renal vascular bed: role of rho-kinase. Nephrology, Dialysis, Transplantation : Official Publication of the European Dialysis and Transplant Association - European Renal Association, 18(9), 1764–9.

Chen, C.-P., Chen, X., Qiao, Y.-N., Wang, P., He, W.-Q., Zhang, C.-H., … Zhu, M.-S. (2015). In vivo roles for myosin phosphatase targeting subunit-1 phosphorylation sites T694 and T852 in bladder smooth muscle contraction. *The Journal of Physiology*, *593*(3), 681–700. doi:10.1113/jphysiol.2014.283853

Chen, S., Crawford, M., Day, R. M., Briones, V. R., Leader, J. E., Jose, P. A., & Lechleider, R. J. (2006). RhoA modulates Smad signaling during transforming growth factor-beta-induced smooth muscle differentiation. The Journal of Biological Chemistry, 281(3), 1765–70. doi:10.1074/jbc.M507771200

Cifarelli, V., Luppi, P., Tse, H. M., He, J., Piganelli, J., & Trucco, M. (2008). Human proinsulin C-peptide reduces high glucose-induced proliferation and NF-kappaB activation in vascular smooth muscle cells. Atherosclerosis, 201(2), 248–57. doi:10.1016/j.atherosclerosis.2007.12.060

Cipolla, M. J. (2009). The Cerebral Circulation [2009] - PubMed - NCBI. Retrieved August 18, 2014, from http://www.ncbi.nlm.nih.gov/pubmed/21452434

Cipolla, M. J., & Bullinger, L. V. (2008). Reactivity of brain parenchymal arterioles after ischemia and reperfusion. Microcirculation (New York, N.Y. : 1994), 15(6), 495–501. doi:10.1080/10739680801986742

Cipolla, M. J., Gokina, N. I., & Osol, G. (2002). Pressure-induced actin polymerization in vascular smooth muscle as a mechanism underlying myogenic behavior. FASEB Journal : Official Publication of the Federation of American Societies for Experimental Biology, 16(1), 72–6. doi:10.1096/cj.01-0104hyp

Clark, E. A., & Brugge, J. S. (1995). Integrins and signal transduction pathways: the road taken. Science (New York, N.Y.), 268(5208), 233–9.

Clements, R. T., Sodha, N. R., Feng, J., Boodhwani, M., Liu, Y., Mieno, S., … Sellke, F. W. (2009). Impaired coronary microvascular dilation correlates with enhanced vascular smooth muscle MLC phosphorylation in diabetes. Microcirculation (New York, N.Y. : 1994), 16(2), 193–206. doi:10.1080/10739680802461950

Cole, W. C., & Welsh, D. G. (2011). Role of myosin light chain kinase and myosin light chain phosphatase in the resistance arterial myogenic response to intravascular pressure. Archives of Biochemistry and Biophysics, 510(2), 160–73. doi:10.1016/j.abb.2011.02.024

Colinas O., Moreno-Domínguez, A., Zhu, H.L., Walsh, E.J., Pérez-García, M.T., Walsh, M.P. and Cole, W.C. (2015). Key role of mechanotransduction by integrin adhesions in the myogenic response of cerebral resistance arteries, The Journal of Biological Chemistry. (submitted)

Copps, K. D., & White, M. F. (2012). Regulation of insulin sensitivity by serine/threonine phosphorylation of insulin receptor substrate proteins IRS1 and IRS2. Diabetologia, 55(10), 2565–82. doi:10.1007/s00125-012-2644-8

Corteling, R. L., Brett, S. E., Yin, H., Zheng, X.-L., Walsh, M. P., & Welsh, D. G. (2007). The functional consequence of RhoA knockdown by RNA interference in rat cerebral arteries. American Journal of Physiology. Heart and Circulatory Physiology, 293(1), H440–7. doi:10.1152/ajpheart.01374.2006

Dandona, P., Aljada, A., & Bandyopadhyay, A. (2004). Inflammation: the link between insulin resistance, obesity and diabetes. Trends in Immunology, 25(1), 4–7.

Dandona, P., Aljada, A., Chaudhuri, A., Mohanty, P., & Garg, R. (2005). Metabolic syndrome: a comprehensive perspective based on interactions between obesity, diabetes, and inflammation. Circulation, 111(11), 1448–54. doi:10.1161/01.CIR.0000158483.13093.9D

Davis, M. J., & Hill, M. A. (1999). Signaling mechanisms underlying the vascular myogenic response. Physiological Reviews, 79(2), 387–423.

Davis, M. J., Wu, X., Nurkiewicz, T. R., Kawasaki, J., Davis, G. E., Hill, M. A., & Meininger, G. A. (2001). Integrins and mechanotransduction of the vascular myogenic response. American Journal of Physiology. Heart and Circulatory Physiology, 280(4), H1427–33.

DeMali, K. A., Wennerberg, K., & Burridge, K. (2003). Integrin signaling to the actin cytoskeleton. Current Opinion in Cell Biology, 15(5), 572–82.

Dessy, C., Matsuda, N., Hulvershorn, J., Sougnez, C. L., Sellke, F. W., & Morgan, K. G. (2000). Evidence for involvement of the PKC-alpha isoform in myogenic contractions of the coronary microcirculation. American Journal of Physiology. Heart and Circulatory Physiology, 279(3), H916–23.

Didion, S. P., Lynch, C. M., Baumbach, G. L., & Faraci, F. M. (2005). Impaired endothelium-dependent responses and enhanced influence of Rho-kinase in cerebral arterioles in type II diabetes. Stroke; a Journal of Cerebral Circulation, 36(2), 342–7. doi:10.1161/01.STR.0000152952.42730.92

Didion, S. P., Lynch, C. M., & Faraci, F. M. (2007). Cerebral vascular dysfunction in TallyHo mice: a new model of Type II diabetes. American Journal of Physiology. Heart and Circulatory Physiology, 292(3), H1579–83. doi:10.1152/ajpheart.00939.2006

Dimopoulos, G. J., Semba, S., Kitazawa, K., Eto, M., & Kitazawa, T. (2007). Ca2+-dependent rapid Ca2+ sensitization of contraction in arterial smooth muscle. Circulation Research, 100(1), 121–9. doi:10.1161/01.RES.0000253902.90489.df

Doronzo, G., Russo, I., Mattiello, L., Riganti, C., Anfossi, G., & Trovati, M. (2006). Insulin activates hypoxia-inducible factor-1alpha in human and rat vascular smooth muscle cells via phosphatidylinositol-3 kinase and mitogen-activated protein kinase pathways: impairment in insulin resistance owing to defects in insulin signalling. Diabetologia, 49(5), 1049–63. doi:10.1007/s00125-006-0156-0

El-Yazbi, A. F., Johnson, R. P., Walsh, E. J., Takeya, K., Walsh, M. P., & Cole, W. C. (2010). Pressure-dependent contribution of Rho kinase-mediated calcium sensitization in serotonin-evoked vasoconstriction of rat cerebral arteries. The Journal of Physiology, 588(Pt 10), 1747–62. doi:10.1113/jphysiol.2010.187146

Eto, M. (2009). Regulation of cellular protein phosphatase-1 (PP1) by phosphorylation of the CPI-17 family, C-kinase-activated PP1 inhibitors. The Journal of Biological Chemistry, 284(51), 35273–7. doi:10.1074/jbc.R109.059972

Faraci, F. M., & Heistad, D. D. (1990). Regulation of large cerebral arteries and cerebral microvascular pressure. Circulation Research, 66(1), 8–17.

Feng, J., Ito, M., Ichikawa, K., Isaka, N., Nishikawa, M., Hartshorne, D. J., & Nakano, T. (1999). Inhibitory phosphorylation site for Rho-associated kinase on smooth muscle myosin phosphatase. The Journal of Biological Chemistry, 274(52), 37385–90.

Flavahan, N. A., Bailey, S. R., Flavahan, W. A., Mitra, S., & Flavahan, S. (2005). Imaging remodeling of the actin cytoskeleton in vascular smooth muscle cells after mechanosensitive arteriolar constriction. American Journal of Physiology. Heart and Circulatory Physiology, 288(2), H660–9. doi:10.1152/ajpheart.00608.2004

Ganne, S., Arora, S. K., Dotsenko, O., McFarlane, S. I., & Whaley-Connell, A. (2007). Hypertension in people with diabetes and the metabolic syndrome: pathophysiologic insights and therapeutic update. Current Diabetes Reports, 7(3), 208–17.

Gao, W., Bihorel, S., DuBois, D. C., Almon, R. R., & Jusko, W. J. (2011). Mechanism-based disease progression modeling of type 2 diabetes in Goto-Kakizaki rats. Journal of Pharmacokinetics and Pharmacodynamics, 38(1), 143–62. doi:10.1007/s10928-010-9182-0

Ge, S., Song, L., & Pachter, J. S. (2005). Where is the blood-brain barrier ... really? Journal of Neuroscience Research, 79(4), 421–7. doi:10.1002/jnr.20313

Gerthoffer, W. T. (2005). Actin cytoskeletal dynamics in smooth muscle contraction. Canadian Journal of Physiology and Pharmacology, 83(10), 851–6. doi:10.1139/y05-088

Gerthoffer, W. T., & Gunst, S. J. (2001). Invited review: focal adhesion and small heat shock proteins in the regulation of actin remodeling and contractility in smooth muscle. Journal of Applied Physiology (Bethesda, Md. : 1985), 91(2), 963–72.

Giorda, C. B., Avogaro, A., Maggini, M., Lombardo, F., Mannucci, E., Turco, S., … Ferrannini, E. (2007). Incidence and risk factors for stroke in type 2 diabetic patients: the DAI study. Stroke; a Journal of Cerebral Circulation, 38(4), 1154–60. doi:10.1161/01.STR.0000260100.71665.2f

Gokina, N. I., & Osol, G. (2002). Actin cytoskeletal modulation of pressure-induced depolarization and Ca(2+) influx in cerebral arteries. American Journal of Physiology. Heart and Circulatory Physiology, 282(4), H1410–20. doi:10.1152/ajpheart.00441.2001

Gokina, N. I., Park, K. M., McElroy-Yaggy, K., & Osol, G. (2005). Effects of Rho kinase inhibition on cerebral artery myogenic tone and reactivity. Journal of Applied Physiology (Bethesda, Md. : 1985), 98(5), 1940–8. doi:10.1152/japplphysiol.01104.2004

Gomez, D., & Owens, G. K. (2012). Smooth muscle cell phenotypic switching in atherosclerosis. Cardiovascular Research, 95(2), 156–64. doi:10.1093/cvr/cvs115

Gonzales, A. L., Yang, Y., Sullivan, M. N., Sanders, L., Dabertrand, F., Hill-Eubanks, D. C., … Earley, S. (2014). A PLCγ1-dependent, force-sensitive signaling network in the myogenic constriction of cerebral arteries. Science Signaling, 7(327), ra49. doi:10.1126/scisignal.2004732

Goralski, K. B., & Sinal, C. J. (2007). Type 2 diabetes and cardiovascular disease: getting to the fat of the matter. Canadian Journal of Physiology and Pharmacology, 85(1), 113–32. doi:10.1139/y06-092

Goto, Y., Suzuki, K., Ono, T., Sasaki, M., & Toyota, T. (1988). Development of diabetes in the non-obese NIDDM rat (GK rat). Advances in Experimental Medicine and Biology, 246, 29–31.

Guilherme, A., & Czech, M. P. (1998). Stimulation of IRS-1-associated phosphatidylinositol 3-kinase and Akt/protein kinase B but not glucose transport by beta1-integrin signaling in rat adipocytes. The Journal of Biological Chemistry, 273(50), 33119–22.

Guilherme, A., Torres, K., & Czech, M. P. (1998). Cross-talk between insulin receptor and integrin alpha5 beta1 signaling pathways. The Journal of Biological Chemistry, 273(36), 22899–903.

Gunst, S. J., & Zhang, W. (2008). Actin cytoskeletal dynamics in smooth muscle: a new paradigm for the regulation of smooth muscle contraction. American Journal of Physiology. Cell Physiology, 295(3), C576–87. doi:10.1152/ajpcell.00253.2008

Guo, Z., Su, W., Allen, S., Pang, H., Daugherty, A., Smart, E., & Gong, M. C. (2005). COX-2 up-regulation and vascular smooth muscle contractile hyperreactivity in spontaneous diabetic db/db mice. Cardiovascular Research, 67(4), 723–35. doi:10.1016/j.cardiores.2005.04.008

Gutsche-Perelroizen, I., Lepault, J., Ott, A., & Carlier, M. F. (1999). Filament assembly from profilin-actin. The Journal of Biological Chemistry, 274(10), 6234–43.

Haffner, S. M., Greenberg, A. S., Weston, W. M., Chen, H., Williams, K., & Freed, M. I. (2002). Effect of rosiglitazone treatment on nontraditional markers of cardiovascular disease in patients with type 2 diabetes mellitus. Circulation, 106(6), 679–84.

Hamilton, S. J., & Watts, G. F. (2013). Endothelial dysfunction in diabetes: pathogenesis, significance, and treatment. *The Review of Diabetic Studies : RDS*, *10*(2-3), 133–56. doi:10.1900/RDS.2013.10.133

Harbeck, B., Hüttelmaier, S., Schluter, K., Jockusch, B. M., & Illenberger, S. (2000). Phosphorylation of the vasodilator-stimulated phosphoprotein regulates its interaction with actin. The Journal of Biological Chemistry, 275(40), 30817–25. doi:10.1074/jbc.M005066200

Harper, S. L., Bohlen, H. G., & Rubin, M. J. (1984). Arterial and microvascular contributions to cerebral cortical autoregulation in rats. The American Journal of Physiology, 246(1 Pt 2), H17–24.

Harris, A. K., Elgebaly, M. M., Li, W., Sachidanandam, K., & Ergul, A. (2008). Effect of chronic endothelin receptor antagonism on cerebrovascular function in type 2 diabetes. American Journal of Physiology. Regulatory, Integrative and Comparative Physiology, 294(4), R1213–9. doi:10.1152/ajpregu.00885.2007

Hayashi, K., Epstein, M., Loutzenhiser, R., & Forster, H. (1992). Impaired myogenic responsiveness of the afferent arteriole in streptozotocin-induced diabetic rats: role of eicosanoid derangements. Journal of the American Society of Nephrology : JASN, 2(11), 1578–86.

Hill, M. A., Falcone, J. C., & Meininger, G. A. (1990). Evidence for protein kinase C involvement in arteriolar myogenic reactivity. The American Journal of Physiology, 259(5 Pt 2), H1586–94.

Hill, M. A., & Meininger, G. A. (2012). Arteriolar vascular smooth muscle cells: mechanotransducers in a complex environment. The International Journal of Biochemistry & Cell Biology, 44(9), 1505–10. doi:10.1016/j.biocel.2012.05.021

Huang, D., Cheung, A. T., Parsons, T., Bryer-ash, M., & Parsons, J. T. (2002). Focal adhesion kinase (FAK) regulates insulin-stimulated glycogen synthesis in hepatocytes. J Biol Chem. 277(20):18151-60. *. doi:10.1074/jbc.M104252200

Huang, D., Khoe, M., Ilic, D., & Bryer-Ash, M. (2006). Reduced expression of focal adhesion kinase disrupts insulin action in skeletal muscle cells. Endocrinology, 147(7), 3333–43. doi:10.1210/en.2005-0382

Huang, P.-H., Sata, M., Nishimatsu, H., Sumi, M., Hirata, Y., & Nagai, R. (2008). Pioglitazone ameliorates endothelial dysfunction and restores ischemia-induced angiogenesis in diabetic mice. Biomedicine & Pharmacotherapy = Biomédecine & Pharmacothérapie, 62(1), 46–52. doi:10.1016/j.biopha.2007.06.014

Huang, L., Li, Q., Li, H., He, Z., Cheng, Z., Chen, J., & Guo, L. (2009). Inhibition of intracellular Ca2+ release by a Rho-kinase inhibitor for the treatment of ischemic damage in primary cultured rat hippocampal neurons. *European Journal of Pharmacology*, *602*(2-3), 238–44. doi:10.1016/j.ejphar.2008.11.053

Ichetovkin, I., Grant, W., & Condeelis, J. (2002). Cofilin produces newly polymerized actin filaments that are preferred for dendritic nucleation by the Arp2/3 complex. Current Biology : CB, 12(1), 79–84.

Ihara, E., & MacDonald, J. A. (2007). The regulation of smooth muscle contractility by zipper-interacting protein kinase. Canadian Journal of Physiology and Pharmacology, 85(1), 79–87. doi:10.1139/y06-103

Ishida, K., Matsumoto, T., Taguchi, K., Kamata, K., & Kobayashi, T. (2012). Protein kinase C delta contributes to increase in EP3 agonist-induced contraction in mesenteric arteries from type 2 diabetic Goto-Kakizaki rats. Pflügers Archiv : European Journal of Physiology, 463(4), 593–602. doi:10.1007/s00424-012-1088-9

Jackson, T. Y., Sun, Z., Martinez-Lemus, L. A., Hill, M. A., & Meininger, G. A. (2010). N-cadherin and integrin blockade inhibit arteriolar myogenic reactivity but not pressure-induced increases in intracellular Ca. Frontiers in Physiology, 1, 165. doi:10.3389/fphys.2010.00165

Jacob, A., Smolenski, A., Lohmann, S. M., & Begum, N. (2004). MKP-1 expression and stabilization and cGK Ialpha prevent diabetes- associated abnormalities in VSMC migration. American Journal of Physiology. Cell Physiology, 287(4), C1077–86. doi:10.1152/ajpcell.00477.2003

Jarajapu, Y. P. R., Guberski, D. L., Grant, M. B., & Knot, H. J. (2008). Myogenic tone and reactivity of cerebral arteries in type II diabetic BBZDR/Wor rat. European Journal of Pharmacology, 579(1-3), 298–307. doi:10.1016/j.ejphar.2007.10.028

Jarajapu, Y. P. R., & Knot, H. J. (2002). Role of phospholipase C in development of myogenic tone in rat posterior cerebral arteries. American Journal of Physiology. Heart and Circulatory Physiology, 283(6), H2234–8. doi:10.1152/ajpheart.00624.2002

Jarajapu, Y. P. R., & Knot, H. J. (2005). Relative contribution of Rho kinase and protein kinase C to myogenic tone in rat cerebral arteries in hypertension. American Journal of Physiology. Heart and Circulatory Physiology, 289(5), H1917–22. doi:10.1152/ajpheart.01012.2004

Johnson, R. P., El-Yazbi, A. F., Takeya, K., Walsh, E. J., Walsh, M. P., & Cole, W. C. (2009). Ca2+ sensitization via phosphorylation of myosin phosphatase targeting subunit at threonine-855 by Rho kinase contributes to the arterial myogenic response. The Journal of Physiology, 587(Pt 11), 2537–53. doi:10.1113/jphysiol.2008.168252

Juliano, R. L. (2002). Signal transduction by cell adhesion receptors and the cytoskeleton: functions of integrins, cadherins, selectins, and immunoglobulin-superfamily members. Annual Review of Pharmacology and Toxicology, 42, 283–323. doi:10.1146/annurev.pharmtox.42.090401.151133

Kanda, T., Wakino, S., Homma, K., Yoshioka, K., Tatematsu, S., Hasegawa, K., … Saruta, T. (2006). Rho-kinase as a molecular target for insulin resistance and hypertension. FASEB Journal : Official Publication of the Federation of American Societies for Experimental Biology, 20(1), 169–71. doi:10.1096/fj.05-4197fje

Kelly-Cobbs, A., Elgebaly, M. M., Li, W., & Ergul, A. (2011). Pressure-independent cerebrovascular remodelling and changes in myogenic reactivity in diabetic Goto-Kakizaki rat in response to glycaemic control. Acta Physiologica (Oxford, England), 203(1), 245–51. doi:10.1111/j.1748-1716.2010.02230.x

Ketsawatsomkron, P., Lorca, R. A., Keen, H. L., Weatherford, E. T., Liu, X., Pelham, C. J., … Sigmund, C. D. (2012). PPARγ regulates resistance vessel tone through a mechanism involving RGS5-mediated control of protein kinase C and BKCa channel activity. Circulation Research, 111(11), 1446–58. doi:10.1161/CIRCRESAHA.112.271577

Kim, H. R., Gallant, C., Leavis, P. C., Gunst, S. J., & Morgan, K. G. (2008). Cytoskeletal remodeling in differentiated vascular smooth muscle is actin isoform dependent and stimulus dependent. American Journal of Physiology. Cell Physiology, 295(3), C768–78. doi:10.1152/ajpcell.00174.2008

Kimura, K., Ito, M., Amano, M., Chihara, K., Fukata, Y., Nakafuku, M., … Kaibuchi, K. (1996). Regulation of myosin phosphatase by Rho and Rho-associated kinase (Rho-kinase). Science (New York, N.Y.), 273(5272), 245–8.

Knot, H. J., & Nelson, M. T. (1995). Regulation of membrane potential and diameter by voltage-dependent K+ channels in rabbit myogenic cerebral arteries. The American Journal of Physiology, 269(1 Pt 2), H348–55.

Knot, H. J., & Nelson, M. T. (1998). Regulation of arterial diameter and wall [Ca2+] in cerebral arteries of rat by membrane potential and intravascular pressure. The Journal of Physiology, 508 (Pt 1), 199–209.

Kobayashi, Y., Naruse, K., Hamada, Y., Nakashima, E., Kato, K., Akiyama, N., … Nakamura, J. (2005). Human proinsulin C-peptide prevents proliferation of rat aortic smooth muscle cells cultured in high-glucose conditions. Diabetologia, 48(11), 2396–401. doi:10.1007/s00125-005-1942-9

Kold-Petersen, H., Brøndum, E., Nilsson, H., Flyvbjerg, a, & Aalkjaer, C. (2012). Impaired myogenic tone in isolated cerebral and coronary resistance arteries from the goto-kakizaki rat model of type 2 diabetes. Journal of Vascular Research, 49(3), 267–78. doi:10.1159/000335487

Lagaud, G. J., Masih-Khan, E., Kai, S., van Breemen, C., & Dubé, G. P. (2001). Influence of type II diabetes on arterial tone and endothelial function in murine mesenteric resistance arteries. Journal of Vascular Research, 38(6), 578–89.

Lam, H.-C., Lee, J.-K., Lu, C.-C., Chu, C.-H., Chuang, M.-J., & Wang, M.-C. (2003). Role of endothelin in diabetic retinopathy. Current Vascular Pharmacology, 1(3), 243–50.

Large, W. A., Saleh, S. N., & Albert, A. P. (2009). Role of phosphoinositol 4,5-bisphosphate and diacylglycerol in regulating native TRPC channel proteins in vascular smooth muscle. Cell Calcium, 45(6), 574–82. doi:10.1016/j.ceca.2009.02.007

Lebrun, P., Baron, V., Hauck, C. R., Schlaepfer, D. D., & Van Obberghen, E. (2000). Cell adhesion and focal adhesion kinase regulate insulin receptor substrate-1 expression. The Journal of Biological Chemistry, 275(49), 38371–7. doi:10.1074/jbc.M006162200

Ledoux, J., Werner, M. E., Brayden, J. E., & Nelson, M. T. (2006). Calcium-activated potassium channels and the regulation of vascular tone. Physiology (Bethesda, Md.), 21, 69–78. doi:10.1152/physiol.00040.2005

Lee, J. H., Palaia, T., & Ragolia, L. (2009). Impaired insulin-mediated vasorelaxation in diabetic Goto-Kakizaki rats is caused by impaired Akt phosphorylation. American Journal of Physiology. Cell Physiology, 296(2), C327–38. doi:10.1152/ajpcell.00254.2008

Legate, K. R., Wickström, S. A., & Fässler, R. (2009). Genetic and cell biological analysis of integrin outside-in signaling. Genes & Development, 23(4), 397–418. doi:10.1101/gad.1758709

Lesniewski, L. A., Donato, A. J., Behnke, B. J., Woodman, C. R., Laughlin, M. H., Ray, C. A., & Delp, M. D. (2008). Decreased NO signaling leads to enhanced vasoconstrictor responsiveness in skeletal muscle arterioles of the ZDF rat prior to overt diabetes and hypertension. American Journal of Physiology. Heart and Circulatory Physiology, 294(4), H1840–50. doi:10.1152/ajpheart.00692.2007

Lessey, E. C., Guilluy, C., & Burridge, K. (2012). From mechanical force to RhoA activation. Biochemistry, 51(38), 7420–32. doi:10.1021/bi300758e

Li, W., Kelly-Cobbs, A. I., Mezzetti, E. M., Fagan, S. C., & Ergul, A. (2010). Endothelin-1-mediated cerebrovascular remodeling is not associated with increased ischemic brain injury in diabetes. Canadian Journal of Physiology and Pharmacology, 88(8), 788–95. doi:10.1139/Y10-040

Li, Y.-J., Hui, Y.-N., Yan, F., & Du, Z.-J. (2007). Up-regulation of integrin-linked kinase in the streptozotocin-induced diabetic rat retina. Graefe's Archive for Clinical and Experimental Ophthalmology = Albrecht von Graefes Archiv Für Klinische Und Experimentelle Ophthalmologie, 245(10), 1523–32. doi:10.1007/s00417-007-0616-3

Lidington, D., Schubert, R., & Bolz, S.-S. (2013). Capitalizing on diversity: an integrative approach towards the multiplicity of cellular mechanisms underlying myogenic responsiveness. Cardiovascular Research, 97(3), 404–12. doi:10.1093/cvr/cvs345

Lin, G., Craig, G. P., Zhang, L., Yuen, V. G., Allard, M., McNeill, J. H., & MacLeod, K. M. (2007). Acute inhibition of Rho-kinase improves cardiac contractile function in streptozotocin-diabetic rats. Cardiovascular Research, 75(1), 51–8. doi:10.1016/j.cardiores.2007.03.009

Liu, Y., Zhou, Y., Wang, Y., Geng, D., & Liu, J. (2011). Roux-en-Y gastric bypass-induced improvement of glucose tolerance and insulin resistance in type 2 diabetic rats are mediated by glucagon-like peptide-1. Obesity Surgery, 21(9), 1424–31. doi:10.1007/s11695-011-0388-z

Livak, K. J., & Schmittgen, T. D. (2001). Analysis of relative gene expression data using real-time quantitative PCR and the 2(-Delta Delta C(T)) method. Methods (San Diego, Calif.), 25(4), 402–8. doi:10.1006/meth.2001.1262

Llagostera, E., Catalucci, D., Marti, L., Liesa, M., Camps, M., Ciaraldi, T. P., … Kaliman, P. (2007). Role of myotonic dystrophy protein kinase (DMPK) in glucose homeostasis and muscle insulin action. PloS One, 2(11), e1134. doi:10.1371/journal.pone.0001134

Loirand, G., Guérin, P., & Pacaud, P. (2006). Rho kinases in cardiovascular physiology and pathophysiology. Circulation Research, 98(3), 322–34. doi:10.1161/01.RES.0000201960.04223.3c

Lorenzi, M., Feke, G. T., Pitler, L., Berisha, F., Kolodjaschna, J., & McMeel, J. W. (2010). Defective myogenic response to posture change in retinal vessels of well-controlled type 1 diabetic patients with no retinopathy. Investigative Ophthalmology & Visual Science, 51(12), 6770–5. doi:10.1167/iovs.10-5785

Loutzenhiser, R., Griffin, K., Williamson, G., & Bidani, A. (2006). Renal autoregulation: new perspectives regarding the protective and regulatory roles of the underlying mechanisms. American Journal of Physiology. Regulatory, Integrative and Comparative Physiology, 290(5), R1153–67. doi:10.1152/ajpregu.00402.2005

Lu, J., Landerholm, T. E., Wei, J. S., Dong, X. R., Wu, S. P., Liu, X., … Majesky, M. W. (2001). Coronary smooth muscle differentiation from proepicardial cells requires rhoA-mediated actin reorganization and p160 rho-kinase activity. Developmental Biology, 240(2), 404–18. doi:10.1006/dbio.2001.0403

Lu, X., Bean, J. S., Kassab, G. S., & Rekhter, M. D. (2011). Protein kinase C inhibition ameliorates functional endothelial insulin resistance and vascular smooth muscle cell hypersensitivity to insulin in diabetic hypertensive rats. Cardiovascular Diabetology, 10, 48. doi:10.1186/1475-2840-10-48

Lucchesi, P. A., Sabri, A., Belmadani, S., & Matrougui, K. (2004). Involvement of metalloproteinases 2/9 in epidermal growth factor receptor transactivation in pressure-induced myogenic tone in mouse mesenteric resistance arteries. Circulation, 110(23), 3587–93. doi:10.1161/01.CIR.0000148780.36121.47

Luykenaar, K. D., El-Rahman, R. A., Walsh, M. P., & Welsh, D. G. (2009). Rho-kinase-mediated suppression of KDR current in cerebral arteries requires an intact actin cytoskeleton. American Journal of Physiology. Heart and Circulatory Physiology, 296(4), H917–26. doi:10.1152/ajpheart.01206.2008

Martinez-Lemus, L. A., Crow, T., Davis, M. J., & Meininger, G. A. (2005). alphavbeta3- and alpha5beta1-integrin blockade inhibits myogenic constriction of skeletal muscle resistance arterioles. American Journal of Physiology. Heart and Circulatory Physiology, 289(1), H322–9. doi:10.1152/ajpheart.00923.2003

Martinez-Lemus, L. A., Wu, X., Wilson, E., Hill, M. A., Davis, G. E., Davis, M. J., & Meininger, G. A. (2003). Integrins as unique receptors for vascular control. Journal of Vascular Research, 40(3), 211–33. doi:71886

Martinez-Lemus, L. A. (2014). Current opinions on the control and role of vascular smooth muscle cell adhesion, calcium sensitization, and the cytoskeleton in vascular structure and function. Microcirculation. 21(3):197-200. doi: 10.1111/micc.12130

Massett, M. P., Ungvari, Z., Csiszar, A., Kaley, G., & Koller, A. (2002). Different roles of PKC and MAP kinases in arteriolar constrictions to pressure and agonists. American Journal of Physiology. Heart and Circulatory Physiology, 283(6), H2282–7. doi:10.1152/ajpheart.00544.2002

Matsumoto, T., Ishida, K., Taguchi, K., Kobayashi, T., & Kamata, K. (2010). Short-term angiotensin-1 receptor antagonism in type 2 diabetic Goto-Kakizaki rats normalizes endothelin-1-induced mesenteric artery contraction. Peptides, 31(4), 609–17. doi:10.1016/j.peptides.2009.12.017

Matsumoto, T., Watanabe, S., Taguchi, K., & Kobayashi, T. (2014). Mechanisms underlying increased serotonin-induced contraction in carotid arteries from chronic type 2 diabetic Goto-Kakizaki rats. Pharmacological Research : The Official Journal of the Italian Pharmacological Society. doi:10.1016/j.phrs.2014.07.001

Mederos y Schnitzler, M., Storch, U., & Gudermann, T. (2011). AT1 receptors as mechanosensors. Current Opinion in Pharmacology, 11(2), 112–6. doi:10.1016/j.coph.2010.11.003

Mederos y Schnitzler, M., Storch, U., Meibers, S., Nurwakagari, P., Breit, A., Essin, K., … Gudermann, T. (2008). Gq-coupled receptors as mechanosensors mediating myogenic vasoconstriction. The EMBO Journal, 27(23), 3092–103. doi:10.1038/emboj.2008.233

Mehta, D., & Gunst, S. J. (1999). Actin polymerization stimulated by contractile activation regulates force development in canine tracheal smooth muscle. The Journal of Physiology, 519 Pt 3, 829–40.

Mishra, R. C., Wulff, H., Cole, W. C., & Braun, A. P. (2014). A pharmacologic activator of endothelial KCa channels enhances coronary flow in the hearts of type 2 diabetic rats. Journal of Molecular and Cellular Cardiology, 72, 364–73. doi:10.1016/j.yjmcc.2014.04.013

Moncada, S., & Higgs, E. A. (2006). The discovery of nitric oxide and its role in vascular biology. British Journal of Pharmacology, 147 Suppl , S193–201. doi:10.1038/sj.bjp.0706458

Moreno-Domínguez, A., Cidad, P., Miguel-Velado, E., López-López, J. R., & Pérez-García, M. T. (2009). De novo expression of Kv6.3 contributes to changes in vascular smooth muscle cell excitability in a hypertensive mice strain. The Journal of Physiology, 587(Pt 3), 625–40. doi:10.1113/jphysiol.2008.165217

Moreno-Domínguez, A., Colinas, O., El-Yazbi, A., Walsh, E. J., Hill, M. A., Walsh, M. P., & Cole, W. C. (2013). Ca2+ sensitization due to myosin light chain phosphatase inhibition and cytoskeletal reorganization in the myogenic response of skeletal muscle resistance arteries. The Journal of Physiology, 591(Pt 5), 1235–50. doi:10.1113/jphysiol.2012.243576

Moreno-Domínguez, A., El-Yazbi, A. F., Zhu, H.-L., Colinas, O., Zhong, X. Z., Walsh, E. J., … Cole, W. C. (2014). Cytoskeletal reorganization evoked by Rho-associated kinase- and protein kinase C-catalyzed phosphorylation of cofilin and heat shock protein 27, respectively, contributes to myogenic constriction of rat cerebral arteries. The Journal of Biological Chemistry. doi:10.1074/jbc.M114.553743

Moriyama, K., Iida, K., & Yahara, I. (1996). Phosphorylation of Ser-3 of cofilin regulates its essential function on actin. Genes to Cells : Devoted to Molecular & Cellular Mechanisms, 1(1), 73–86.

Mueed, I., Zhang, L., & MacLeod, K. M. (2005). Role of the PKC/CPI-17 pathway in enhanced contractile responses of mesenteric arteries from diabetic rats to alpha-adrenoceptor stimulation. British Journal of Pharmacology, 146(7), 972–82. doi:10.1038/sj.bjp.0706398

Mufti, R. E., Brett, S. E., Tran, C. H. T., Abd El-Rahman, R., Anfinogenova, Y., El-Yazbi, A., … Welsh, D. G. (2010). Intravascular pressure augments cerebral arterial constriction by inducing voltage-insensitive Ca2+ waves. The Journal of Physiology, 588(Pt 20), 3983–4005. doi:10.1113/jphysiol.2010.193300

Mulvany, M. J., & Aalkjaer, C. (1990). Structure and function of small arteries. Physiological Reviews, 70(4), 921–61.

Muniyappa, R., Montagnani, M., Koh, K. K., & Quon, M. J. (2007). Cardiovascular actions of insulin. Endocrine Reviews, 28(5), 463–91. doi:10.1210/er.2007-0006

Muniyappa, R., & Quon, M. J. (2007). Insulin action and insulin resistance in vascular endothelium. Current Opinion in Clinical Nutrition and Metabolic Care, 10(4), 523–30. doi:10.1097/MCO.0b013e32819f8ecd

Murányi, A., MacDonald, J. A., Deng, J. T., Wilson, D. P., Haystead, T. A. J., Walsh, M. P., … Hartshorne, D. J. (2002). Phosphorylation of the myosin phosphatase target subunit by integrin-linked kinase. The Biochemical Journal, 366(Pt 1), 211–6. doi:10.1042/BJ20020401

Murányi, A., Zhang, R., Liu, F., Hirano, K., Ito, M., Epstein, H. F., & Hartshorne, D. J. (2001). Myotonic dystrophy protein kinase phosphorylates the myosin phosphatase targeting subunit and inhibits myosin phosphatase activity. FEBS Letters, 493(2-3), 80–4.

Muris, D. M. J., Houben, A. J. H. M., Schram, M. T., & Stehouwer, C. D. A. (2013). Microvascular dysfunction: An emerging pathway in the pathogenesis of obesity-related insulin resistance. Reviews in Endocrine and Metabolic Disorders, 14(1), 29–38. doi:10.1007/s11154-012-9231-7

Murphy, T. V, Spurrell, B. E., & Hill, M. A. (2002). Cellular signalling in arteriolar myogenic constriction: involvement of tyrosine phosphorylation pathways. Clinical and Experimental Pharmacology & Physiology, 29(7), 612–9.

Nakamura, J., Kasuya, Y., Hamada, Y., Nakashima, E., Naruse, K., Yasuda, Y., … Hotta, N. (2001). Glucose-induced hyperproliferation of cultured rat aortic smooth muscle cells through polyol pathway hyperactivity. Diabetologia, 44(4), 480–7. doi:10.1007/s001250051646

Nie, J., Xue, B., Sukumaran, S., Jusko, W. J., Dubois, D. C., & Almon, R. R. (2011). Differential muscle gene expression as a function of disease progression in Goto-Kakizaki diabetic rats. Molecular and Cellular Endocrinology, 338(1-2), 10–7. doi:10.1016/j.mce.2011.02.016

Nigro, J., Osman, N., Dart, A. M., & Little, P. J. (2006). Insulin resistance and atherosclerosis. Endocrine Reviews, 27(3), 242–59. doi:10.1210/er.2005-0007

Nobe, K., Hashimoto, T., & Honda, K. (2012). Two distinct dysfunctions in diabetic mouse mesenteric artery contraction are caused by changes in the Rho A-Rho kinase signaling pathway. European Journal of Pharmacology, 683(1-3), 217–25. doi:10.1016/j.ejphar.2012.03.022

Nobe, K., Yamazaki, T., Tsumita, N., Hashimoto, T., & Honda, K. (2009). Glucose-dependent enhancement of diabetic bladder contraction is associated with a rho kinase-regulated protein kinase C pathway. The Journal of Pharmacology and Experimental Therapeutics, 328(3), 940–50. doi:10.1124/jpet.108.144907

Noll, C., Lacraz, G., Ehses, J., Coulaud, J., Bailbe, D., Paul, J.-L., … Janel, N. (2011). Early reduction of circulating homocysteine levels in Goto-Kakizaki rat, a spontaneous nonobese model of type 2 diabetes. Biochimica et Biophysica Acta, 1812(6), 699–702. doi:10.1016/j.bbadis.2011.03.011

O'Rourke, C. M., Davis, J. A., Saltiel, A. R., & Cornicelli, J. A. (1997). Metabolic effects of troglitazone in the Goto-Kakizaki rat, a non-obese and normolipidemic rodent model of non-insulin-dependent diabetes mellitus. Metabolism: Clinical and Experimental, 46(2), 192–8.

Okon, E. B., Szado, T., Laher, I., McManus, B., & van Breemen, C. (2003). Augmented contractile response of vascular smooth muscle in a diabetic mouse model. Journal of Vascular Research, 40(6), 520–30. doi:75238

Opazo Saez, A., Zhang, W., Wu, Y., Turner, C. E., Tang, D. D., & Gunst, S. J. (2004). Tension development during contractile stimulation of smooth muscle requires recruitment of paxillin and vinculin to the membrane. American Journal of Physiology. Cell Physiology, 286(2), C433–47. doi:10.1152/ajpcell.00030.2003

Osol, G., Brekke, J. F., McElroy-Yaggy, K., & Gokina, N. I. (2002). Myogenic tone, reactivity, and forced dilatation: a three-phase model of in vitro arterial myogenic behavior. American

Journal of Physiology. Heart and Circulatory Physiology, 283(6), H2260–7. doi:10.1152/ajpheart.00634.2002

Osol, G., Laher, I., & Cipolla, M. (1991). Protein kinase C modulates basal myogenic tone in resistance arteries from the cerebral circulation. Circulation Research, 68(2), 359–67.

Ostenson, C.-G., & Efendic, S. (2007). Islet gene expression and function in type 2 diabetes; studies in the Goto-Kakizaki rat and humans. Diabetes, Obesity & Metabolism, 9 Suppl 2, 180–6. doi:10.1111/j.1463-1326.2007.00787.x

Owens, G. K., Kumar, M. S., & Wamhoff, B. R. (2004). Molecular regulation of vascular smooth muscle cell differentiation in development and disease. Physiological Reviews, 84(3), 767–801. doi:10.1152/physrev.00041.2003

Pavalko, F. M., Adam, L. P., Wu, M. F., Walker, T. L., & Gunst, S. J. (1995). Phosphorylation of dense-plaque proteins talin and paxillin during tracheal smooth muscle contraction. The American Journal of Physiology, 268(3 Pt 1), C563–71.

Pfeifle, B., & Ditschuneit, H. (1981). Effect of insulin on growth of cultured human arterial smooth muscle cells. Diabetologia, 20(2), 155–8.

Plane, F., Johnson, R., Kerr, P., Wiehler, W., Thorneloe, K., Ishii, K., … Cole, W. (2005). Heteromultimeric Kv1 channels contribute to myogenic control of arterial diameter. Circulation Research, 96(2), 216–24. doi:10.1161/01.RES.0000154070.06421.25

Polikandriotis, J. A., Mazzella, L. J., Rupnow, H. L., & Hart, C. M. (2005). Peroxisome proliferator-activated receptor gamma ligands stimulate endothelial nitric oxide production through distinct peroxisome proliferator-activated receptor gamma-dependent mechanisms. Arteriosclerosis, Thrombosis, and Vascular Biology, 25(9), 1810–6. doi:10.1161/01.ATV.0000177805.65864.d4

Porter, K. E., & Riches, K. (2013). The vascular smooth muscle cell: a therapeutic target in Type 2 diabetes? Clinical Science (London, England : 1979), 125(4), 167–82. doi:10.1042/CS20120413

Portha, B. (2005). Programmed disorders of beta-cell development and function as one cause for type 2 diabetes? The GK rat paradigm. Diabetes/metabolism Research and Reviews, 21(6), 495–504. doi:10.1002/dmrr.566

Portha, B., Giroix, M.-H., Tourrel-Cuzin, C., Le-Stunff, H., & Movassat, J. (2012). The GK rat: a prototype for the study of non-overweight type 2 diabetes. Methods in Molecular Biology (Clifton, N.J.), 933, 125–59. doi:10.1007/978-1-62703-068-7_9

Portha, B., Lacraz, G., Kergoat, M., Homo-Delarche, F., Giroix, M.-H., Bailbé, D., … Movassat, J. (2009). The GK rat beta-cell: a prototype for the diseased human beta-cell in type 2 diabetes? Molecular and Cellular Endocrinology, 297(1-2), 73–85. doi:10.1016/j.mce.2008.06.013

Potocnik, S. J., & Hill, M. A. (2001). Pharmacological evidence for capacitative Ca(2+) entry in cannulated and pressurized skeletal muscle arterioles. British Journal of Pharmacology, 134(2), 247–56. doi:10.1038/sj.bjp.0704270

Putnam, T. J. (1937). The Cerebral Circulation: Some New Points in its Anatomy, Physiology and Pathology. The Journal of Neurology and Psychopathology, 17(67), 193–212.

Ragolia, L., Palaia, T., Koutrouby, T. B., & Maesaka, J. K. (2004). Inhibition of cell cycle progression and migration of vascular smooth muscle cells by prostaglandin D2 synthase: resistance in diabetic Goto-Kakizaki rats. American Journal of Physiology. Cell Physiology, 287(5), C1273–81. doi:10.1152/ajpcell.00230.2004

Rao, M. Y., Soliman, H., Bankar, G., Lin, G., & MacLeod, K. M. (2013). Contribution of Rho kinase to blood pressure elevation and vasoconstrictor responsiveness in type 2 diabetic Goto-Kakizaki rats. Journal of Hypertension, 31(6), 1160–9. doi:10.1097/HJH.0b013e328360383a

Rice, D. C., Dobrian, A. D., Schriver, S. D., & Prewitt, R. L. (2002). Src autophosphorylation is an early event in pressure-mediated signaling pathways in isolated resistance arteries. Hypertension, 39(2 Pt 2), 502–7.

Rosen, E. D., & Spiegelman, B. M. (2001). PPARgamma : a nuclear regulator of metabolism, differentiation, and cell growth. The Journal of Biological Chemistry, 276(41), 37731–4. doi:10.1074/jbc.R100034200

Sachidanandam, K., Hutchinson, J. R., Elgebaly, M. M., Mezzetti, E. M., Dorrance, A. M., Motamed, K., & Ergul, A. (2009). Glycemic control prevents microvascular remodeling and increased tone in type 2 diabetes: link to endothelin-1. American Journal of Physiology. Regulatory, Integrative and Comparative Physiology, 296(4), R952–9. doi:10.1152/ajpregu.90537.2008

Saito, S. Y., Hori, M., Ozaki, H., & Karaki, H. (1996). Cytochalasin D inhibits smooth muscle contraction by directly inhibiting contractile apparatus. Journal of Smooth Muscle Research = Nihon Heikatsukin Gakkai Kikanshi, 32(2), 51–60.

Sandu, O. A., Ragolia, L., & Begum, N. (2000). Diabetes in the Goto-Kakizaki rat is accompanied by impaired insulin-mediated myosin-bound phosphatase activation and vascular smooth muscle cell relaxation. Diabetes, 49(12), 2178–89.

Sarwar, N., Gao, P., Seshasai, S. R. K., Gobin, R., Kaptoge, S., Di Angelantonio, E., … Danesh, J. (2010). Diabetes mellitus, fasting blood glucose concentration, and risk of vascular disease: a collaborative meta-analysis of 102 prospective studies. Lancet, 375(9733), 2215–22. doi:10.1016/S0140-6736(10)60484-9

Sasaki, Y., Suzuki, M., & Hidaka, H. (2002). The novel and specific Rho-kinase inhibitor (S)-(+)-2-methyl-1-[(4-methyl-5-isoquinoline)sulfonyl]-homopiperazine as a probing molecule for Rho-kinase-involved pathway. Pharmacology & Therapeutics, 93(2-3), 225–32.

Satoh, K., Fukumoto, Y., & Shimokawa, H. (2011). Rho-kinase : important new therapeutic target in cardiovascular diseases. Am J Physiol Heart Circ Physiol, 301(2):H287-96, doi:10.1152/ajpheart.00327.2011.

Sauzeau, V., Le Jeune, H., Cario-Toumaniantz, C., Smolenski, A., Lohmann, S. M., Bertoglio, J., … Loirand, G. (2000). Cyclic GMP-dependent protein kinase signaling pathway inhibits RhoA-induced Ca2+ sensitization of contraction in vascular smooth muscle. The Journal of Biological Chemistry, 275(28), 21722–9. doi:10.1074/jbc.M000753200

Sauzeau, V., Rolli-Derkinderen, M., Lehoux, S., Loirand, G., & Pacaud, P. (2003). Sildenafil prevents change in RhoA expression induced by chronic hypoxia in rat pulmonary artery. Circulation Research, 93(7), 630–7. doi:10.1161/01.RES.0000093220.90027.D9

Schaeffer, G., Levak-Frank, S., Spitaler, M. M., Fleischhacker, E., Esenabhalu, V. E., Wagner, A. H., … Graier, W. F. (2003). Intercellular signalling within vascular cells under high D-glucose involves free radical-triggered tyrosine kinase activation. Diabetologia, 46(6), 773–83. doi:10.1007/s00125-003-1091-y

Schofield, I., Malik, R., Izzard, A., Austin, C., & Heagerty, A. (2002). Vascular structural and functional changes in type 2 diabetes mellitus: evidence for the roles of abnormal myogenic responsiveness and dyslipidemia. Circulation, 106(24), 3037–43.

Schubert, R., Lidington, D., & Bolz, S.-S. (2008). The emerging role of Ca2+ sensitivity regulation in promoting myogenic vasoconstriction. Cardiovascular Research, 77(1), 8–18. doi:10.1016/j.cardiores.2007.07.018

Schubert, R., & Mulvany, M. J. (1999). The myogenic response: established facts and attractive hypotheses. Clinical Science (London, England : 1979), 96(4), 313–26.

Shaw, L., Ahmed, S., Austin, C., & Taggart, M. J. (2003). Inhibitors of actin filament polymerisation attenuate force but not global intracellular calcium in isolated pressurised resistance arteries. Journal of Vascular Research, 40(1), 1–10; discussion 10. doi:68940

Shiraishi, T., Sakaki, S., & Uehara, Y. (1986). Architecture of the media of the arterial vessels in the dog brain: a scanning electron-microscopic study. Cell and Tissue Research, 243(2), 329–35.

Socha, M. J., Behringer, E. J., & Segal, S. S. (2012). Calcium and electrical signalling along endothelium of the resistance vasculature. Basic & Clinical Pharmacology & Toxicology, 110(1), 80–6. doi:10.1111/j.1742-7843.2011.00798.x

Somlyo, A. P., & Somlyo, A. V. (2000). Signal transduction by G-proteins, rho-kinase and protein phosphatase to smooth muscle and non-muscle myosin II. The Journal of Physiology, 522 Pt 2, 177–85.

Somlyo, A. P., & Somlyo, A. V. (2003). Ca2+ sensitivity of smooth muscle and nonmuscle myosin II: modulated by G proteins, kinases, and myosin phosphatase. Physiological Reviews, 83(4), 1325–58. doi:10.1152/physrev.00023.2003

Spurrell, B. E., Murphy, T. V, & Hill, M. A. (2000). Tyrosine phosphorylation modulates arteriolar tone but is not fundamental to myogenic response. American Journal of Physiology. Heart and Circulatory Physiology, 278(2), H373–82.

Spurrell, B. E., Murphy, T. V, & Hill, M. A. (2003). Intraluminal pressure stimulates MAPK phosphorylation in arterioles: temporal dissociation from myogenic contractile response. American Journal of Physiology. Heart and Circulatory Physiology, 285(4), H1764–73. doi:10.1152/ajpheart.00468.2003

Standaert, M. L., Sajan, M. P., Miura, A., Kanoh, Y., Chen, H. C., & Farese, R. V. (2004). Insulin-induced activation of atypical protein kinase C, but not protein kinase B, is maintained in diabetic (ob/ob and Goto-Kakazaki) liver. Contrasting insulin signaling patterns in liver versus muscle define phenotypes of type 2 diabetic and high fat-i. The Journal of Biological Chemistry, 279(24), 24929–34. doi:10.1074/jbc.M402440200

Su, J., Lucchesi, P. A., Gonzalez-Villalobos, R. A., Palen, D. I., Rezk, B. M., Suzuki, Y., … Matrougui, K. (2008). Role of advanced glycation end products with oxidative stress in resistance artery dysfunction in type 2 diabetic mice. Arteriosclerosis, Thrombosis, and Vascular Biology, 28(8), 1432–8. doi:10.1161/ATVBAHA.108.167205

Surks, H. K., Mochizuki, N., Kasai, Y., Georgescu, S. P., Tang, K. M., Ito, M., … Mendelsohn, M. E. (1999). Regulation of myosin phosphatase by a specific interaction with cGMP- dependent protein kinase Ialpha. Science (New York, N.Y.), 286(5444), 1583–7.

Suzuki, L. A., Poot, M., Gerrity, R. G., & Bornfeldt, K. E. (2001). Diabetes accelerates smooth muscle accumulation in lesions of atherosclerosis: lack of direct growth-promoting effects of high glucose levels. Diabetes, 50(4), 851–60.

Swärd, K., Mita, M., Wilson, D. P., Deng, J. T., Susnjar, M., & Walsh, M. P. (2003). The role of RhoA and Rho-associated kinase in vascular smooth muscle contraction. Current Hypertension Reports, 5(1), 66–72.

Takano, H., & Komuro, I. (2009). Peroxisome proliferator-activated receptor gamma and cardiovascular diseases. Circulation Journal : Official Journal of the Japanese Circulation Society, 73(2), 214–20.

Takeya, K., Loutzenhiser, K., Shiraishi, M., Loutzenhiser, R., & Walsh, M. P. (2008). A highly sensitive technique to measure myosin regulatory light chain phosphorylation: the first quantification in renal arterioles. American Journal of Physiology. Renal Physiology, 294(6), F1487–92. doi:10.1152/ajprenal.00060.2008

Takizawa, N., Koga, Y., & Ikebe, M. (2002). Phosphorylation of CPI17 and myosin binding subunit of type 1 protein phosphatase by p21-activated kinase. Biochemical and Biophysical Research Communications, 297(4), 773–8.

Tang, D. D., & Gunst, S. J. (2001). Depletion of focal adhesion kinase by antisense depresses contractile activation of smooth muscle. American Journal of Physiology. Cell Physiology, 280(4), C874–83.

Tang, D. D., & Gunst, S. J. (2004). The small GTPase Cdc42 regulates actin polymerization and tension development during contractile stimulation of smooth muscle. The Journal of Biological Chemistry, 279(50), 51722–8. doi:10.1074/jbc.M408351200

Tang, D. D., & Tan, J. (2003). Role of Crk-associated substrate in the regulation of vascular smooth muscle contraction. Hypertension, 42(4), 858–63. doi:10.1161/01.HYP.0000085333.76141.33

Tang, D. D., Zhang, W., & Gunst, S. J. (2005). The adapter protein CrkII regulates neuronal Wiskott-Aldrich syndrome protein, actin polymerization, and tension development during contractile stimulation of smooth muscle. The Journal of Biological Chemistry, 280(24), 23380–9. doi:10.1074/jbc.M413390200

Tejani, A. D., Walsh, M. P., & Rembold, C. M. (2011). Tissue length modulates "stimulated actin polymerization," force augmentation, and the rate of swine carotid arterial contraction. American Journal of Physiology. Cell Physiology, 301(6), C1470–8. doi:10.1152/ajpcell.00149.2011

Thomas, S. M., & Brugge, J. S. (1997). Cellular functions regulated by Src family kinases. Annual Review of Cell and Developmental Biology, 13, 513–609. doi:10.1146/annurev.cellbio.13.1.513

Thorneloe, K. S., Chen, T. T., Kerr, P. M., Grier, E. F., Horowitz, B., Cole, W. C., & Walsh, M. P. (2001). Molecular composition of 4-aminopyridine-sensitive voltage-gated K(+) channels of vascular smooth muscle. Circulation Research, 89(11), 1030–7.

Tontonoz, P., Hu, E., & Spiegelman, B. M. (1994). Stimulation of adipogenesis in fibroblasts by PPAR gamma 2, a lipid-activated transcription factor. Cell, 79(7), 1147–56.

Touyz, R. M., & Schiffrin, E. L. (2006). Peroxisome proliferator-activated receptors in vascular biology-molecular mechanisms and clinical implications. Vascular Pharmacology, 45(1), 19–28. doi:10.1016/j.vph.2005.11.014

Tsai, E. J., & Kass, D. A. (2009). Cyclic GMP signaling in cardiovascular pathophysiology and therapeutics. Pharmacology & Therapeutics, 122(3), 216–38. doi:10.1016/j.pharmthera.2009.02.009

Tsui, H., Paltser, G., Chan, Y., Dorfman, R., & Dosch, H. M. (2011). “Sensing” the link between type 1 and type 2 diabetes. Diabetes/metabolism Research and Reviews, 27(8), 913–8. doi:10.1002/dmrr.1279

Ueta, K., Ishihara, T., Matsumoto, Y., Oku, A., Nawano, M., Fujita, T., Arakawa, K. (2005). Long-term treatment with the Na+-glucose cotransporter inhibitor T-1095 causes sustained improvement in hyperglycemia and prevents diabetic neuropathy in Goto-Kakizaki Rats. Life Sciences, 76(23), 2655–68. doi:10.1016/j.lfs.2004.09.038

Wakabayashi, I., Nakano, T., & Takahashi, Y. (2010). Enhancement of interleukin-1beta-induced iNOS expression in cultured vascular smooth muscle cells of Goto-Kakizaki diabetes rats. European Journal of Pharmacology, 629(1-3), 1–6. doi:10.1016/j.ejphar.2009.11.054

Wakino, S., Hayashi, K., Kanda, T., Tatematsu, S., Homma, K., Yoshioka, K., … Saruta, T. (2004). Peroxisome proliferator-activated receptor gamma ligands inhibit Rho/Rho kinase pathway by inducing protein tyrosine phosphatase SHP-2. Circulation Research, 95(5), e45–55. doi:10.1161/01.RES.0000142313.68389.92

Walsh, M. P., Bridenbaugh, R., Hartshorne, D. J., & Kerrick, W. G. (1982). Phosphorylation-dependent activated tension in skinned gizzard muscle fibers in the absence of Ca2+. The Journal of Biological Chemistry, 257(11), 5987–90.

Walsh, M. P., & Cole, W. C. (2013). The role of actin filament dynamics in the myogenic response of cerebral resistance arteries. Journal of Cerebral Blood Flow & Metabolism, 33(1), 1–12. doi:10.1038/jcbfm.2012.144

Walsh, M. P., Thornbury, K., Cole, W. C., Sergeant, G., Hollywood, M., & McHale, N. (2011). Rho-associated kinase plays a role in rabbit urethral smooth muscle contraction, but not via enhanced myosin light chain phosphorylation. American Journal of Physiology. Renal Physiology, 300(1), F73–85. doi:10.1152/ajprenal.00011.2010

Wang, C. C. L., Goalstone, M. L., & Draznin, B. (2004). Molecular mechanisms of insulin resistance that impact cardiovascular biology. Diabetes, 53(11), 2735–40.

Wang, C. C. L., Gurevich, I., & Draznin, B. (2003). Insulin affects vascular smooth muscle cell phenotype and migration via distinct signaling pathways. Diabetes, 52(10), 2562–9.

Wertheimer, E., Taylor, S. I., & Tennenbaum, T. (1998). Insulin receptor regulation of cell surface integrins: a possible mechanism contributing to the development of diabetic complications. Proceedings of the Association of American Physicians, 110(4), 333–9.

Wilson, D. P., Susnjar, M., Kiss, E., Sutherland, C., & Walsh, M. P. (2005). Thromboxane A2-induced contraction of rat caudal arterial smooth muscle involves activation of Ca2+ entry and Ca2+ sensitization: Rho-associated kinase-mediated phosphorylation of MYPT1 at Thr-855, but not Thr-697. The Biochemical Journal, 389(Pt 3), 763–74. doi:10.1042/BJ20050237

Wu, X., Davis, G. E., Meininger, G. A., Wilson, E., & Davis, M. J. (2001). Regulation of the L-type calcium channel by alpha 5beta 1 integrin requires signaling between focal adhesion proteins. The Journal of Biological Chemistry, 276(32), 30285–92. doi:10.1074/jbc.M102436200

Xie, X., Peng, J., Chang, X., Huang, K., Huang, J., Wang, S., … Huang, H. (2013). Activation of RhoA/ROCK regulates NF-κB signaling pathway in experimental diabetic nephropathy. Molecular and Cellular Endocrinology, 369(1-2), 86–97. doi:10.1016/j.mce.2013.01.007

Xie, Z., Su, W., Guo, Z., Pang, H., Post, S. R., & Gong, M. C. (2006). Up-regulation of CPI-17 phosphorylation in diabetic vasculature and high glucose cultured vascular smooth muscle cells. Cardiovascular Research, 69(2), 491–501. doi:10.1016/j.cardiores.2005.11.002

Yang, Y., Murphy, T. V, Ella, S. R., Grayson, T. H., Haddock, R., Hwang, Y. T., … Hill, M. A. (2009). Heterogeneity in function of small artery smooth muscle BKCa: involvement of the beta1-subunit. The Journal of Physiology, 587(Pt 12), 3025–44. doi:10.1113/jphysiol.2009.169920

Youn, T., Kim, S. A., & Hai, C. M. (1998). Length-dependent modulation of smooth muscle activation: effects of agonist, cytochalasin, and temperature. The American Journal of Cell Physiology, 274(6 Pt 1), C1601–7.

Yuen, S. L., Ogut, O., & Brozovich, F. V. (2014). Differential phosphorylation of LZ+/LZ- MYPT1 isoforms regulates MLC phosphatase activity. Archives of Biochemistry and Biophysics, 562, 37–42. doi:10.1016/j.abb.2014.08.011

Yuen, S., Ogut, O., & Brozovich, F. V. (2011). MYPT1 protein isoforms are differentially phosphorylated by protein kinase G. The Journal of Biological Chemistry, 286(43), 37274–9. doi:10.1074/jbc.M111.282905

Zhang, W., Wu, Y., Wu, C., & Gunst, S. J. (2007). Integrin-linked kinase regulates N-WASp-mediated actin polymerization and tension development in tracheal smooth muscle. The Journal of Biological Chemistry, 282(47), 34568–80. doi:10.1074/jbc.M704966200

Zhong, X. Z., Abd-Elrahman, K. S., Liao, C.-H., El-Yazbi, A. F., Walsh, E. J., Walsh, M. P., & Cole, W. C. (2010). Stromatoxin-sensitive, heteromultimeric Kv2.1/Kv9.3 channels contribute to myogenic control of cerebral arterial diameter. The Journal of Physiology, 588(Pt 22), 4519–37. doi:10.1113/jphysiol.2010.196618

Zhong, X. Z., Harhun, M. I., Olesen, S. P., Ohya, S., Moffatt, J. D., Cole, W. C., & Greenwood, I. A. (2010). Participation of KCNQ (Kv7) potassium channels in myogenic control of cerebral arterial diameter. The Journal of Physiology, 588(Pt 17), 3277–93. doi:10.1113/jphysiol.2010.192823